

# Magnetotelluric Data Processing and Analysis

Alan G. Jones

Geological Survey of Canada  
ajones@nrcan.gc.ca

*Processing* takes the time series and derives estimates of the MT impedance tensor. *Analysis* occurs when the MT impedance tensor estimates are studied for their characteristics.

## Processsing Overview

The processing of magnetotelluric (MT) data takes the *data* from time series, with digital values every sampling interval, to MT *responses*, as a function of frequency. These responses are analysed, modeled and inverted to yield the electrical resistivity structure of the Earth below the recording locations, and its variation both laterally and vertically. An attempt was made by Kunetz (1972) to determine MT responses in the time domain as impulse response functions. However, this did not prove fruitful, and has not been followed since.

The time series data are first pre-conditioned then transformed into the frequency domain. Once in the frequency domain, the MT impedance tensor elements are estimated using a variety of methods, with the most reliable and smoothest responses coming from application of modern robust statistical procedures.

Pertinent to response estimation is consideration of linear systems. These are discussed below, starting with the basic single-input/single-output noise-free case to the multiple-input/multiple-output noise contaminated case.

## Analytical signal

On occasion it is useful to inspect the behavior of the time series to determine certain characteristics. One useful tool is to derive the *analytic signal* and, from it, the instantaneous frequency (or wavenumber in the case of series in space, such as profiles of magnetic measurements), amplitude and phase. The analytic signal has no content at negative frequencies in the Fourier domain. An analytic signal can be derived from any real-values time series from

$$z(t) = x(t) + iH [x(t)]$$

where the operator  $H$  denotes the Hilbert transform operator (Hilbert transformation is discussed further below), and  $i$  is the imaginary (square root of  $-1$ ). The analytic signal is useful for detecting time-local (or space-local) properties. It has been used in magnetics for source localization (Nabighian, 1972, 1974).

In magnetotellurics recently the analytic signal approach has been used to identify times when there is likely source field contamination (Jones and Spratt, 2001). Other applications exist.

## Data Pre-conditioning

Prior to any attempt to transform the data from the time domain into frequency domain Fourier spectral estimates, the time series must be pre-conditioned, using a windowing function, to reduce the effect of the finite observation length and trends. In addition, there needs to be some form of severe noise removal, especially spikes, as they have frequency content over the entire spectrum and can distort all frequency estimates.

Standard windowing functions are treated in the standard literature. The Hamming, Hanning, Parzen etc. windows all can perform a reasonable job. Thompson has shown that the best windows are what he terms “prolate spheroidal” windows, and these offer the greatest side-lobe protection.

## Fourier estimation

After pre-conditioning, the time series are transformed into the frequency domain using some form of Fast Fourier Transform (FFT). The standard one is Cooley and Tukey’s Base-2 algorithm, but other algorithms exist that use other bases (Base-3, Base-5)

### Standard spectral methods

Standard spectral estimation methods are discussed in the standard literature. They will not be covered here. Please refer to e.g. Jenkins and Watts, 1968; Bendat and Piersol, 1971; Otnes and Enochson, 1972.

### Cascade decimation

A new approach to time series processing was introduced by Wight and Bostick (1980) and is called *cascade decimation*. This approach has the significant advantage that it computes the spectral estimates in real-time, and was introduced into MT in Phoenix’s MT-16 system in the early 1980s.

### Wavelet methods

Some attempts have been made recently to use wavelet methods in an attempt to time-localize signals in the presence of high noise levels. Garcia and Jones (2003?) will have a paper submitted soon on the work.

## Linear System Transfer Function Estimation

Maxwell’s equations are linear – that is, if the amplitude of the magnetic field is doubled, then the induced electric field is doubled in Faraday’s Law (Eqn. 1.3). Accordingly, we can appeal to the procedures used for linear system estimation. These are given in many standard texts on time series analysis (Jenkins and Watts, 1968; Bendat and Piersol, 1971; Otnes and Enochson, 1972) but they are restated here because of their intrinsic importance to understanding some basic mathematical procedures used in MT impedance tensor estimation.

### Single-input/Single-Output Noise Free Linear System

Consider the single-input/single-output noise-free linear system shown in Fig. 1.

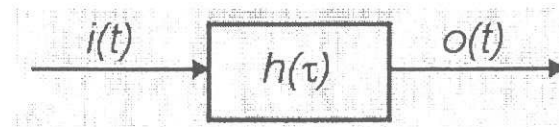


Figure 1: Single-input/single-output noise-free linear system

The input,  $i(t)$ , is related to the output,  $o(t)$ , by the dynamic characteristics of the system, described by the response function,  $h(\tau)$ , through the convolution integral, namely

$$o(t) = \int_{-\infty}^{\infty} h(\tau) i(t - \tau) d\tau \quad (1)$$

(Bendat and Piersol, 1971, Eqn. 2.2). The response function  $h(\tau)$ , is called the *impulse response function*, or *weighting response function*, because the output is exactly the response function for an unit delta function at  $t=0$  on the input.

Any physically-realizable system cannot respond prior to any input, which implies that  $h(\tau) = 0$  for  $\tau < 0$ . Hence, the lower limit of the integration can be set to zero. This requirement is called *causality*, and it results in a set of conditions that can be placed on the impulse response function.

One can determine an estimate of  $h(\tau)$  using auto-correlation methods, but this is unwise because of poor statistical properties of the resulting estimates (Jenkins and Watts, 1968, pp. 422-429). These difficulties may be removed by estimating the Fourier transform of the impulse response function,  $H(\omega)$ , given by

$$H(\omega) = \int_{-\infty}^{\infty} h(\tau) e^{-i\omega\tau} d\tau \quad (2)$$

This function is derived by Fourier transforming the input and output series to yield  $I(\omega)$  and  $O(\omega)$  respectively, from the Fourier transform of the convolution integral above

$$O(\omega) = H(\omega) \cdot I(\omega) \quad (3)$$

Because of the causality requirement of all physically-realizable linear systems, the real and imaginary parts of the complex transfer function  $H(\omega)$  are related by the Hilbert transform relationship. This relationship occurs in many branches of the sciences. It was discovered independently in geomagnetism by Kertz (19xx), and was called the *Kertz transform* through the 1960s.

One least-squares estimate of  $H(\omega)$ ,  $H'(\omega)$ , is given from the Wiener-Hopf integral equation, which states

$$c_{io}(u) = \int_{-\infty}^{\infty} h(\tau) c_{io}(u-\tau) d\tau \quad (4)$$

(Jenkins and Watts, 1968, pp. 204-205), where  $c_{io}(u)$  is the cross-correlation of  $i(t)$  with  $o(t)$ . The Fourier transform of the Wiener-Hopf integral equation is

$$S_{io}(\omega) = H'(\omega) \cdot S_{ii}(\omega) \quad (5)$$

where  $S_{io}(\omega)$  is the cross-spectral density between  $I(\omega)$  and  $O(\omega)$ , from which  $H'(\omega)$ , the least-squares estimate of  $H(\omega)$ , can be derived.

However, one does not know these auto- and cross-spectra. One only has estimates of them based on an observation period from  $(0, T)$ . Thus, the least-squares estimate of  $H(\omega)$  is given by

$$H'(\omega, T) = \frac{S_{io}(\omega, T)}{S_{ii}(\omega, T)} \quad (6)$$

$$\text{where } S_{io}(\omega, T) = I^*(\omega, T) \cdot O^*(\omega, T)$$

$$\text{and } S_{ii}(\omega, T) = I^*(\omega, T) \cdot I^*(\omega, T)$$

The estimates of the auto- and cross-spectra of  $I(\omega)$  and  $O(\omega)$  must be averaged, either over frequency bandwidth or over individual realizations at a particular frequency, to reduce their variances. The greater the averaging, then the lower the variances (assuming all estimates are independent and consistent with the same linear system model). Thus, the smoothed estimate of  $H(\omega)$  is given by

$$\bar{H}_d(\omega, T) = \frac{\bar{S}_{io}(\omega, T)}{\bar{S}_{ii}(\omega, T)} \quad (7)$$

$$\text{where } \bar{S}_{io}(\omega, T) = \langle I^*(\omega, T) \cdot O^*(\omega, T) \rangle$$

$$\text{and } \bar{S}_{ii}(\omega, T) = \langle I^*(\omega, T) \cdot I^*(\omega, T) \rangle$$

and the *random error* associated with the estimates can be reduced by sufficient averaging. Strictly, the above is only valid if the smoothed auto- and cross-spectra are derived at a discrete frequency  $\omega$  from an

ensemble of events. However, if  $H(\omega)$  is a slowly varying function of frequency, then smoothing of the raw estimates may be done by averaging over estimates at neighboring frequencies.

An alternative estimate of  $H(\omega)$  comes from reversing the inputs and outputs to the system, and constructing the auto- and cross-spectra using the output series,  $o(t)$ , instead of the input series. This leads to a second estimate of  $H(\omega)$  given by

$$\bar{H}_u(\omega, T) = \frac{\bar{S}_{oo}(\omega, T)}{\bar{S}_{oi}(\omega, T)} \quad (8)$$

$$\text{where } \bar{S}_{oo}(\omega, T) = \langle O^*(\omega, T) \cdot O(\omega, T) \rangle$$

$$\text{and } \bar{S}_{oi}(\omega, T) = \langle O^*(\omega, T) \cdot I^*(\omega, T) \rangle$$

The reasons for the subscripts “d” and “u” will be made obvious in the below.

### **Single-input/Single-Output Noise Contaminated Linear System**

#### **Noise on output**

Consider the effect of their existing white noise,  $n_y(t)$ , on the output series, so that the measured output,  $y(t)$ , is given by the sum of the true output,  $o(t)$ , plus the white noise. This is shown in Fig. 2.

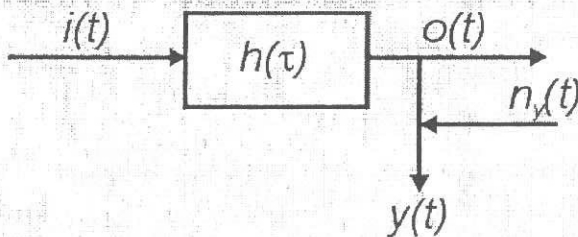


Figure 2: Single-input/Single-output system with output noise

The mathematical model for the linear system is expressed as

$$y(t) = o(t) + n_y(t) = \int_{-\infty}^{\infty} h(\tau) i(t-\tau) d\tau + n_y(t) \quad (9)$$

with the Fourier transform being

$$Y(\omega) = O(\omega) + N_y(\omega) = H(\omega) \cdot I(\omega) + N_y(\omega) \quad (10)$$

If the noise is orthogonal, i.e., totally uncorrelated, to the input series,  $i(t)$ , then

$$\langle n_y(\tau) \cdot i(t+\tau) \rangle = 0$$

(Bendat and Piersol, 1973, p. 161), and the smoothed cross-spectral density between them will also be zero, i.e.,

$$\bar{S}_{in_y}(\omega) = \langle I^*(\omega) \cdot N_y(\omega) \rangle = 0 \quad (11)$$

The auto-spectral density of the input series is unaffected by the output noise. However, the auto-spectral density of the output series is given by

$$\begin{aligned}
S_{yy}(\omega) &= Y^*(\omega) \cdot Y(\omega) \\
&= (O(\omega)) + Ny(\omega))^* \cdot (O(\omega)) + Ny(\omega)) \\
&= O(\omega)^* \cdot O(\omega) + O(\omega)^* \cdot Ny(\omega) + O(\omega) \cdot Ny(\omega)^* + Ny(\omega)^* Ny(\omega) \\
&= S_{oo}(\omega) + S_{n_y n_y}(\omega)
\end{aligned}$$

on the assumption that the output noise is orthogonal to the output series.

Thus, our estimate of  $H(\omega)$  given by Eqn. (7) is

$$\bar{H}_d(\omega) = \frac{\bar{S}_{iy}(\omega)}{\bar{S}_{ii}(\omega)} = \frac{\bar{S}_{io}(\omega) + \bar{S}_{in_y}(\omega)}{\bar{S}_{ii}(\omega)} = \frac{\bar{S}_{io}(\omega)}{\bar{S}_{ii}(\omega)} \quad (12)$$

and the estimate of  $H(\omega)$  is the same as for the noise-free case.

However, our estimate of  $H(\omega)$  given by Eqn. (8) is

$$\bar{H}_u(\omega) = \frac{\bar{S}_{yy}(\omega)}{\bar{S}_{yi}(\omega)} = \frac{\bar{S}_{oo}(\omega) + \bar{S}_{n_y n_y}}{\bar{S}_{oi}(\omega)} \quad (13)$$

and this estimate is *upward-biased* in the presence of output noise, hence the subscript “u”.

### Noise on input

When noise exists on the input, as shown in Fig. 3,

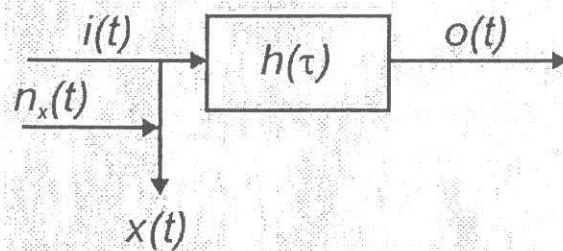


Figure 3: Single-input/single-output with input noise

then the measured input,  $x(t)$ , is the sum of the true input,  $i(t)$ , plus a noise contribution,  $n_x(t)$ . As above, the auto- and cross-spectral densities of the observed quantities are given by:

$$\begin{aligned}
S_{xx}(\omega) &= S_{ii}(\omega) + S_{n_x n_x}(\omega) \\
S_{xo}(\omega) &= S_{io}(\omega) \\
S_{oo}(\omega) &= S_{oo}(\omega)
\end{aligned}$$

Our two estimates of  $H(\omega)$  from Eqns. (7) and (8) are given by:

$$\bar{H}_d(\omega) = \frac{\bar{S}_{xo}(\omega)}{\bar{S}_{xx}(\omega)} = \frac{\bar{S}_{io}(\omega)}{\bar{S}_{ii}(\omega) + \bar{S}_{n_x n_x}(\omega)}$$

and

$$\bar{H}_u(\omega) = \frac{\bar{S}_{oo}(\omega)}{\bar{S}_{ox}(\omega)} = \frac{\bar{S}_{oo}(\omega)}{\bar{S}_{oi}(\omega)}$$

and our estimate  $H_u(\omega)$  is correct, but  $H_d(\omega)$  is *downward-biased* by noise on the input.

### Noise on both input and output

In the general case of there existing noise on both the input and output series, shown by Fig. 4.

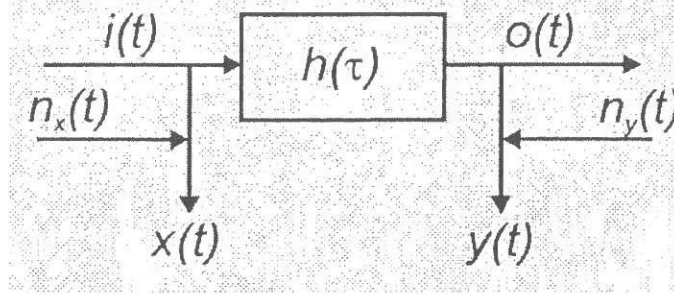


Figure 4: Single-input/Single-output system with noise

then neither estimate given by Eqns. (7) and (8) are unbiased. They are

$$\bar{H}_d(\omega) = \frac{\bar{S}_{xy}(\omega)}{\bar{S}_{xx}(\omega)} = \frac{\bar{S}_{io}(\omega)}{\bar{S}_{ii}(\omega) + \bar{S}_{n_x n_x}(\omega)}$$

and

$$\bar{H}_u(\omega) = \frac{\bar{S}_{yy}(\omega)}{\bar{S}_{yx}(\omega)} = \frac{\bar{S}_{oo}(\omega) + \bar{S}_{n_y n_y}}{\bar{S}_{oi}(\omega)}$$

These *bias-errors* cannot be reduced by averaging

### Remote reference series

To address the bias problems associated with transfer function estimation in the presence of noise, Riersol (1950; see also Akaike, 1967) introduced the concept of *instrumental variables* in economic theory. An instrumental variable is a third time series, other than the observed ones  $x(t)$  and  $y(t)$ , which correlates with the true signals  $i(t)$  and  $o(t)$  but not their respective noise contributions. We shall denote the true instrumental variable by  $a(t)$ , but in the general case, this series is also contaminated by noise, and we observe  $r(t)$ , as shown in Fig. 5.

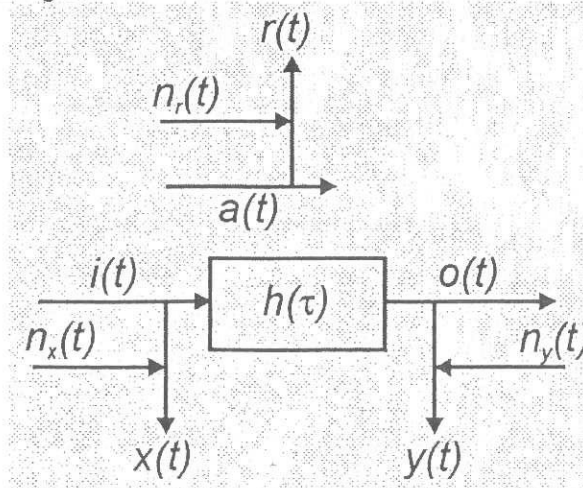


Figure 5: Single-input/Single-output system with instrumental variable

Following from Eqn. (6) above, a least-squares estimate of the transfer function is given by

$$H'(\omega, T) = \frac{\bar{S}_{ao}(\omega, T)}{\bar{S}_{ai}(\omega, T)} \quad (14)$$

On the assumption that all three noise contributions are orthogonal to the three true series and to each other, then our remote-reference estimate of the transfer function, similar to Eqns. (7) and (8), is

$$\begin{aligned} \bar{H}_r(\omega) &= \frac{\bar{S}_{ry}(\omega)}{\bar{S}_{rx}(\omega)} = \frac{\bar{S}_{ao}(\omega) + \bar{S}_{an_y}(\omega) + \bar{S}_{n_r o}(\omega) + \bar{S}_{n_r n_y}(\omega)}{\bar{S}_{ai}(\omega) + \bar{S}_{an_x}(\omega) + \bar{S}_{n_r i}(\omega) + \bar{S}_{n_r n_x}(\omega)} \\ &= \frac{\bar{S}_{ao}(\omega)}{\bar{S}_{ai}(\omega)} \end{aligned}$$

which is an unbiased estimate of Eqn. (14).

This concept of using additional correlated series to yield noise unbiased estimates was introduced into magnetotellurics by Gamble et al. (1979).

### **Ordinary coherence function**

A measure of the noise in the system can be obtained from the coherence between the input ( $x(t)$ ) and output ( $y(t)$ ) series. Coherence is the frequency domain equivalent of the cross-correlation function. The coherence between two series is called an *ordinary coherence function*, and is defined by:

$$\gamma^2_{xy}(\omega) = \frac{|S_{xy}(\omega)|^2}{S_{xx}(\omega) \cdot S_{yy}(\omega)} \quad (15)$$

and is a real number that satisfies  $0 < \gamma^2 < 1$  for all frequencies (Bendat and Piersol, 1973, pp. 79-80). (This parameter is occasionally termed the *magnitude-squared coherency* in the literature.) If the two series are totally uncorrelated, then the coherence function is theoretically zero. If they are totally correlated, the function will be unity. If the function lies between these limits, then one of three conditions exists

1. extraneous noise present in the measurements
2. the system relating  $x(t)$  to  $y(t)$  is not linear, or
3. the output  $y(t)$  is due to other inputs than just  $x(t)$ .

Consider the value of the coherence function in the presence of noise on both input and output, then

$$\begin{aligned} \gamma^2_{xy}(\omega) &= \frac{|S_{xy}(\omega)|^2}{S_{xx}(\omega) \cdot S_{yy}(\omega)} \\ &= \frac{|S_{io}(\omega)|^2}{(S_{ii}(\omega) + S_{n_x n_x}(\omega)) \cdot (S_{oo}(\omega) + S_{n_y n_y}(\omega))} \end{aligned} \quad (16)$$

which is less than unity.

### **Bias in coherence function estimate**

Although the expectation value of the true coherence function between two random series,  $r_1(\omega)$  and  $r_2(\omega)$ , is zero, the expectation value of the estimate of the coherence function is not zero, due to bias. That is

$$E[\gamma^2_{r_1 r_2}] = 0 \quad \text{but} \quad E[\bar{\gamma}^2_{r_1 r_2}] > 0$$

The bias is given by

$$\begin{aligned} B(\bar{\gamma}_{rr_2}^2) &= E[\bar{\gamma}_{rr_2}^2 - \gamma_{rr_2}^2] \\ &= E[\bar{\gamma}_{rr_2}^2] - E[\gamma_{rr_2}^2] \\ &= E[\bar{\gamma}_{rr_2}^2] \end{aligned}$$

(Kendall and Stuart, 1958, p. 51). Hence, the bias of the estimate is given by the expectation value of the estimate. The bias between two normal, ergodic, random series is

$$B(\bar{\gamma}_{rr_2}^2) = \frac{I}{T}$$

where  $I = \int_{-\infty}^{\infty} W^2(\omega) d\omega$ , the integrated squared smoothing window function

and  $T$  = data set length

(Jenkins and Watts, 1968, pp. 396-399). The ratio  $I/T$  is called the variance ratio, and, if the spectrum is smooth with respect to the spectral window, is given by

$$\frac{I}{T} = \frac{2}{n}$$

(Jenkins and Watts, 1968, pp. 252-254), where  $n$  is the number of degrees of freedom associated with the estimate. Hence,

$$E[\bar{\gamma}_{rr_2}^2] = \frac{2}{n}$$

which shows that smoothing over only a few frequencies can yield misleadingly high coherence estimates, even for poorly correlated series.

### Error estimation

In the event that all noise contributions are random, and that the signals are Gaussian, the error in the estimate of the transfer function  $H(\omega)$  is given by a circle in the complex plane, defined by

$$\hat{r}(\omega) \geq |\hat{H}(\omega) - H(\omega)|$$

is given by

$$\hat{r}^2(\omega) = \frac{2}{n-2} F_{2,n-2,\alpha} (1 - \hat{\gamma}_{xy}^2(\omega)) \frac{\hat{S}_{yy}(\omega)}{\hat{S}_{xx}(\omega)}$$

where  $F_{2,n-2,\alpha}$  = 100 $\alpha$  percentage point of an F-distribution.

### Two-input/Single-Output Noise Contaminated Linear System

The magnetotelluric method estimates four transfer functions that relate the two magnetic field components (as inputs) to the two electric field components (as outputs). This linear system can be divided into two separate two-input/single-output linear systems. In the general noise-contaminated case, the system is as in Fig. 6

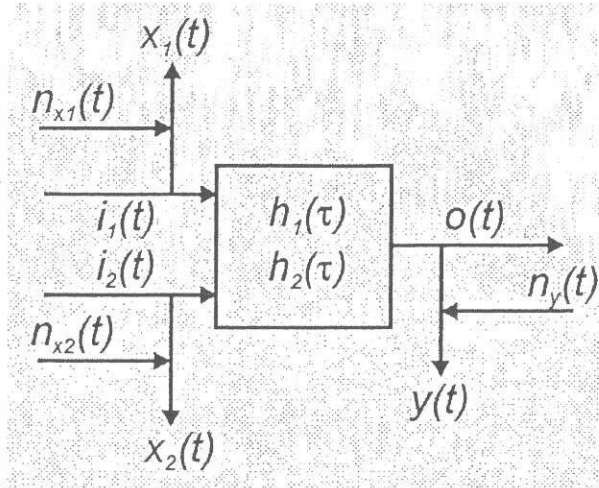


Figure 6: Two-input/Single-output noise contaminated linear system

The impulse response functions in most general noise-contaminated system possible are described by the convolution integral

$$y(t) - n_y(t) = \int_{-\infty}^{\infty} h_1(\tau)(x_1(t-\tau) - n_{x_1}(t-\tau)) d\tau + \int_{-\infty}^{\infty} h_2(\tau)(x_2(t-\tau) - n_{x_2}(t-\tau)) d\tau$$

which, in the frequency domain, is

$$Y(\omega) - N_y(\omega) = H_1(\omega) \cdot (X_1(\omega) - N_{x_1}(\omega)) + H_2(\omega) \cdot (X_2(\omega) - N_{x_2}(\omega)) \quad (17)$$

Multiplying Eqn. (16) by the complex conjugate of the two input series, \$X\_1^\*(\omega)\$ and \$X\_2^\*(\omega)\$, yields two auto- and cross-spectral equations

$$\begin{aligned} S_{1y} &= H_1 \cdot (S_{11} - S_p) + H_2 \cdot S_{12} \\ \text{and} \\ S_{2y} &= H_1 \cdot S_{21} + H_2 \cdot (S_{22} - S_q) \end{aligned} \quad (18)$$

where \$S\_{1y} = S\_{x1y}\$, etc., \$S\_p = S\_{n1n1}\$ and \$S\_q = S\_{n2n2}\$ (dependence on frequency assumed), and it is assumed that the noise series are uncorrelated to any other series. These equations can be solved simultaneously to yield the true transfer function estimates from

$$\begin{aligned} H_1 &= \frac{(S_{22} - S_q)S_{1y} - S_{12}S_{2y}}{(S_{11} - S_p)(S_{22} - S_q) - S_{12}S_{21}} \\ &= \frac{S_{1y} \left[ 1 - \frac{S_{12}S_{2y}}{(S_{22} - S_q)S_{1y}} \right]}{(S_{11} - S_p) \left[ 1 - \frac{|S_{12}|^2}{(S_{11} - S_p)(S_{22} - S_q)} \right]} \end{aligned} \quad (19)$$

(similarly for \$H\_2\$). However, the noise contributions are unknown, so the estimate of \$H\_1\$ is given by

$$\begin{aligned}\bar{H}_1 &= \frac{\bar{S}_{22}S_{1y} - S_{12}S_{2y}}{\bar{S}_{11}\bar{S}_{22} - S_{12}S_{21}} \\ &= \frac{S_{1y} \left[ 1 - \frac{S_{12}S_{2y}}{\bar{S}_{22}S_{1y}} \right]}{\bar{S}_{11} \left[ 1 - \bar{\gamma}_{12}^2 \right]}\end{aligned}$$

As with the single-input/single-output case, the estimate  $\bar{H}_1$  is a downward-biased underestimate of  $H_1$  in the presence of noise on the inputs.

### Multiple coherence function

As with the single-input/single-output case, there are coherences between the various signals. The multiple coherence function is a quantitative measure of how well the output is predicted from the inputs convolved with the estimated impulse response functions. The multiple coherence function is given by

$$\begin{aligned}\gamma_{y12}^2 &= \frac{S_{11}S_{2y}S_{y2} + S_{22}S_{1y}S_{y1} - S_{12}S_{2y}S_{y1} - S_{1y}S_{y2}S_{21}}{S_{yy}S_{11}S_{22} - S_{yy}S_{12}S_{21}} \\ &= \frac{S_{11}|S_{2y}|^2 + S_{22}|S_{1y}|^2 - 2\operatorname{Re}(S_{12}S_{2y}S_{y1})}{S_{yy}S_{11}S_{22}(1 - \gamma_{12}^2)} \\ &= \frac{\gamma_{2y}^2 + \gamma_{1y}^2 - 2\operatorname{Re}(S_{12}S_{2y}S_{y1}) / S_{yy}S_{11}S_{22}}{(1 - \gamma_{12}^2)}\end{aligned}\quad (20)$$

(dependence on frequency assumed) (Jenkins and Watts, 1968, p. 488), where  $y$  denotes the output, and 1 and 2 denote the two inputs. Note the ordinary coherence term in the denominator. In the event that the two input series are perfectly correlated, i.e.,  $\gamma_{12}^2 = 0$ , then the multiple coherence is indeterminable.

### Partial coherence function

If the ordinary coherence functions between either of the inputs and the output,  $\gamma_{12}^2$  and  $\gamma_{21}^2$ , are calculated from Eqn. (15), then their values may be misleadingly high or low. The input series  $x_2(t)$ , when computing  $\gamma_{12}^2$ , appears as a correlating “noise” component at the output,  $y(t)$ . Thus, although there may be either little correlation or a true linear relationship between  $x_1(t)$  and  $y(t)$ , it will be masked by the effect of  $x_2(t)$ . To determine the true coherence between one of the inputs and the output, the effect of the other input must be removed from the output. This is accomplished in a least-squares sense by computing the *partial coherence functions* (Bendat and Piersol, 1972, pp. 153-160). For the two-input/single-output linear system, these two functions are given by

$$\gamma_{y1.2}^2 = \frac{\gamma_{y12}^2 - \gamma_{2y}^2}{1 - \gamma_{2y}^2} \quad \text{and} \quad (21)$$

$$\gamma_{y2.1}^2 = \frac{\gamma_{y12}^2 - \gamma_{1y}^2}{1 - \gamma_{1y}^2}$$

(Jenkins and Watts, 1968, p. 489).

### Bias of multiple and partial coherence function estimates

Similar to the ordinary coherence function case, the estimates of the multiple and partial coherence functions are biased estimates. As the expectation value for three totally uncorrelated series is zero, i.e.,

$E[\gamma_{r3r1r2}^2] = 0$ , then the bias is given directly by the expectation value of the estimate of the coherences. For the multiple coherence function, this is

$$\begin{aligned} E[\bar{\gamma}_{y12}^2] &= E\left[\frac{\bar{\gamma}_{y1}^2 - \bar{\gamma}_{y1}^2 - 2 \operatorname{Re}(\bar{S}_{12}\bar{S}_{2y}\bar{S}_{y1})/\bar{S}_{11}\bar{S}_{22}\bar{S}_{yy}}{1 - \bar{\gamma}_{12}^2}\right] \\ &= \frac{E[\bar{\gamma}_{y1}^2] - E[\bar{\gamma}_{y1}^2] - E[2 \operatorname{Re}(\bar{S}_{12}\bar{S}_{2y}\bar{S}_{y1})/\bar{S}_{11}\bar{S}_{22}\bar{S}_{yy}]}{1 - E[\bar{\gamma}_{12}^2]} \end{aligned}$$

Assuming that the expectation value of the third term in the numerator is small compared to the first two terms, then this reduces to

$$\begin{aligned} E[\bar{\gamma}_{y12}^2] &= \frac{E[\bar{\gamma}_{y1}^2] - E[\bar{\gamma}_{y1}^2]}{1 - E[\bar{\gamma}_{12}^2]} \\ &= \frac{\frac{2}{n} + \frac{2}{n}}{1 - \frac{2}{n}} \\ &= \frac{4}{n-2} \end{aligned} \tag{22}$$

For the partial coherence function, then, from Eqn. (21), the expectation value is given by

$$\begin{aligned} E[\bar{\gamma}_{y1.2}^2] &= \frac{E[\bar{\gamma}_{y12}^2] - E[\bar{\gamma}_{y2}^2]}{1 - E[\bar{\gamma}_{y2}^2]} \\ &= \frac{\frac{4}{n-2} + \frac{2}{n}}{1 - \frac{2}{n}} \\ &= \frac{2n+4}{(n-2)^2} \end{aligned} \tag{23}$$

which reduces to the expectation value for multiple coherence (Eqn. (22)) for  $n$  large.

Note that there are two degrees of freedom for each Fourier coefficient, which is the real and imaginary parts. Thus, averaging over only three coefficients will mean  $n = 6$ , and the expectation value of the multiple and partial coherences is unity even for random series.

### Error estimation

As with the single-input/single-output case, if all noise contributions are random, and that the signals are Gaussian, the error in the estimate of the transfer function  $H_i(\omega)$  is given by a circle in the complex plane, defined by

$$\hat{r}_i(\omega) \geq |\hat{H}_i(\omega) - H_i(\omega)|$$

is given by

$$\hat{r}_i^2(\omega) = \frac{4}{n-4} F_{4:n-4:\alpha} \frac{(1 - \hat{\gamma}_{y12}^2(\omega)) \hat{S}_{yy}(\omega)}{(1 - \hat{\gamma}_{12}^2(\omega)) \hat{S}_i(\omega)}$$

## MT Tensor Estimation

### Conventional single-site estimates

The MT tensor is a 2x2 complex tensor that relates the horizontal components of the magnetic field,  $H_x$  and  $H_y$ , to the horizontal components of the electric field,  $E_x$  and  $E_y$ . Thus, it is a two-input/two-output linear system, and the approaches given above can be applied. Given that there are four series, and any two can be used to form the auto- and cross-spectra, this leads to six possible estimates for each of the four tensor elements.

Sims et al. (1971) list the six possible estimates for  $\bar{Z}_{xy}$ , and they are:

$$\begin{aligned}\bar{Z}_{xy}(ExEy) &= \frac{\bar{S}_{HxEx}\bar{S}_{ExEy} - \bar{S}_{HxEy}\bar{S}_{ExEx}}{\bar{S}_{HxEx}\bar{S}_{HyEy} - \bar{S}_{HxEy}\bar{S}_{HyEx}} \\ \bar{Z}_{xy}(ExHx) &= \frac{\bar{S}_{HxEx}\bar{S}_{ExHx} - \bar{S}_{HxHx}\bar{S}_{ExEx}}{\bar{S}_{HxEx}\bar{S}_{HyHx} - \bar{S}_{HxHx}\bar{S}_{HyEx}} \\ \bar{Z}_{xy}(ExHy) &= \frac{\bar{S}_{HxEx}\bar{S}_{ExHy} - \bar{S}_{HxHy}\bar{S}_{ExEx}}{\bar{S}_{HxEx}\bar{S}_{HyHy} - \bar{S}_{HxHy}\bar{S}_{HyEx}} \\ \bar{Z}_{xy}(EyHx) &= \frac{\bar{S}_{HxEy}\bar{S}_{ExHx} - \bar{S}_{HxHx}\bar{S}_{ExEy}}{\bar{S}_{HxEy}\bar{S}_{HyHx} - \bar{S}_{HxHx}\bar{S}_{HyEy}} \\ \bar{Z}_{xy}(EyHy) &= \frac{\bar{S}_{HxEy}\bar{S}_{ExHy} - \bar{S}_{HxHy}\bar{S}_{ExEy}}{\bar{S}_{HxEy}\bar{S}_{HyHy} - \bar{S}_{HxHy}\bar{S}_{HyEy}}\end{aligned}\tag{24}$$

and

$$\bar{Z}_{xy}(HxHy) = \frac{\bar{S}_{HxHx}\bar{S}_{ExHy} - \bar{S}_{HxHy}\bar{S}_{ExHx}}{\bar{S}_{HxHx}\bar{S}_{HyHy} - \bar{S}_{HxHy}\bar{S}_{HyHx}}$$

(dependency on frequency assumed) where the components in parentheses denotes the two used to construct the auto- and cross-spectra. The first and last of these two,  $Z_{xy}(ExEy)$  and  $Z_{xy}(HxHy)$ , can be recognized as upward-biased and downward-biased estimators equivalent to Eqns. (7) and (8), for noise on the electric and magnetic fields respectively. The others are mixed-bias estimators.

As pointed out by Sims et al. (1971), for a one-dimensional (1-D) Earth with unpolarized incident fields, then the spectral terms  $S_{ExEy}$ ,  $S_{ExHx}$ ,  $S_{EyHy}$ , and  $S_{HxHy}$  tend to zero, so that estimates  $Z_{xy}(ExHy)$  and  $Z_{xy}(EyHx)$  become indeterminant.

Typically in MT application, the electric fields are far noisier than the magnetic fields. This means that estimate  $Z_{xy}(HxHy)$  is both the least-biased and statistically the best.

### Remote-reference estimates

Gamble et al. (1978) introduced the concept of using instrumental variables into magnetotellurics, and termed it the *remote-reference* method. A second MT site records the same (!) MT fields at a sufficient distance from the base site that noise at the base site is uncorrelated with noise at the remote site. The noise can take the form of instrumentation noise, for which the remote site need be only a few metres away, to wind-induced noise, for which the remote needs to be some hundreds of metres away, to cultural disturbances, for which in extreme cases the remote has to be many tens to hundreds of kilometers away.

The remote-reference estimates are given by equations such as the below for  $Z_{xy}$ ,

$$\bar{Z}_{xy}(RxRy) = \frac{\bar{S}_{HxRx}\bar{S}_{ExRy} - \bar{S}_{HxRy}\bar{S}_{ExRx}}{\bar{S}_{HxRx}\bar{S}_{HyRy} - \bar{S}_{HxRy}\bar{S}_{HyRx}} \quad (25)$$

where the remote fields are denoted by  $Rx$  and  $Ry$ . As with single-station tensor estimation, typically the magnetic fields contain less noise than the electric fields, and thus the remote fields used for Eqn. (25) are the remote magnetic fields.

Gamble et al. (1979) undertake an error analysis for remote reference MT, using parametric methods and standard error propagation.

## Robust processing

Through the 1980s a number of robust processing schemes were proposed and developed to optimally derive the MT impedance tensor elements in a manner that is unbiased by outliers.

The earliest was the heuristic scheme of Jones and Jödicke (1984), which appears to be successful in many situations. In this scheme, discussed also in Jones et al. (1989), the ensemble of available estimates from all available combinations of data windowing and remote references are inspected using a *delete-1* iterative approach to try to obtain the best estimates possible. In the original version, the multiple coherence was maximized. Later, Jones found that superior results were obtained from minimizing variance, rather than maximizing coherence. This scheme has been used commercially by Phoenix Geophysics for over 15 years.

In the mid-1980s, Chave (Chave et al., 1987; Chave and Thompson, 1989, 2002) and Egbert (Egbert and Booker, 1986; Egbert, 1997) presented formal robust procedures. Larsen (1989; Larsen et al., 1996) presented a hybrid approach, using some formal aspects of robust estimation but coupling it with “event selection” based on implementing the Hilbert transform relationship.

All four of these codes are available. In the majority of cases, they will return reasonably-alike estimates. In the case of severe noise contributions, then they will perform differently depending on the nature of the noise.

## Analysis Overview

The primary purpose of MT impedance tensor analysis is to determine what the intrinsic *dimensionality* and *directionality* of the tensor are, and how those change with decreasing frequency (increasing period), which is our proxy for depth, and to derive response functions that can be interpreted fully consistently with our assumptions about the Earth.

The observed estimated MT impedance tensor looks like

$$\hat{\mathbf{Z}} = \begin{bmatrix} \hat{Z}_{xx} & \hat{Z}_{xy} \\ \hat{Z}_{yx} & \hat{Z}_{yy} \end{bmatrix}$$

(dependence on frequency assumed).

If the world is 1-D, then the tensor should look like

$$\mathbf{Z}_{1D} = \begin{bmatrix} 0 & Z_{xy} \\ -Z_{xy} & 0 \end{bmatrix}$$

that is, the two estimates of the apparent resistivity curves should lie on top of each other, and the phases should be exactly 180° apart. The XY phase should lie in the first quadrant (0° - 90°), and the YX phase should lie in the third quadrant (-90° - -180°).

If the Earth is 2-D beneath the recording location, then the observed impedance tensor looks like

$$\mathbf{Z}_{obs} = \mathbf{R} \mathbf{Z}_{2D} \mathbf{R}^T$$

where  $\mathbf{R}$  is the Cartesian rotation matrix, and the 2-D impedance tensor is given by

$$\mathbf{Z}_{2D} = \begin{bmatrix} 0 & Z_{xy} \\ Z_{yx} & 0 \end{bmatrix}$$

The primary goal in this case is to derive the appropriate strike angle and to rotate the data into the interpretation reference frame.

If the Earth is fully 3-D, then the MT tensor must be interpreted accordingly.

The useful approximation that has been used over the last decade is to fit a model with near-surface distortion over a body that can be approximated by 2-D. This is the 3D/2D galvanic distortion of the electric fields approach was first introduced by Richards et al. (1982), and has been used by Bahr (1984, 1988), Zhang et al. (1987) and Bailey and Groom (1987; Groom and Bailey 1989, 1991).

### **Properties of the MT impedance tensor**

#### **Rotation**

The Cartesian rotation matrix operates on the impedance tensor to yield rotated versions of each element. In matrix rotation, this is given by

$$\mathbf{Z}(\theta) = \mathbf{R}(\theta) \mathbf{Z}(0) \mathbf{R}(\theta)^T$$

and the elements are

$$Z_{xx}(\theta) = Z_{xx} \cos^2(\theta) + (Z_{xy} + Z_{yx}) \sin(\theta) \cos(\theta) + Z_{yy} \sin^2(\theta)$$

$$Z_{xy}(\theta) = Z_{xy} \cos^2(\theta) + (Z_{yy} - Z_{xx}) \sin(\theta) \cos(\theta) - Z_{yx} \sin^2(\theta)$$

$$Z_{yx}(\theta) = Z_{yx} \cos^2(\theta) + (Z_{yy} - Z_{xx}) \sin(\theta) \cos(\theta) - Z_{xy} \sin^2(\theta)$$

and

$$Z_{yy}(\theta) = Z_{yy} \cos^2(\theta) - (Z_{xy} + Z_{yx}) \sin(\theta) \cos(\theta) + Z_{xx} \sin^2(\theta)$$

These are used below.

#### **Rotational invariants**

From the above rotated forms of the impedance tensor, we can determine that several combinations of impedance tensors are *rotationally invariant*, that is, they have the same value whatever the angle of rotation is.

Consider the sum of the diagonal elements,  $Z_{xx} + Z_{yy}$ . From the above

$$\begin{aligned} Z_{xx}(\theta) + Z_{yy}(\theta) &= Z_{xx} \cos^2(\theta) + (Z_{xy} + Z_{yx}) \sin(\theta) \cos(\theta) + Z_{yy} \sin^2(\theta) \\ &\quad + Z_{yy} \cos^2(\theta) - (Z_{xy} + Z_{yx}) \sin(\theta) \cos(\theta) + Z_{xx} \sin^2(\theta) \\ &= Z_{xx}(\cos^2(\theta) + \sin^2(\theta)) + Z_{yy}(\cos^2(\theta) + \sin^2(\theta)) \\ &= Z_{xx} + Z_{yy} \end{aligned}$$

Similarly, it is possible to show that the difference of the off-diagonal elements,  $Z_{xy} - Z_{yx}$ , is also rotationally invariant.

### **Dimensionality measures**

#### **Amplitude-based measure: Skew**

The first measure of dimensionality was introduced by Swift (1967), in his deservedly renowned and well-read Ph.D. thesis, and is MT *skew*. The skew is defined in the same manner that the skew of any  $2 \times 2$  tensor is defined, namely

$$\text{skew} = \left| \frac{Z_{xx} + Z_{yy}}{Z_{xy} - Z_{yx}} \right|$$

Note from our discussion above that this is rotationally invariant.

In 1-D and 2-D cases, skew should be zero. Large departures from zero were taken in the past as indicators of three-dimensionality. Typically, values below 0.2 were taken to indicate that the responses could be interpreted in a 1-D or 2-D manner.

There are two problems with this. The first is that there is no statistical basis for assuming that a value of 0.2 means that the responses are from a 1-D or 2-D Earth. Measures such as these need to be put into a firm statistical framework with reference to the errors in the data. Second, the amplitudes of the impedance tensor elements can be distorted by static shifts (see below), so one can obtain large values of skew even for 1-D or 2-D Earths due to the local distorting inhomogeneities.

#### **Phase-based measure: Phase sensitive skew**

Bahr's phase sensitive skew.

### **Directionality measures**

If it is considered from dimensionality analysis that the Earth can be validly described by a 2-D model (or at least parts of the data can), then one needs to derive the strike direction consistent with the majority of the data.

#### **Amplitude-based measures**

- rotation to maximize off-diagonal elements ( $Z_{xy}, Z_{yx}$ ) or minimize diagonal elements ( $Z_{xx}, Z_{yy}$ )
- rotation to maximize coherences
- analytical schemes

- Haak's MINMAX method

### **Phase-based measures**

### **Static Shift**

As a consequence of static shifts (Jones, 1988), in 1-D the apparent resistivity curves may be apart, but the phases may be exactly alike (apart from the shift by  $\pi$ ). This case was first studied by Larsen (1977) for distortions on Hawaii due to the ocean. The amplitude shifts of the curves cannot be determined from the data alone, and yield a 1-D model that is incorrect (resistivities scaled by the amount of the shift, and layer depths scaled by the square-root of the shift).

### **References**

- Bahr, K., 1984. Elimination of local 3D distortion of the magnetotelluric tensor impedance allowing for two different phases. *Seventh Wkshp. Electromagnetic Induction in the Earth and Moon*. Ile-Ife, Nigeria, August 15-22.
- Bahr, K., 1988. Interpretation of the magnetotelluric impedance tensor: regional induction and local telluric distortion. *J. Geophys.* **62**: 119-127.
- Bailey, R.C. and R.W. Groom, 1987. Decomposition of the magnetotelluric impedance tensor which is useful in the presence of channeling. Expanded abstracts of the 57th annual international Society of Exploration Geophysicists meeting and exposition, Tulsa, OK, **57**, 154-156.
- Chave, A.D. and Thomson, D.J., 1989. Some comments on magnetotelluric response function estimation. *J. Geophys. Res.*, **94**: 14,215-14,225.
- Chave, A.D., and Thomson, D.J., 2002. Robust, controlled leverage processing of magnetotelluric data, *Geophys. J Internat.*, submitted.
- Chave, A.D., Thomson, D.J. and Ander M.E., 1987. On the robust estimation of power spectra, coherences, and transfer functions. *J. Geophys. Res.*, **92**, 633-648.
- Groom, R.W. and Bailey, R.C., 1989. Decomposition of magnetotelluric impedance tensors in the presence of local three-dimensional galvanic distortion. *J. Geophys. Res.*, **94**: 1913-1925.
- Groom, R.W. and Bailey, R.C., 1991. Analytical investigations of the effects of near-surface three-dimensional galvanic scatterers on MT tensor decomposition. *Geophysics*, **56**: 496-518.
- Egbert, G.D., 1997. Robust multiple-station magnetotelluric data processing. *Geophys. J. Internat.*, **130**, 475-496.
- Egbert, G.D. and Booker, J.R., 1986. Robust estimation of geomagnetic transfer functions. *Geophys. J.R. Astron. Soc.*, **87**: 173-194.
- Jones, A.G., 1988a. Static shift of magnetotelluric data and its removal in a sedimentary basin environment. *Geophysics*, **53**: 967-978.
- Kunetz, G., 1972. Processing and interpretation of magnetotelluric soundings. *Geophysics*, **37**, 1005-1021.
- Larsen, J.C., 1977. Removal of local surface conductivity effects from low frequency mantle response curves. *Acta Geodaeet. Geophys. et Montanist. Acad. Sci. Hung.*, **12**: 183-186.
- Larsen, J.C., 1989. Transfer functions: smooth robust estimates by least-squares and remote reference methods. *Geophys. J. Internat.*, **99**: 645-663.
- Larsen, J.C., Mackie, R.L., Manzella, A., Fiordelisi, A., and Rieven, S., 1996. Robust smooth magnetotelluric transfer functions. *Geophys. J. Internat.*, **124**: 801-819.
- Nabighian, M.N., 1972. The analytic signal of two-dimensional magnetic bodies with polygonal cross section: its properties and use for automated anomaly interpretation. *Geophysics*, **37**, 507-517.

Phx library  
283

- Nabighian, M.N., 1974. Additional comments on the analytic signal of two-dimensional magnetic bodies with polygonal cross section. *Geophysics*, 39,
- Richards, M.L., U. Schmucker, and E. Steveling, 1982. Entzerrung der Impedanzkurven von magnetotellurischen Messungen in der Schwäbischen Alb. In *Protokol über das 9 Kolloquium Elektromagnetische Tiefenforschung* (Abstracts from 9<sup>th</sup> Electromagnetic Deep Sounding Symposium), held in Neustadt, Weinstraße, 22-26 March, 27-40.
- Swift, C.M., 1967. A magnetotelluric investigation of an electrical conductivity anomaly in the south-western United States. *Ph.D. thesis, Dept. Geology Geophys., M.I.T.*, Cambridge, Mass.
- Zhang, P., Roberts, R.G. and Pedersen, L.B., 1987. Magnetotelluric strike rules. *Geophysics*, 52: 267-278.



# Magnetotellurics for Natural Resources

## From Acquisition through Interpretation

SEG  
October 5&6, 2002  
Salt Lake City

Presented by:  
Karen R. Christopherson, Chinook Geoconsulting, Inc.  
Alan Jones, Geological Survey of Canada  
Randall Mackie, GSY-USA

## MT Short Course

### Day 1:

1. Introduction
2. History of MT
  - a. Formulation of the technique
  - b. First field trials
  - c. Developments over the past few decades
3. Theory
  - a. Maxwell's Equations
  - b. Source fields
  - c. Signal strengths
  - d. Tensor components
  - e. Various computed parameters
4. Acquisition
  - a. Equipment
  - b. Noise sources
  - c. Good field practices

### Day 2:

1. Processing
  - a. Standard
  - b. Robust schemes
  - c. Decomposition techniques
2. Interpretation
  - a. Review of data parameters (dimensionality, strike, good vs. bad data, cultural noise)
  - b. Selection of TE/TM modes
  - c. 1D forward and inverse modeling
  - d. 2D forward and inverse modeling
  - e. 3D inversion
3. Applications and Case Histories

Co-teachers with Karen R. Christopherson

Randall Mackie, Geosystem  
Alan Jones, Geol. Survey of Canada

## **1 MAGNETOTELLURICS - MT**

### **1.1.1 Definition**

The magnetotelluric technique is a passive surface measurement of the Earth's electric and magnetic fields, in the time domain, used to infer the electrical resistivity structure of the subsurface.

### **1.1.2 Application of Magnetotellurics to Resource Exploration**

Resistivity Contrasts Essential

In general, lateral and/or vertical resistivity contrasts in the subsurface are essential for MT to be an effective exploration tool. Fortunately there are many geologic environments where such contrasts are present, and knowledge of their structure provides useful information for interpretation of subsurface geology. There are two broad classes of application of MT to exploration: (1) large scale regional reconnaissance, and (2) detail surveys.

#### **Reconnaissance Applications**

Regional reconnaissance can be subdivided into (a) detection of sedimentary basins beneath cover and (b) general regional structural interpretation for siting detailed surveys. These surveys are typically done on a grid with 2 to 6 kilometer station spacing.

#### **Detail Application**

Detail surveys are those where the acquisition is targeted for mapping the specifics of a resource. Examples would be

- Mapping aquifers
- Mapping mineralized zones
- Defining petroleum traps (structural or stratigraphic)
- Mapping geothermal horizons

These types of surveys are typically done as profiles or grids with 0.1 to 1 kilometer station spacing.

## **2 Brief History of Development of MT Technique**

### **Milestones in MT Technology - Early**

The invention of the MT technique is credited jointly to Tikhonov, 1950, and Cagniard, 1953. However, Cagniard was the first to actually perform scalar field measurements (1956).

Scalar measurements do not take into account variations with azimuth in the natural induced electromagnetic field. The tensor MT method was proposed by Cantwell, 1960, at MIT. This approach defines and measures a tensor relationship between the electric and magnetic fields at the earth's surface. This accommodates the sometimes large variations in the fields with azimuth.

Development of a commercial tensor MT system was undertaken by GeoScience, Inc. in 1966, under the sponsorship of several major U.S. oil companies. The first field survey contract services were subsequently offered in 1968.

As more powerful computers were developed in the late 1960's, it became practical to do quantitative modeling of MT field data. A one-dimensional direct inversion algorithm, for scalar MT data, was developed by Wu, 1969. A two-dimensional network analogy forward modeling algorithm was developed by Madden and Swift, 1969.

#### Milestones in MT Technology - Recent

The MT technique did not become useful, on a practical basis, for exploration until the 1980's. Several developments were responsible for this. First came an understanding of the mechanisms of three-dimensional effects in MT data, along with the development of a practical three-dimensional modeling algorithm by Hohmann, 1975. Then there was the development of (a) real-time data processing by Wight and Bostick, 1977, (b) a two-dimensional direct inversion algorithm by Jupp and Vozoff, 1977, and (c) the remote reference noise reduction technique by Gamble, 1978.

The first offering of state-of-the-art real-time remote reference data acquisition contract services by Woodward-Clyde Consultants in 1980, marked the beginning of industry wide application to petroleum exploration. The first commercial backpack/helicopter portable system became available from Phoenix Geophysics in 1982.

The 1990's saw the production of 24-bit A-to-D acquisition units. The increase in bandwidth provided for better S/N ratio and less problems with saturation in the instrumentation. The new systems also took advantage of GPS for synchronization between stations. This made MT acquisition more flexible as stations no longer needed to be hardwired together. Other advances, such as increased computing power, robust processing and improvements to modeling codes, have meant that MT data are higher in quality and more readily interpreted.

## Magnetotelluric Theory

Alan G. Jones

Geological Survey of Canada

### Magnetotelluric Overview

The magnetotelluric (MT) method uses the time-varying Earth's electromagnetic (EM) field as its source, and depth penetration from a few hundred metres to about 200 km is generally assured. At high frequencies (about 8 Hz and higher), the EM fields penetrate typically to about mid-crustal depths. These variations are caused by distant lightning storms, perhaps half the globe away. The time variations at deep-crustal and mantle-probing depths are caused by the interaction of the solar plasma with the Earth's magnetosphere - the most visible form of this interaction is the *northern lights*. The EM energy from both of these sources is trapped within the Earth-ionosphere waveguide.

By Faraday's Law of Induction, this varying magnetic field induces an electric current within the Earth, and by Ohm's Law this current generates an electric (called "telluric") field. The strength of the electric field is dependent on the conductivity of the medium and the strength of the inducing source magnetic field. Hence, by observing the magnetic and electric fields simultaneously, and determining their ratios at varying frequencies (equivalent to depths by the skin depth phenomenon), one can derive the conductivity variation with both depth and distance.

It can be shown that for a one-dimensional (1-D) Earth, i.e., an Earth in which the conductivity varies with depth alone, when one has perfect data at all frequencies then there exists only one model that will fit the data (Bailey, 1970; Weidelt, 1972). This uniqueness property separates EM generally, and MT in particular, from other potential field methods, such as gravity and magnetics, where non-uniqueness is an inherent property. It is, of course, never possible to obtain perfect data, but the existence of this uniqueness theorem drives MT people to make more and more accurate and precise estimates of the Earth responses by improving instrumentation, processing and analysis methods.

On the surface of the Earth, one measures the time variations of the three components of the magnetic field ( $H_x$ ,  $H_y$  and  $H_z$ ), and the two horizontal components of the Earth's electric field ( $E_x$  and  $E_y$ ). An example of their variation over a twenty-four hour period is shown in Figure 1 from a site in northern Canada near Yellowknife for 12th January, 1997 (UT). Local magnetic midnight (based on geomagnetic coordinates, rather than geographic ones) at Yellowknife is at approximately 09:00 UT (01:00 local time), when there is a strong negative excursion of  $H_x$ . Two hours later is a substorm event rich in long period activity, followed by high signal activity at shorter periods.

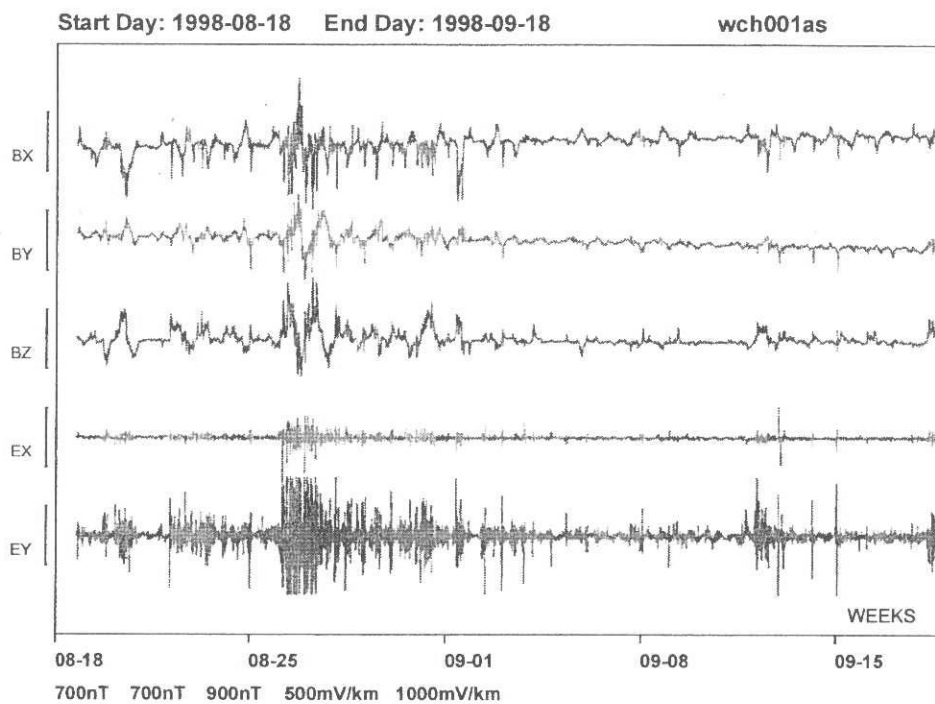


**Figure 1.** Typical magnetotelluric time series. Shown are the time variations of one month of data recorded at an MT site close to Rankin Inlet, northern Canada. The scale represent 700 nT, 700 nT, 900 nT, 500 mV/km and 1000 mV/km for Hx, Hy, Hz, Ex and Ey respectively.

There are two frequency bands that are problem areas for MT data acquisition. The most well-known one is the so-called *MT dead band*, and is at frequencies between about 0.1 – 10 Hz. Not only is there low signal at these frequencies – which are the cross-over frequencies between lightning-induced energy and ionospheric-induced energy – but also there is a natural maximum in the near-surface microseismic noise due to coupling of the wind with the ground. This low signal and high noise needs to be combated with overnight acquisition and extra effort with sensor installation. The other problem occurs at frequencies around 1 kHz – 5 kHz, and is the so-called *AMT dead band*, for audio-MT. The energy from distant lightning storms comes from cloud-to-stratosphere at about 10 Hz – 1 kHz frequencies, and cloud-to-ground at 5 kHz – 100 kHz and higher frequencies. There is a natural minimum in energy at 1 kHz – 5 kHz due to this.

These minima undergo diurnal, seasonal and solar-cycle variation. In particular, during the sunlit daytime there is absorption of the EM energy by the photo-ionized atmospheric particles. Propagation is far more efficient during the nighttime. The AMT dead band is so deep during the daytime, that the magnetic signals are estimated to be two orders of magnitude smaller in amplitude than the noise levels of the currently best available coil sensors (Garcia and Jones, 2002). This means that AMT sounding for mineral exploration yields the broadest spectrum with overnight acquisition.

## Theory of Magnetotelluric Sounding

### *Maxwell's equations*

No treatise on electromagnetism (EM) could be complete without including the founding principles of EM, which are Maxwell's equations, and a brief explanation of them. In a uniform medium, they are:

$$\operatorname{div} \mathbf{B} = 0 \quad \text{Gauss' Law for magnetic field} \quad (1.1)$$

$$\operatorname{div} \mathbf{D} = q \quad \text{Gauss' Law for electric field} \quad (1.2)$$

$$\operatorname{curl} \mathbf{E} = -\partial \mathbf{B} / \partial t \quad \text{Faraday's Law} \quad (1.3)$$

$$\operatorname{curl} \mathbf{H} = \mathbf{J} + \partial \mathbf{D} / \partial t \quad \text{Ampere's Law with Maxwell's Term} \quad (1.4)$$

plus the constitutive relationships:

$$\mathbf{B} = \mu \mathbf{H}, \quad \mathbf{D} = \epsilon \mathbf{E}, \quad \mathbf{J} = \sigma \mathbf{E} \quad (2)$$

where  $q$  is the electric charge density (the amount of charge per unit volume),  $\sigma$  is the electrical conductivity,  $\epsilon$  is the electric permittivity,  $\mathbf{J}$  is the electric current density (the rate at which charge flows through a unit area per second), and  $c$  is the speed of light. These four elegant formulae, describing the complete classical theory of the interactions between the vector electric ( $\mathbf{E}$ ) and magnetic ( $\mathbf{H}$ ) fields, were derived by James Clerk Maxwell and published in his renowned *Treatise on Electricity and Magnetism* in 1873. Maxwell was a brilliant man, and the first to realize that light comprises electromagnetic waves.

The two mathematical operators, *div* and *curl*, operate on vector fields. The *div*, short for *divergence*, of a vector at a point  $P$  is the integral (sum) of the outgoing flux (flow) of the vector in the neighbourhood of  $P$ . The *curl*, short for *circulation*, of a vector is the integral of the tangential component of the vector along a defined path. These odd names come from the attention during the mid-1800s on the flow of fluids.

Gauss' Law (Johann Carl Friedrich Gauss, 1777-1855) for magnetic fields states that the net flux of magnetic field lines through a closed surface must be zero, i.e., if you have a bag of magnetic poles, then the lines of magnetic field force leaving the bag must be the same as those entering the bag. This means that there cannot be any magnetic monopoles - there must be as many "north" magnetic poles inside the bag as "south" magnetic poles. Gauss' Law for electric fields states that the electric field is proportional to the net charge, i.e., if you have a bag of electric charges, then the net lines of electric field force leaving the bag is proportional to the net charge inside (positive minus negative charges).

Faraday's Law of Induction (Michael Faraday, 1791 - 1867) states that electric field is generated by a time-changing magnetic field. Faraday was not a theoretician like many of his contemporaries, but an experimentalist. Many scientists knew by the 1820s that there was some relationship between magnetism and electricity, but it was Faraday who realized in 1839 that to "generate", or induce, an electric field, the magnetic field had to be moving in time.

Ampère's Law (André-Marie Ampère, 1775-1836), the first term in the last equation, relates the magnetic field to static current flow, which is  $\sigma E$ , i.e., a current flowing in a wire produces a

magnetic field. Ampère explained Oersted's 1821 observation that a current flowing through a wire deflects a compass needle.

However, these four laws, of Gauss, Faraday and Ampère, are not internally consistent. Electric charge is not conserved. It was Maxwell who recognized that there had to be another term added to Ampère's Law to unify the equations for magnetic and electric fields. This term relates to the time-varying electric field, and leads to what are called *displacement currents*.

Thus, in English, Maxwell's Equations say

$$(\text{Flux of } \mathbf{B} \text{ through a closed surface}) = 0$$

$$(\text{Flux of } \mathbf{D} \text{ through a closed surface}) = (\text{Charge inside})$$

$$(\text{Line integral of } \mathbf{E} \text{ around a loop}) = -d/dt (\text{Flux of } \mathbf{B} \text{ through the loop})$$

$$(\text{Integral of } \mathbf{H} \text{ around a loop}) = (\text{Current through the loop})$$

$$+ d/dt (\text{Flux of } \mathbf{D} \text{ through the loop})$$

(Feynman, 1964). Maxwell unified electricity and magnetism into an electromagnetic theory. When calculating the speed of these electromagnetic waves in 1862, Maxwell found that they flowed at close to the speed of light. He then drew the astounding conclusion that light was comprised of electromagnetic waves!

*We can scarcely avoid the conclusion that light consists in the transverse undulations of the same medium which is the cause of electric and magnetic phenomena.*

Einstein said of Maxwell that his work resulted in the most profound change in the conception of reality in physics since the time of Newton.

Another important relationship in EM studies, called a constitutive equation, is Ohm's Law (Georg Simon Ohm, 1798-1854). The most common form of this law is  $V = I R$ , the electromotive force is given by the current times the resistance in the wire. In terms of current density,  $\mathbf{J}$ , it can be written as

$$\mathbf{J} = \sigma \mathbf{E}$$

Ohm's Law

which has significant implications for charge accumulation at a boundary (see below).

As well as these formulae that govern how EM waves travel through a uniform medium, there are conditions that must be met by the EM fields at the boundary where two media of differing conductivity are in contact. These boundary conditions specify that the normal component of the current density,  $J_n$ , the normal component of the magnetic field,  $B_n$ , and the transverse

component of the electric field,  $E_t$ , must all be continuous, i.e., they must be of the same value immediately on either side of the boundary.

### Electromagnetic Propagation

Recasting Faraday's and Ampère-Maxwell Laws using the constitutive equations and the time dependence ( $\exp(-i\omega t)$ ) of the fields gives:

$$\begin{aligned} \text{curl } \mathbf{E} &= -\partial \mathbf{B} / \partial t \\ &= i\omega\mu\mathbf{H} \end{aligned} \quad (3.1)$$

$$\begin{aligned} \text{curl } \mathbf{H} &= \mathbf{J} + \partial \mathbf{D} / \partial t \\ &= (\sigma + i\omega\epsilon)\mathbf{E} \end{aligned} \quad (3.2)$$

Taking the *curl* of both of these equations, and substituting, gives:

$$\begin{aligned} \text{curl curl } \mathbf{E} &= i\omega\mu \text{curl } \mathbf{H} \\ &= i\omega\mu(\sigma + i\omega\epsilon)\mathbf{E} \end{aligned} \quad (4.1)$$

$$\begin{aligned} \text{curl curl } \mathbf{H} &= (\sigma + i\omega\epsilon)\text{curl } \mathbf{E} \\ &= (\sigma + i\omega\epsilon)i\omega\mu\mathbf{H} \end{aligned} \quad (4.2)$$

Using the vector identity

$$\text{curl curl } \mathbf{F} = -\nabla^2 \mathbf{F} + \text{grad div } \mathbf{F}$$

and that, in a source-free medium (no charges), the divergence of both the  $\mathbf{B}$  and  $\mathbf{E}$  fields is zero, then the equations are in the form of the vector Helmholtz differential equation (an elliptical partial differential equation)

$$\nabla^2 \mathbf{F} - k^2 \mathbf{F} = 0$$

(dependence on frequency assumed) where  $k$  is the propagation constant in the medium and is given by

$$\begin{aligned} k^2 &= i\omega\mu\sigma - \omega^2\mu\epsilon \\ &= \omega\mu(i\sigma - \omega\epsilon) \end{aligned}$$

where  $\sigma$ ,  $\mu$  and  $\epsilon$  are the uniform conductivity, permeability and permittivity of the medium, and  $\omega$  is the radian frequency.

At the very low EM frequencies of <20 kHz used in magnetotellurics, mathematical treatment of the penetration of the electromagnetic (EM) fields into the Earth can be simplified by

considering only the term describing the diffusion of the EM fields ( $\omega\mu\sigma$ ) and neglecting the wave propagation term ( $\omega^2\mu\epsilon$ ). The former describes the flow of *conduction currents* within the medium, whereas the latter describes the *displacement currents*, first identified by Maxwell in the 1860s. Although it is convenient mathematically to drop the wave propagation term, it still exists physically, even though its effects are small. Without it, electric and magnetic waves would not be coupled as waves.

For this to be valid, the ratio of  $\sigma$  to  $\omega\epsilon$  must be large. The worst case is for very low conductivity shield rocks ( $\sigma$  of  $10^{-5}$  S/m) at high frequencies (10 kHz), but such rocks have very low permittivities.

Given the low magnetic susceptibilities ( $k$ ) of most Earth materials, one can replace  $\mu$  ( $\mu=\mu_0(1+k)$ ) with the free-space value,  $\mu_0$ , which, in S.I. units, is  $4\pi \cdot 10^{-7}$  H/m (Henry/metres). Thus, the physical parameter dominantly being sensed in a low frequency geophysical electromagnetic experiment is electrical conductivity, and its lateral and vertical variation within a volume of physical dimension given by an inductive scale length at exciting frequency  $\omega$ .

Thus, the wave propagation term,  $k$ , reduces to

$$k^2 = i\omega\mu_0\sigma \quad (5)$$

and the vector Helmholtz equation reduces to a diffusion equation

$$\nabla^2 \mathbf{F} - i\omega\mu_0\sigma \mathbf{F} = 0 \quad (6)$$

that describes the diffusion of EM fields into the medium.

The scalar forms of Eqns. 3.1 and 3.2 (dropping the displacement currents term) for the electric field in the  $x$ -direction ( $E_x$ ) and the magnetic field in the  $y$ -direction ( $H_y$ ) are:

$$dE_x/dz = i\omega\mu_0H_y \quad (7.1)$$

$$dH_y/dz = -\sigma E_x \quad (7.2)$$

(the negative sign on Eqn. 7.2 is to have a consistent right-hand rule). Differentiating with respect to depth,  $z$ , yields

$$\begin{aligned}
 d^2 E_x / dz^2 &= i \omega \mu_0 d H_y / dz \\
 &= -i \omega \mu_0 \sigma E_x \\
 &= -i k^2 E_x
 \end{aligned} \tag{8.1}$$

$$\begin{aligned}
 d^2 H_y / dz^2 &= -\sigma d E_x / dz \\
 &= -i \omega \mu_0 \sigma H_y \\
 &= -i k^2 H_y
 \end{aligned} \tag{8.2}$$

Solutions to Eqns. 8.1 and 8.2 are in the form:

$$E_x = A \exp(-ikz) + B \exp(ikz) \tag{9.1}$$

$$H_y = \frac{k}{\omega \mu_0} (A \exp(-ikz) - B \exp(ikz)) \tag{9.2}$$

where the first terms in the two equations describe electric and magnetic horizontal fields that decrease in amplitude with depth (downward-traveling waves), whereas the second terms describe fields that increase with depth (upward-traveling, i.e., reflected, waves).

### Uniform Half-Space

Following from the field equations valid for propagation in a uniform space, Eqns. 9.1 and 9.2, we can see that for a uniform half space then the (complex-valued) *impedance* within the medium is given by:

$$Z_{xy}(\omega) = \frac{E_x(\omega)}{H_y(\omega)} = \frac{\omega \mu_0}{k} \tag{10}$$

Similar to DC resistivity, one can scale the magnitude-squared of the impedance to give an *apparent resistivity* by

$$\begin{aligned}
 \rho_{a,xy}(\omega) &= \frac{1}{\omega\mu_0} \left| \frac{E_x(\omega)}{H_y(\omega)} \right|^2 \\
 &= \frac{1}{\omega\mu_0} \left| \frac{\omega\mu_0}{k} \right|^2 = \frac{\omega\mu_0}{|k|^2} \\
 &= \frac{1}{\sigma} = \rho
 \end{aligned}$$

which is the true resistivity of the half space at all frequencies. The phase can be shown also to be frequency independent, and is 45°.

### Skin Depth

In a uniform medium, a measure of inductive scale length is given by the *skin depth*,  $\delta$ , which is the distance by which the exponentially decaying amplitude becomes  $1/e$ 'th (37%) of its surface value, given by:

$$\delta(\omega) = \sqrt{\frac{2}{\omega\mu_0\sigma}} \quad (\text{m}) \quad (14)$$

which reduces to

$$\delta(\omega) \approx 0.5 \sqrt{\rho T} \quad (\text{km})$$

for  $\mu = \mu_0$ , and where  $\rho$  is the electrical resistivity (in  $\Omega \cdot \text{m}$ ), given by  $1/\sigma$ , and  $T$  is the period of oscillation (in s), given by  $2\pi/\omega$ . Accordingly, with electromagnetic methods theoretically penetration to all depths is assured from the skin depth phenomenon - one merely needs to measure at lower and lower frequency (longer and longer period) to probe deeper and deeper into the Earth.

A representation of this phenomenon is shown in Figure 2 for a schematic 2-layer Earth. High frequencies (short periods) only penetrate shallowly to the surface, and thus give information about the conductivity of the top layer ( $\sigma_1 = 1/\rho_1$ ), whereas low frequencies (long periods) pass through the top layer virtually without any effects, and give information about the conductivity of the base layer ( $\sigma_2 = 1/\rho_2$ ). In a time-domain EM system, these two are equivalent to the early-time and late-time responses respectively. The frequencies (or times) at which the EM response changes from seeing the top layer to seeing the base layer gives information about the thickness of the top layer ( $h_1$ ).

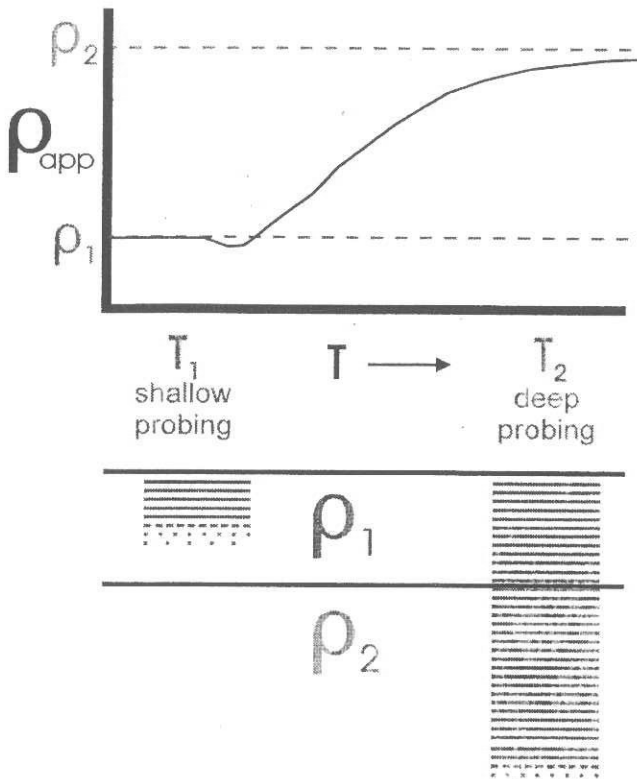


Figure 2: Skin depth phenomenon

## Two-layered Earth

Consider an Earth comprising two layers, the upper one of conductivity  $\sigma_1$  (resistivity  $\rho_1$ ) and thickness  $h$ , and the lower layer of conductivity  $\sigma_2$  (resistivity  $\rho_2$ ), and of infinite depth extent. As described above, at sufficiently high frequencies (short periods), the penetration depth is less than  $h_1$ , so the Earth seems like a uniform half space, and the apparent resistivity is the true resistivity of the top layer. At sufficiently long periods (low frequencies), the EM fields pass through the top layer without being modified, and so the apparent resistivity monotonically approaches  $\rho_2$ .

From Eqn. 9.1, the horizontal electric fields in the two layers are given by:

$$E_x(z) = A_1 \exp(-ik_1 z) + B_1 \exp(ik_1 z) \quad \text{for } z < h \quad (15.1)$$

$$E_x(z) = A_2 \exp(-ik_2 z) \quad \text{for } z > h \quad (15.2)$$

(dependence on frequency assumed) where  $k_1$  and  $k_2$  are the propagation (diffusion) coefficients in the two layers, given by Eqn. 5. Note that there are both downward ( $A_1$ ) and upward ( $B_1$ ) traveling waves in the upper layer, but only downward ( $A_2$ ) traveling waves in the lower layer. Similar expressions can be written for the orthogonal horizontal magnetic field,  $H_y$ , in the two layers following Eqn. 9.2:

$$H_y(z) = \frac{k_1}{\omega\mu_0} (A_1 \exp(-ik_1 z) - B_1 \exp(ik_1 z)) \quad \text{for } z < h \quad (16.1)$$

$$H_y(z) = \frac{k_2}{\omega\mu_0} (A_2 \exp(-ik_2 z)) \quad \text{for } z > h \quad (16.2)$$

The impedance at any depth is given by Eqn. (13),  $Z_{xy}(z) = E_x(z)/H_y(z)$ , and is, in layers 1 and 2:

$$Z_{1,xy}(z) = \frac{\omega\mu_0}{k_1} \left( \frac{A_1 \exp(-ik_1 z) + B_1 \exp(ik_1 z)}{A_1 \exp(-ik_1 z) - B_1 \exp(ik_1 z)} \right) \quad \text{for } z < h \quad (17.1)$$

$$Z_{2,xy}(z) = \frac{\omega\mu_0}{k_2} \left( \frac{A_1 \exp(-ik_1 z)}{A_1 \exp(-ik_1 z)} \right) = \frac{\omega\mu_0}{k_2} \quad \text{for } z > h \quad (17.2)$$

and note that the impedance in the lower layer is the same as the impedance for a half-space. The lower layer is unaffected by anything above it. The surface impedance is given by:

$$Z_{1,xy}(0) = \frac{\omega\mu_0}{k_1} \left( \frac{A_1 + B_1}{A_1 - B_1} \right) \quad (18)$$

and we require knowledge of the propagation terms,  $A_1$  and  $B_1$ , to determine this value.

The general expression for the impedance in the upper layer can be re-written in terms of hyperbolic sines and cosines,

$$\cosh(x) = \frac{1}{2}(\exp(x) + \exp(-x))$$

$$\sinh(x) = \frac{1}{2}(\exp(x) - \exp(-x))$$

by dividing both the numerator and denominator by  $\sqrt{(A_1 B_1)}$ ,

$$Z_{1,xy}(z) = \frac{\omega\mu_0}{k_1} \left( \frac{\sqrt{\frac{A_1}{B_1}} \exp(-ik_1 z) + \sqrt{\frac{B_1}{A_1}} \exp(ik_1 z)}{\sqrt{\frac{A_1}{B_1}} \exp(-ik_1 z) - \sqrt{\frac{B_1}{A_1}} \exp(ik_1 z)} \right) \quad \text{for } z < h \quad (19)$$

Using the identity  $\sqrt{(A_1 B_1)} = \exp(\ln(\sqrt{(A_1 B_1)}))$ , then we have

$$\begin{aligned}
 Z_{1,xy}(z) &= \frac{\omega\mu_0}{k_1} \begin{cases} \frac{\exp(\ln \sqrt{\frac{A_1}{B_1}} - ik_1 z) + \exp(-\ln \sqrt{\frac{A_1}{B_1}} + ik_1 z)}{\exp(\ln \sqrt{\frac{A_1}{B_1}} - ik_1 z) - \exp(-\ln \sqrt{\frac{A_1}{B_1}} + ik_1 z)} & \text{for } z < h \\ \frac{\cosh(\ln \sqrt{\frac{A_1}{B_1}} - ik_1 z)}{\sinh(\ln \sqrt{\frac{A_1}{B_1}} - ik_1 z)} & \text{for } z < h \end{cases} \\
 Z_{1,xy}(z) &= \frac{\omega\mu_0}{k_1} \frac{\cosh(\ln \sqrt{\frac{A_1}{B_1}} - ik_1 z)}{\sinh(\ln \sqrt{\frac{A_1}{B_1}} - ik_1 z)} = \frac{\omega\mu_0}{k_1} \coth\left(\ln \sqrt{\frac{A_1}{B_1}} - ik_1 z\right) \quad (20)
 \end{aligned}$$

We obtain this from using the continuity conditions on the electric and magnetic fields at the interface (i.e.,  $z = h$ ), which require that the fields be the same, and so the impedances must be the same. Thus, from Eqns. (17.2) and (20)

$$Z_{xy}(h) = \frac{\omega\mu_0}{k_1} \coth\left(\ln \sqrt{\frac{A_1}{B_1}} - ik_1 h\right) = \frac{\omega\mu_0}{k_2} \quad (21)$$

Thus,

$$\left( \ln \sqrt{\frac{A_1}{B_1}} \right) = \coth^{-1}\left(\frac{k_1}{k_2}\right) - ik_1 h$$

and the impedance on the surface is given by substituting this expression into (20) for  $z=0$ ,

$$\begin{aligned}
 Z_{1,xy}(0) &= \frac{\omega\mu_0}{k_1} \coth\left(\coth^{-1}\left(\frac{k_1}{k_2}\right) - ik_1 h\right) \\
 Z_{1,xy}(0) &= \frac{\omega\mu_0}{k_1} \coth\left(\coth^{-1}\left(\frac{k_1 Z_{2,xy}(h)}{\omega\mu_0}\right) - ik_1 h\right) \quad (22)
 \end{aligned}$$

and in the second form the equation for the surface impedance is cast as a recurrence equation involving the impedance at the interface ( $z=h$ ).

## Multi-Layered Earth

For multiple layers, the recurrence equation is extended by substitution. The impedance in each layer is a function of the conductivity of that layer, and the parameters (conductivity and thickness) of the layers below.

From the ratios of any two field components in the frequency domain, one can define a complex impedance,  $Z_{xy}(\omega)$ , at radial frequency  $\omega$  between e.g. the northward -directed electric field  $E_x(\omega)$  and the perpendicular eastward-directed magnetic field component  $H_y(\omega)$ , from

$$Z_{xy}(\omega) = \frac{E_x(\omega)}{H_y(\omega)} \quad (10)$$

and the S.I. units of  $Z$  are ohms. The ratios of the powers of the fields can be scaled as an *apparent resistivity*, akin to DC resistivity exploration,

$$\rho_{a,xy}(\omega) = \frac{1}{\omega\mu_0} \left| \frac{E_x(\omega)}{H_y(\omega)} \right|^2 \quad (11)$$

and the phase lead of the electric field over the magnetic field is given by

$$\varphi_{xy}(\omega) = \tan^{-1} \left( \frac{E_x(\omega)}{H_y(\omega)} \right) \quad (12)$$

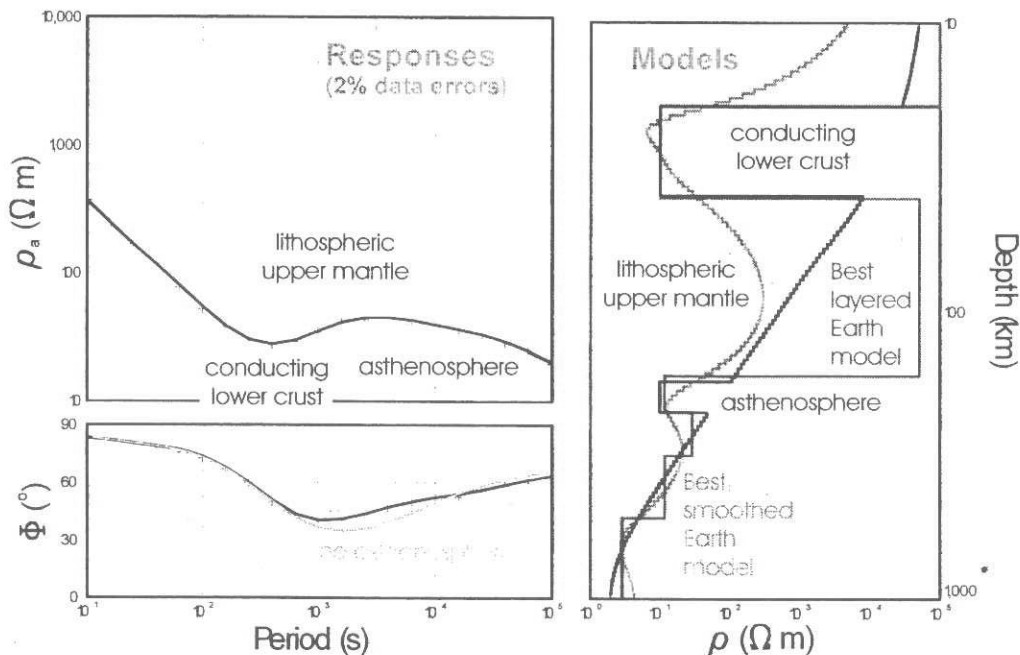


**Figure 3.** Synthetic data (with 2% scatter and error) generated from a theoretical reference model containing a lower crustal conductor and an asthenospheric zone (heavy line). The two

other models, one a smooth inversion and the other a 7-layer inversion, fit the synthetic data to an RMS of 1.0. The fourth response is for a model without an asthenospheric layer.

For a multi-layered Earth, the two parameters vary with frequency, and their variation with frequency can be inverted to reveal the structure. Figure 3 shows the MT responses for four 1D models. One model has no crustal conductor, nor an electrical asthenosphere (dashed line), whereas the others have both. The short periods (typically  $<1,000$  s) are sensing the crust, whereas the longer periods (typically  $>1,000$  s) sense the mantle lithosphere, asthenosphere, and below.

### Multi-Dimensional Earth

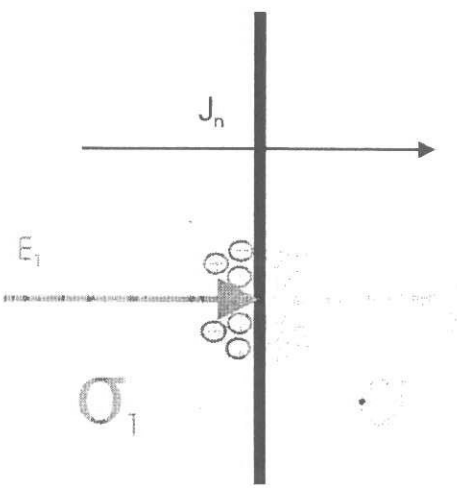
Since the mid-1960s methods have been developed for treating a more complex Earth in which the electrical conductivity varies horizontally as well as vertically. When the geological structures are relatively long compared to their width, then *two-dimensional* (2-D) approaches can be used. In 2-D then the equations decouple into two different modes of propagation. In one mode, electric currents are flowing parallel to the strike of the structures, and is termed the *transverse-electric* (TE) mode (also *E-polarization* and *E-parallel* is used). The other mode describes currents crossing the structures, and is called the *transverse-magnetic* (TM) mode (also *B-polarization*, *H-polarization*, and *E-perpendicular*). The appropriate MT methods are still being developed in areas where the complexity is fully *three-dimensional* (3D). In some cases restricted 2D interpretation of the 3D data may be valid.

When there are discontinuities in electrical conductivity, then there will be charges generated on those boundaries. This can be seen from consideration of Ohm's Law (above), where  $\mathbf{J} = \sigma \mathbf{E}$ , and the boundary condition requiring that  $J_n$  be continuous. As  $J_n = \sigma E_n$ , then at a contact between two media of differing conductivity,  $\sigma_1$  and  $\sigma_2$  (Figure 4), for  $J_n$  to be continuous  $E_n$  must be discontinuous. This is accomplished through charges on the surface which deflect electric field away. These charges do not exist in 1D, only in the TM-mode in 2D and in 3D.

**Figure 4.** Ohm's Law. At a boundary the normal current density must be continuous, and so the electric fields must have different amplitudes on either side of the boundary.

MORE TEXT AND MATHS HERE ABOUT

- 1) 2-D CASE
- 2) SKEW AND OTHER INVARIANTS



$$\sigma_1 >$$

## References

- Bailey, R.C., 1970. Inversion of the geomagnetic induction problem. *Proc. Roy. Soc. London, Ser. A*, **315**, 185-194.
- Cavaliere, T. and Jones, A.G., 1984. On the identification of a transition zone in electrical conductivity between the lithosphere and asthenosphere: a plea for more precise phase data. *J. Geophys.* **55**: 23-30.
- Constable, S.C., Parker, R.L. and Constable, C.G., 1987. Occam's inversion: a practical algorithm for generating smooth models from electromagnetic sounding data. *Geophysics*, **52**, 289-300.
- Gamble, T.D., Goubaud, W.M. and Clarke, J., 1979. Magnetotellurics with a remote reference. *Geophysics*, **44**: 53-68.
- Haak, V. and Hutton, V.R.S., 1986. Electrical resistivity in continental lower crust. In: The Nature of the Lower Continental Crust. Editors: J.B. Dawson, D.A. Carswell, J. Hall and K.H. Wedepohl. Geol. Soc. London, Spec. Publ. **24**, 35-49.
- Hashin, Z. and Shtrikman, S., 1963. A variational approach to the theory of the elastic behaviour of multiphase materials. *J. Mech. Phys. Solids*, **11**, 12-140.
- Kellett, R.L., Mareschal, M. and Kurtz, R.D., 1992. A model of lower crustal electrical anisotropy for the Pontiac Subprovince of the Canadian Shield. *Geophys. J. Int.*, **111**: 141-150.
- Kurtz, R.D., Craven, J.A., Niblett, E.R. and Stevens, R.A., 1993. The conductivity of the crust and mantle beneath the Kapuskasing Uplift: electrical anisotropy in the upper mantle. *Geophys. J. Int.*, **113**: 483-498.
- Madden, T.D., 1976. Random networks and mixing laws. *Geophys.*, **41**, 1104-1125.
- Madden, T.D., 1983. Microcrack connectivity in rocks: a renormalization group approach to the critical phenomena of conduction and failure in crystalline rocks. *J. Geophys. Res.*, **88**, 585-592.
- Maxwell, J.C., 1892. *A Treatise on Electricity and Magnetism*. 3rd. ed. (2), Clarendon Press, Oxford.
- Nesbitt, B.E., 1993. Electrical resistivities of crustal fluids. *J. Geophys. Res.*, **98**, 4301-4310.
- Oldenburg D.W., Whittall K.P. and Parker R.L., 1984. Inversion of ocean bottom magnetotelluric data revisited. *J. Geophys. Res.*, **89**, 1829-1833.
- Osipova, I.L., Hjelt, S.-E., and Vanyan, L.L., 1989. Source field problems in northern parts of the Baltic shield. *Phys. Earth Planet. Inter.*, **53**, 337-342.
- Reiersol, O., 1950. Identifiability of a linear relation between variables which are subject to error. *Econometrica*, **18**: 375-389.
- Sato, H., M.H. Manghnani, B.R. Lienert and A.T. Weiner, 1986. Effects of electrode polarization on the electrical properties of partially molten rock. *J. Geophys. Res.*, **91**, 9,325-9,332.
- Schilling, F.R., G.M. Partzsch, H. Brasse and G. Schwarz, 1997. Partial melting below the magmatic arc in the central Andes deduced from geoelectromagnetic field experiments and laboratory data. *Phys. Earth Planet. Inter.*, **103**, 17-31.
- Schmeling, H., 1985. Numerical models on the influence of partial melt on elastic, anelastic and electrical properties of rocks. Part I: Elasticity and anelasticity. *Phys. Earth Planet. Inter.*, **41**, 105-110.
- Schmeling, H., 1986. Numerical models on the influence of partial melt on elastic, anelastic and electrical properties of rocks. Part II: Electrical conductivity. *Phys. Earth Planet. Inter.*, **43**, 123-136.
- Senechal, G., Rondenay, S., Mareschal, M., Guilbert, J. and Poupinet, G., 1996. Seismic and electrical anisotropies in the lithosphere across the Grenville Front, Canada. *Geophys. Res. Lett.*, **23**, 2255-2258.
- Smith, J.T. and Booker, J.R., 1988. Magnetotelluric inversion for minimum structure. *Geophysics*, **53**: 1565-1576.
- Tarits, P., 1986. Conductivity and fluids in the oceanic upper mantle. *Phys. Earth Planet. Inter.*, **42**, 215-226.
- Tozer, D.C., 1972. The present thermal state of the terrestrial planets. *Phys. Earth Planet. Inter.*, **6**, 182-

- 197.
- Tozer, D.C., 1979. The interpretation of upper mantle electrical conductivities. *Tectonophys.*, **56**, 147-163.
- Tozer, D.C., 1981. The mechanical and electrical properties of Earth's asthenosphere. *Phys. Earth Planet. Inter.*, **25**, 280-296.
- Tyburczy, J.A. and J.J. Roberts, 1990. Low frequency electrical response of polycrystalline olivine compacts; grain boundary transport. *Geophys. Res. Lett.*, **17**, 1985-1988.
- Vanyan, L.L., 1984. Electrical conductivity of the asthenosphere. *J. Geophys.*, **55**, 179-181.
- Vanyan, L.L., Berdichevsky, M.N., Fainberg, E.B. and Fiskina, M.V., 1977. The study of the asthenosphere of the East European platform by electromagnetic sounding. *Phys. Earth Planet. Inter.*, **14**, P1-P2 (Letter section).
- Vanyan, L.L., I.V. Yegorov, P.P. Shilovsky, I.M. Al'perovich, V.M. Nikiforov and O.V. Volkova, 1983. Characteristics of deep electrical conductivity of northern Sakhlin. *Izvestiya*, **19**, 208-214.
- Velikhov, Y.P., Zhamaletdinov, A.A., Belkov, I.V., Gorbunov, G.I., Hjelt, S.-E., Lisin, A.S., Vanyan, L.L., Zhdanov, M.S., Demidova, T.A., Korja, T., Kirillov, S.K., Kuksa, Y.I., Poltanov, A.Y., Tokarev, A.D. and Yevstigneyev, V.V., 1986. Electromagnetic studies on the Kola peninsula and in northern Finland by means of a powerful controlled source. *J. Geodyn.*, **5**, 237-256.
- Velikhov, Y.P., M.S. Zhdanov and M.A. Frenkel, 1987. Interpretation of MHD-sounding data from the Kola Peninsula by the electromagnetic migration method. *Phys. Earth Planet. Inter.*, **45**, 149-160.
- Vidale, J.E., X.-Y. Ding and S.P. Grand, 1995. The 410-km-depth discontinuity: A sharpness estimate from near-critical reflections. *Geophys. Res. Lett.*, **22**, 2557-2560.
- Vladimirov, N.P., 1976. Deep magnetotelluric surveys in the Baltic-Scandinavian Shield and the Kokchetav Block. In: Geoelectric and geothermal studies . A. Adam (editor). Publ. by Akad. Kiado. Budapest, Hungary, 615-616.
- Watanabe, T. and K. Kurita, 1993. The relationship between electrical conductivity and melt fraction in a partially molten simple system: Archie's law behavior. *Phys. Earth Planet. Inter.*, **78**, 9-17.
- Watanabe, T. and K. Kurita, 1994. Simultaneous measurements of the compressional-wave velocity and the electrical conductivity in a partially molten material. *J. Phys. Earth.*, **42**, 69-87.
- Weidelt, P., 1972. The inverse problem of geomagnetic induction. *Z. Geophys.*, **38**, 257-289.
- Wickens, A. J., 1971. Variations in lithospheric thickness in Canada. *Can. J. Earth Sci.*, **8**: 1154-1162.
- Xu, Y. B.T. Poe, T.J. Shankland and D.C. Rubie, 1998. Electrical conductivity of olivine, wadsleyite and ringwoodite under upper-mantle conditions. *Science*, **280**, 1415-1418.



### 3 Source Field

There are two major mechanisms which give rise to the MT signal. These are micropulsations and spherics. There are other lesser mechanisms. The nature of the naturally occurring electromagnetic fields and waves is given in numerous texts and papers. A multitude of data can be found on websites and literature searches.

#### 3.1 Low Frequencies - Micropulsations

- 3.1.3 In the range of about .001 to 1.0 Hz, the major source mechanism for natural electromagnetic fields is called micropulsations. These arise from complex interactions of the charged particles in the solar wind with the earth's magnetic field and charged particles in the ionosphere (see Figure 1).
- 3.1.4 This source field can vary in magnitude on a daily, weekly, and yearly basis. This can effect recording at times, where the natural signal strength is not strong enough to produce high S/N data. In these cases, longer recording may be required. Figure 2 shows how sunspot activity varies over yearly cycles.
- 3.1.5 Solar forecasts are available through a variety of sources and can aid in acquisition planning.

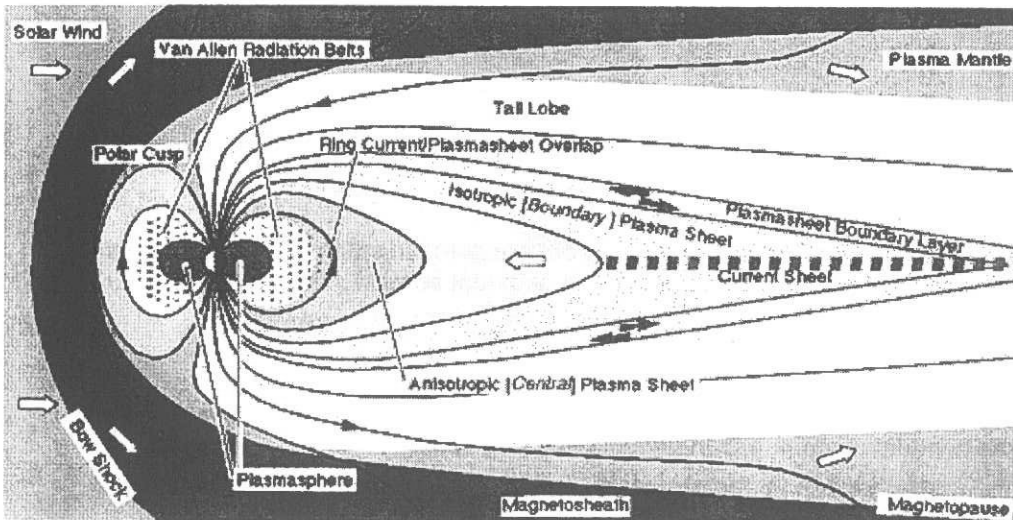


Figure 1: Effect of solar wind on Earth's magnetosphere (from NASA)

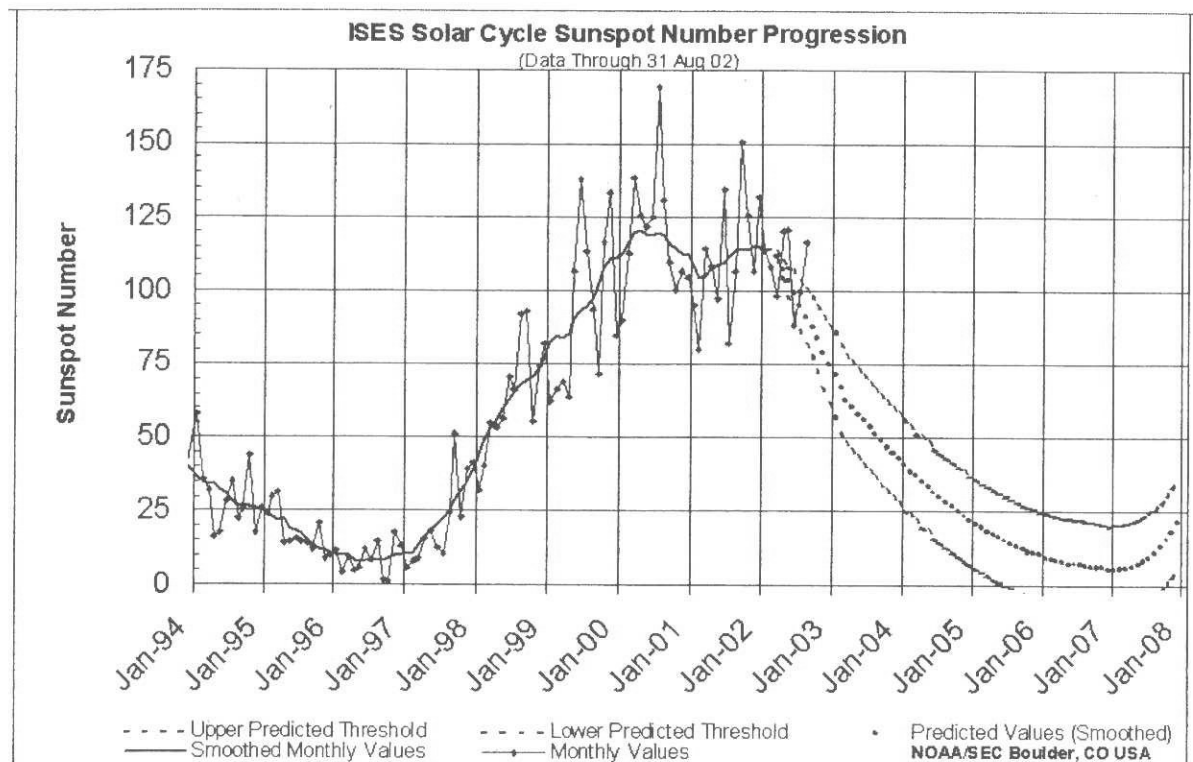


Figure 2: Solar sunspot levels (from NOAA)

### 3.2 High Frequencies - Spherics

- 3.2.3 In the range of 1.0 to 1000 Hz and higher, the major source mechanism is the propagation of electromagnetic energy from distant thunderstorms on a global scale. These storms occur primarily in the equatorial regions.
- 3.2.4 The energy propagates in the spherical cavity wave guide formed by the earth's atmosphere (bounded by the conducting earth and the conducting ionosphere).  
Figure 3 shows the mechanism for the propagation. Figure 4 shows a snapshot of lightning activity around the world.

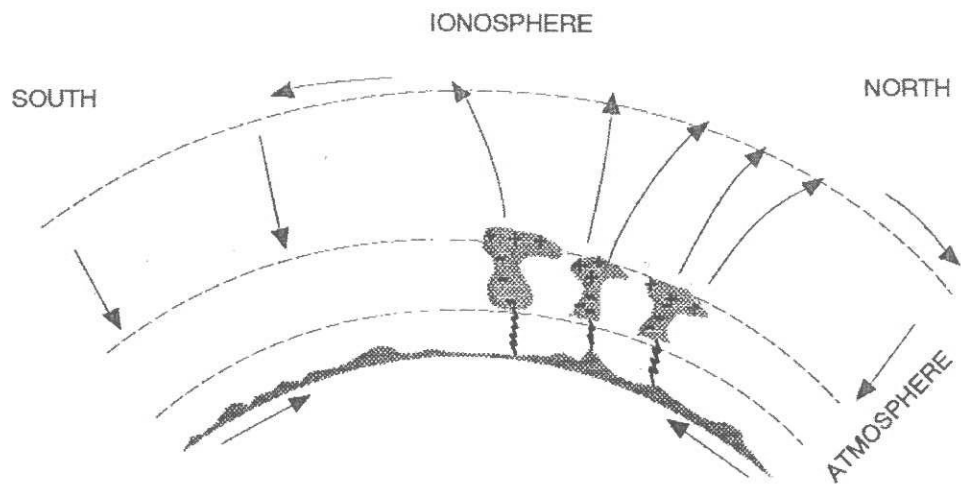


Figure 3: Spherics activity (from Zhdanov and Keller, 1994)

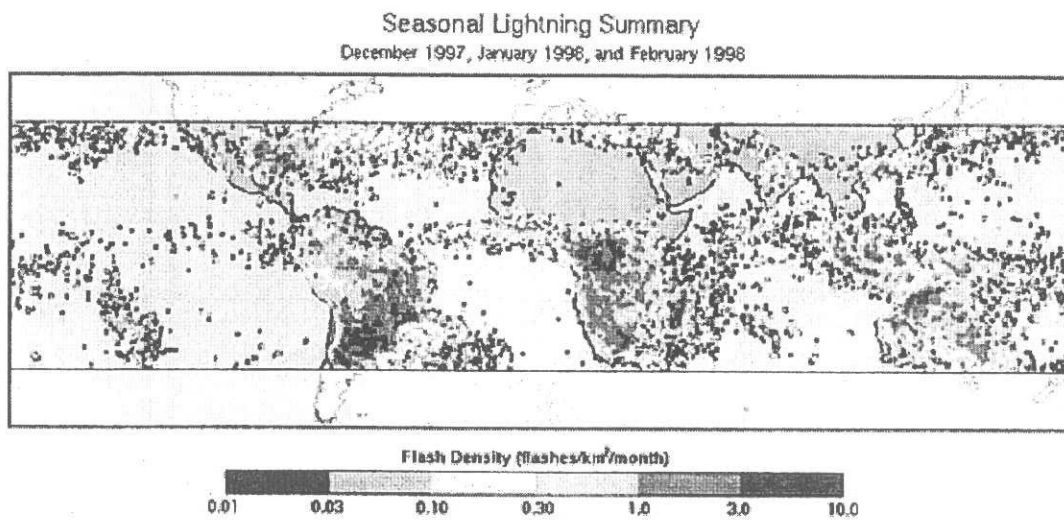


Figure 4: Worldwide lightning activity

### 3.3 Plane Wave Assumption

Because of the high resistivity contrast between the earth and the atmosphere, it can be assumed that all source waves are effectively refracted to vertical incidence (by Snell's law). Therefore, in Magnetotellurics it is assumed that the source is a plane wave impinging vertically upon the earth.

### 3.4 Typical Energy Spectra

- 3.4.3 Figures 5, 6, and 7 are typical measured energy density spectra for telluric (electric) and magnetic fields respectively. Figure 8 shows a summary of magnetic field spectra amplitude over the entire MT/AMT frequency range. Note that the maximum density occurs at low frequencies (less than 0.1 Hz) and that a minimum occurs at about 1 Hz. Signal also falls off at very high frequencies
- 3.4.4 The low mid-frequency energy results in a poor signal-to-noise ratio over the range of about 5 Hz to 0.1 Hz. This band of data is the most difficult to acquire in practice.

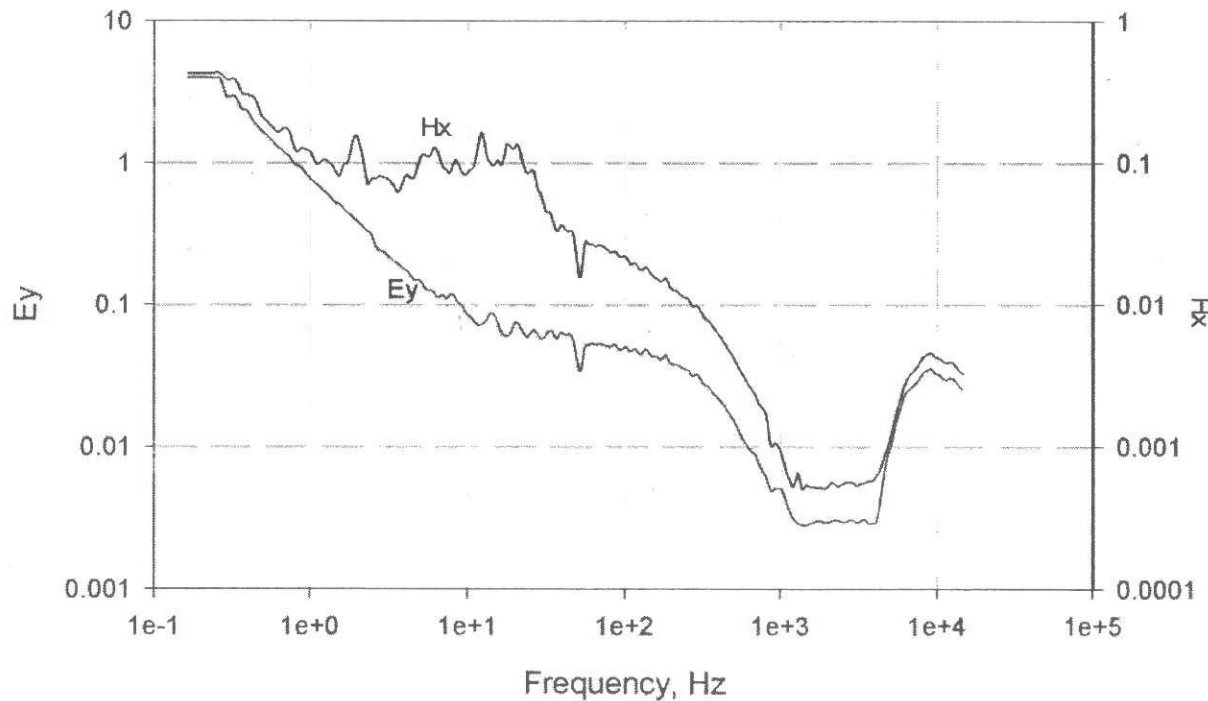


Figure 5: Typical higher frequency (AMT) amplitude spectra

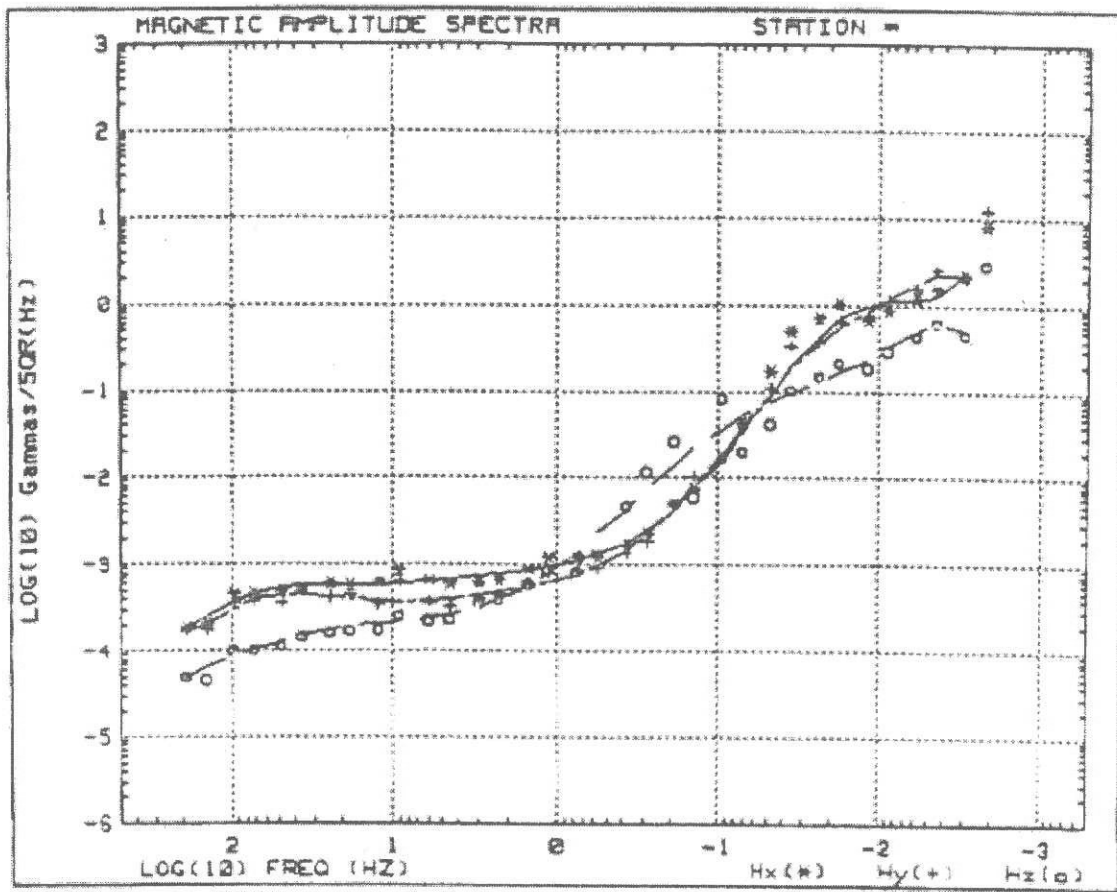


Figure 6: Typical MT magnetic amplitude spectra

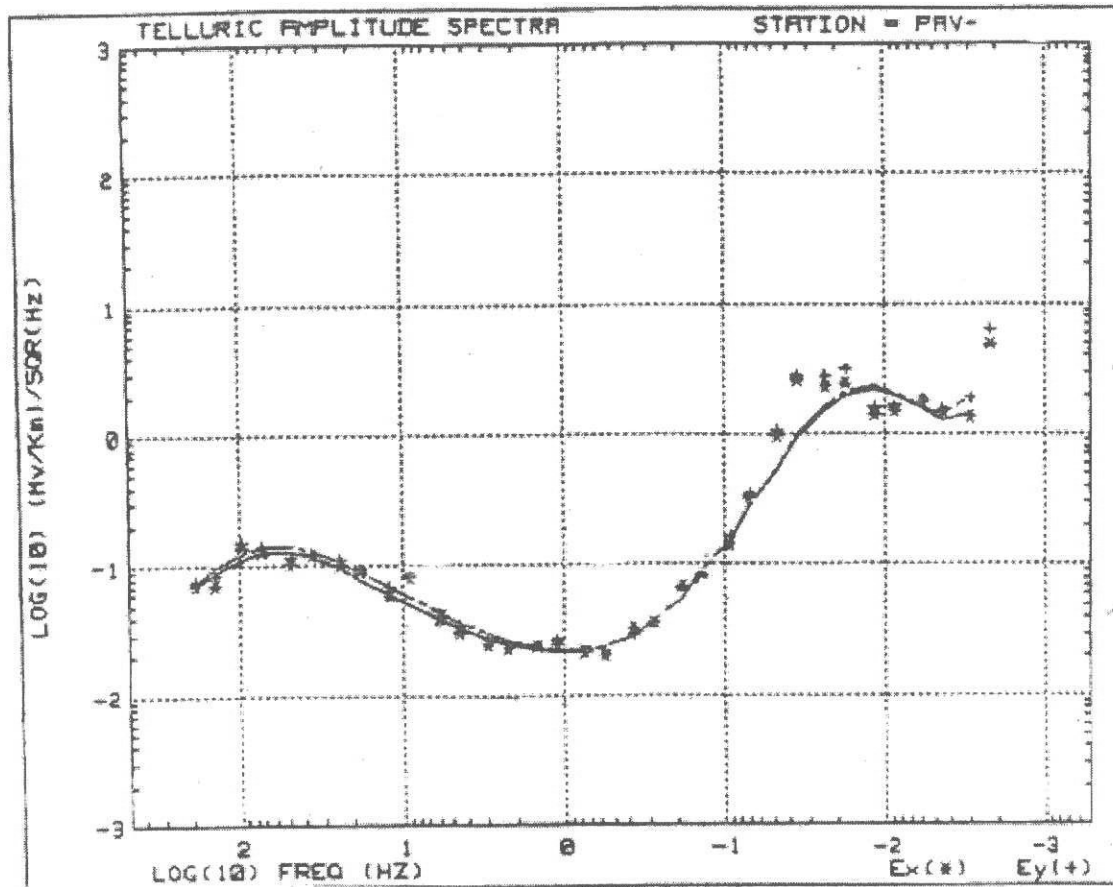


Figure 7: Typical MT telluric (electric field) amplitude spectra

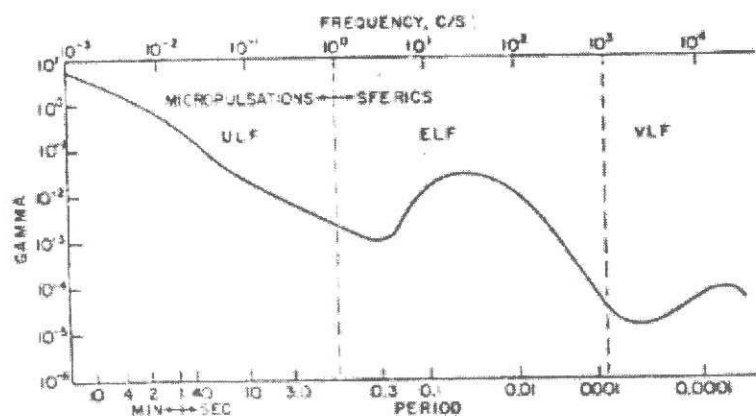


Figure 8: Summary of H-field spectra over MT/AMT frequency range

## 4. MT Data Acquisition

### 4.1. Data Input at Each Station: Ex, Ey, Hy, Hx, Hz

4.1.1. There are five channels of data input at each station. These are two components of electric field ( $E_x$  and  $E_y$  time series) and three components of the magnetic field ( $H_x$ ,  $H_y$ , and  $H_z$  time series). Note that boundary conditions require that  $E_z = 0$ , so a full three-dimensional vector measurement is being made. Figure 1 shows a typical MT station sensor layout.

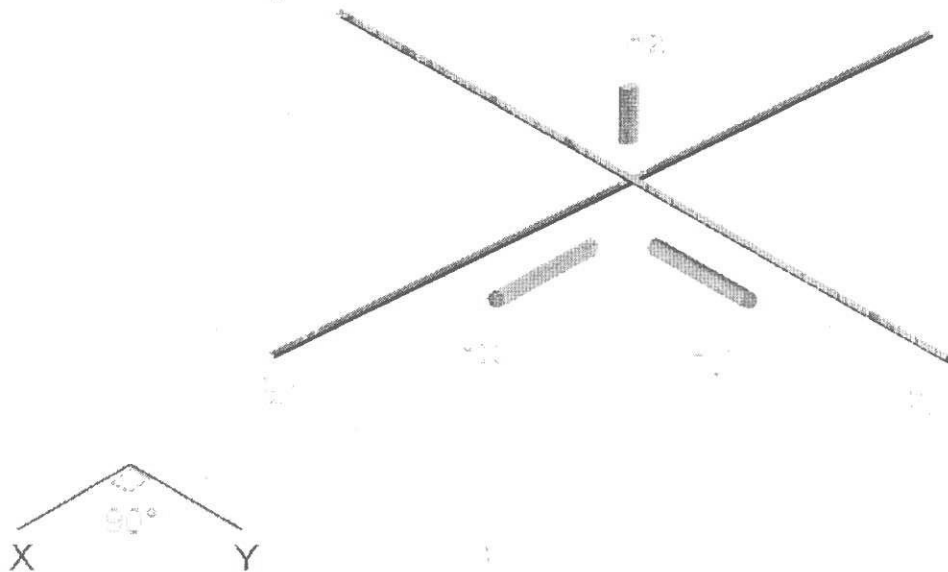


Figure 1: Typical MT sensor layout

### 4.2. Typical Sensors

4.2.1. Figure 2 shows a typical sensor layout for an MT station. The electric field components ( $E_x$  and  $E_y$ ) are measured by orthogonal pairs of non-polarizable porous pot electrodes connected by cables. The magnetic field components ( $H_x$ ,  $H_y$  and  $H_z$ ) are normally measured with ferrous-cored coils

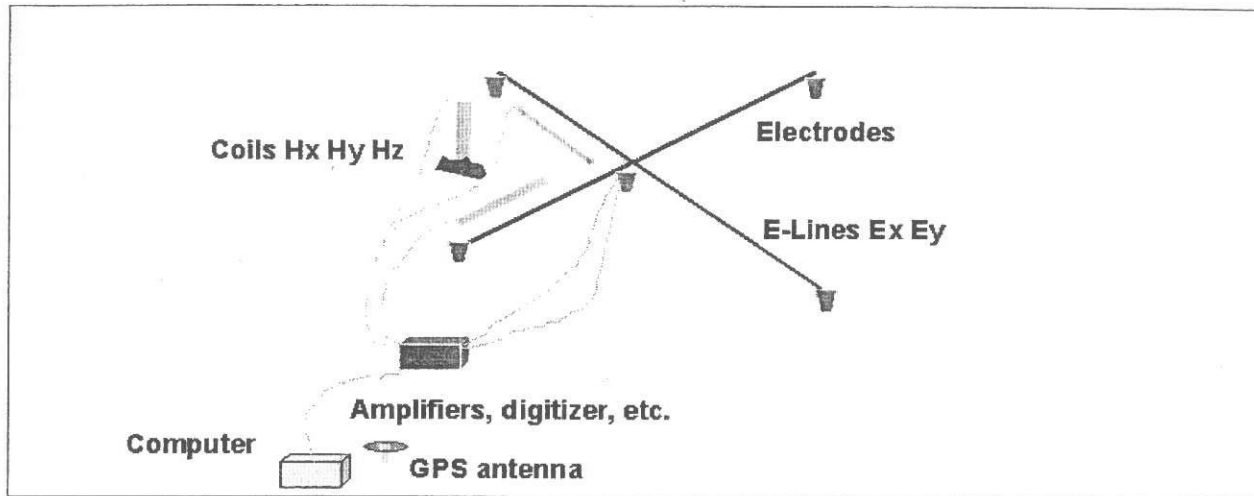


Figure 2: Typical MT station layout

#### 4.3. Components:

##### 4.3.1. Coils:

4.3.1.1. The two horizontal magnetic field components ( $H_x$  and  $H_y$ ) are measured by calibrated ferrous cored coils, typically about 4 to 8 cm in diameter and 1 to 3 meters in length, weighing about 2 to 10 kg. They are usually buried about a foot below the surface to get them out of the surface noise environment. The vertical magnetic field is measured by a vertical coil (buried as much as possible) or by an "air coil" consisting of several turns of wire with a diameter of about 30 feet (oriented so the axis of the coil is vertical). This is also buried a few inches. Figure 3 shows some typical coils.

4.3.1.2. An alternative sensor for all three magnetic field components is a three-component SQUID (Super-conducting Quantum Interference Device) magnetometer. These have the advantage of being extremely sensitive with excellent low frequency response. However, they require liquid helium, which may be a logistics problem at some locations, and have poor high frequency response. Low frequency data acquired with a SQUID are generally higher quality but more expensive than those acquired with conventional coil sensors. High frequency data are generally lower quality.

4.3.1.3. Coils are built and calibrated for certain frequency ranges, i.e. recording to low frequencies (such as 1000 seconds) may require a different coil than needed to record very high frequencies (e.g. 1 KHz). Figure 4 shows an example of calibrated ranges. In some surveys, where both very low and very high frequencies are desired, it may be necessary to record the high frequency data with a separate set of coils. Fortunately, this can be done in a matter of minutes, with the lower frequency data

being recorded separately for a minimum of several hours, either before or after the high frequency data.

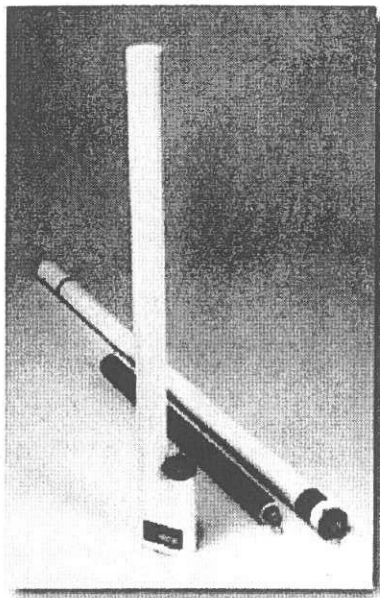


Figure 3: Typical MT coils (from EMI Instruments)

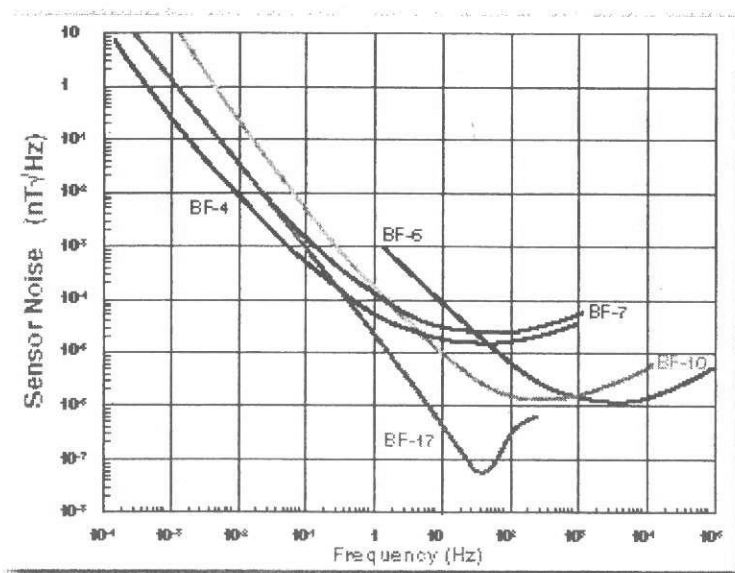


Figure 4: Example of coil calibrated frequency ranges

#### 4.3.2. Electrodes:

- 4.3.2.1. Porous pots consist of a metal electrode in contact with a container of concentrated solution of a salt of the same metal (e.g. Pb-PbCl<sub>2</sub>, Cu-CuSO<sub>4</sub>). Contact with the

ground is made from the salt solution through a porous ceramic surface. Alternatively, metal stakes can be used as electrodes (normally for AMT surveys). Contact resistance should be low and can be minimized by pouring water, a salt solution, or a drilling mud in the hole. This also stabilizes the electrode over the time of recording. Figure 5 shows an example (cross-section) through one type of porous pot.

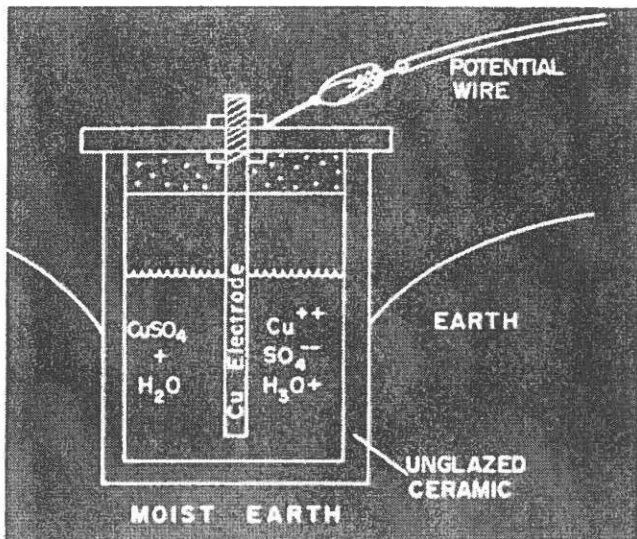


Figure 5: Diagram of porous pot electrode

#### 4.3.3. Cables:

Various connection cables or wires are used to connect sensors to the recording unit or to each other. They are shielded and completely waterproof when installed. The E-lines, which connect the porous pots together, will vary in length depending on the frequency range being recorded. AMT will use short E-lines, e.g. 25 m long. MT typically uses longer E-lines, e.g. 100m long.

#### 4.3.4. Batteries:

Power supply for the recording unit and other equipment is normally 12V batteries which need to be changed every day. They are recharged and returned to the field every other day. In some instances, the equipment can be powered by solar cells (recharging the batteries).

#### 4.3.5. Recording Unit:

Most are 24-bit A-to-D (since the mid-90's). This provides for a larger dynamic range and hence better signal-to-noise and less saturation. The data are recorded and transferred by the means of compact flash cards. The units are light weight (5 to 7 Kg) and enclosed in some form of weatherproof casing.

4.3.5.1. Recording units are built to receive up to 6 channels, just E or H, or full 5 channels (E and H). Synchronization with other sites is via built-in GPS receivers and timing mechanisms.

4.3.5.2. These units digitize the time series for all channels over the period of recording. The units include gain settings (either automatic or manual) in order to record a range of signal strengths. They also have filters (such as 60/50Hz and harmonics) and amplifiers. Normally these units provide raw processing of the data in the field so that data can be inspected on site.

4.3.5.3. Figures 6 and 7 show examples of the acquisition units. Each channel enters the 'box' by its own connection which is waterproof and tight.

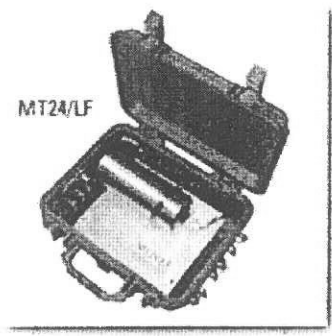


Figure 6: Example of MT acquisition/recording unit (EMI Instruments)

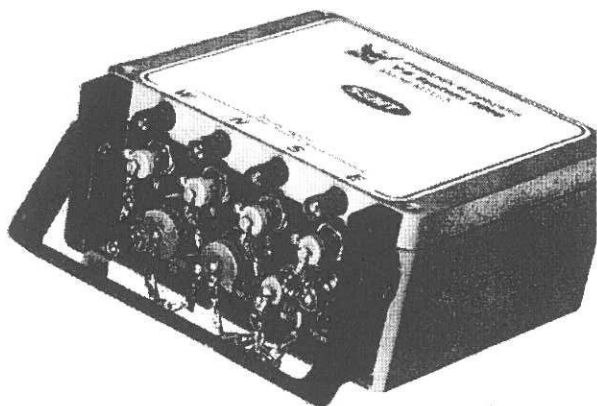


Figure 7: Example of MT acquisition/recording unit (Phoenix Geophysics)

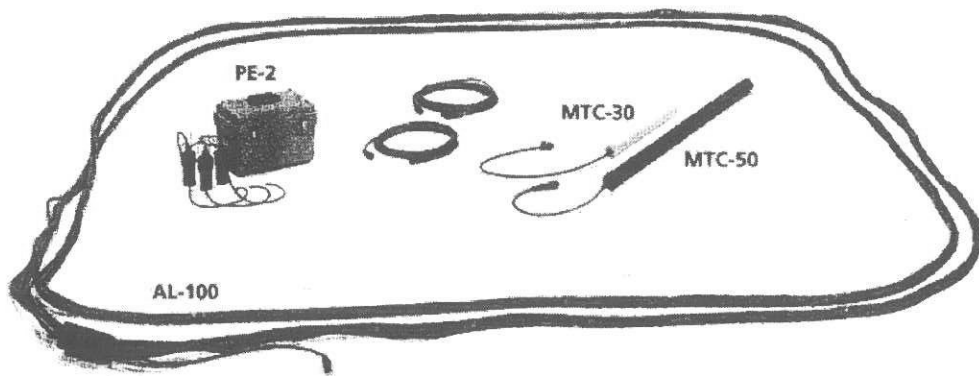


Figure 8: Coils, porous pots, battery, cable and air loop (for Hz) – (Phoenix Geophysics)

#### 4.4. Remote Reference Acquisition

- 4.4.1. Since 1979, standard field practice has made use of the remote reference noise reduction technique (see Gamble, 1978). This technique takes advantage of the fact that at two sites, separated by a significant distance, the electromagnetic noise fields are uncorrelated. However, the plane wave MT source fields are correlated. Noise at a given site can therefore be reduced substantially by cross-correlating appropriate field components between local and remote sites.
- 4.4.2. Remote referencing was an extremely important development since it allowed recording of consistently accurate mid-frequency data for the first time.
- 4.4.3. Present state-of-the-art systems record and process data at two, three, or more stations simultaneously. Most systems use GPS signals to synchronize between stations. Usually, the magnetic field is used as the reference. This reference can be another station recorded on the survey, or a stationary reference for an entire survey (or portion of survey). Reference stations can be any distance away, from ~0.5km to 100's of kilometers. The source of the severe noise usually determines where the reference station should be. In extreme cases, where noise sources are widespread in an area (such as train rails), a reference site will have to be placed outside of the noisy territory. In some areas, where there is little noise, a remote reference can be a neighboring station or a remote reference may not be necessary.

#### 4.5. Noise

##### 4.5.1. Cultural (Man-made)

Vehicles – both the vibrations from motion and EM from starting vehicle

Powerlines – any size; amount of noise can depend on grounding, leaky transformers, etc.

Pipelines (transmitting current) – Cathodic protection

Electric fences – Pulsating usually around 1 Hz.

Electrified rail lines – Can be major problem with signal traveling for many kilometers

Water and other pumps -

#### 4.5.2. Natural

Lightning storms – Can cause noise (hi-amplitude spikes) and will travel further where surface is resistive. Energy from lightning storms can damage gear if it strikes near station. Recording should be ceased and equipment ‘unhooked’ when severe electrical storms are present and threatening.

Wind – Vibrations on both the coils and E-lines can be caused by wind.

Animals (chewing wires, tripping wires, digging up pots)

People (taking wire or gear)

#### 4.5.3. Terrain Effects

Locating a station on top of a topographic high will usually cause effects in the data, primarily caused by distortion of the fields by the feature. For example, recording on top of a butte places a station basically ‘up in the air’ (which is highly resistive).

Terrain can also cause problems if the E-lines are laid out on extreme slopes, effectively shortening the length without the acquisition unit (and processing) recognizing the problem.

#### 4.5.4. Solutions

4.5.4.1. Efforts should be made to reduce noise during acquisition. This is best done by placing stations as far as possible from known cultural noise sources. It is difficult to provide a rule-of-thumb, but at least a half-kilometer separation between station and powerline/house/ pumps is suggested. Noise can often be minimized by filters and processing but it is best to avoid it if possible.

4.5.4.2. Recording is often stopped during lightning storms, as a strike near a station can damage electronics. Noise from lightning will travel further in areas where the ground is highly resistive. When working in a lightning-prone area, it is good practice to shift acquisition schedules so that recording is not done during that part of the day when thunderstorms are active.

4.5.4.3. Wind can cause noise on both the electric and magnetic field sensors, primarily from vibration. Coils should be buried under a few inches of soil. E-lines should be placed near or on the ground; E-lines hanging from bushes or between trees can sway in the wind.

4.5.4.4. Laying E-lines close to the ground should also minimize damage caused by animals (deer, cows, etc.) tripping on the wires and breaking them. Some animals (rabbits, rats) will also chew wires. With persistent animals, rubbing or spraying the E-lines with ammonia or other deterrents should help.

- 4.5.4.5. Some animals (pigs, bears) have been known to dig up electrodes. In these situations the pots may have to be covered for protection.
- 4.5.4.6. Stations should not be placed on top of topographic highs. It is better to place them on the side of slopes. E-lines should be laid out as level as possible. Coils should always be leveled to horizontal or vertical. In areas of topography, 2D and 3D modeling should incorporate topography.

#### 4.6. Typical MT field crew

Operators – The Operators are responsible for setting up and tearing down site. They are also responsible for the site location and should attempt to avoid noise sources. They also record the location of the station (via map or gps) and record pertinent information about the station layout.

Field assistants – Assistants aid the operators in carrying and laying/picking up gear. They can be locally hired personnel.

Processor – processes field data. Data are processed after the operators return from the field.

Crew Chief – responsible for general crew ops; oversees all activities

Client rep – sometimes the client will have a rep in the field to QC field acquisition and processing, or to interpret the data as soon as the processor is finished.

#### 4.7. QC'ing a Field Survey

- 4.7.1. Quality Control (QC) by a client is necessitated when the client feels it is pertinent. In some cases, this is company policy. In others, it will depend on how confident the client is in the contractor. It may also depend on what type of rate the contractor has been hired, i.e. Per station or per day rate.

#### 4.7.2. Recommendations for QC of an MT field survey

- ✓ Ensure that the field sensors have been calibrated and tested and are in good working order.
- ✓ Visit the field crews and observe their procedures. Are they:
  - ✓ Placing sensors with care, burying magnetometers (coils), placing E-lines near ground (if windy or animals are present)?
  - ✓ Recording for sufficient amounts of time
  - ✓ Recording their physical location (such as UTM or lat-long) accurately so that the client can be sure of the station location?
  - ✓ Hooking up sensors properly (i.e. the correct sensors into the correct slots in the recording equipment)?
  - ✓ Placing sensors in the correct orientation (orthogonal components)
  - ✓ Checking for contact resistance of electrodes – Contact resistance should be minimized and less than 1K Ohms.
  - ✓ Employing good safety practices
  - ✓ Are they representing the client appropriately (i.e. no poor behavior which would reflect badly on client)
  - ✓ Are they behaving in an environmentally-responsible manner (much more critical in some areas and surveys than others)?

#### 4.7.3. Observe the processing

- ✓ Is all care being taken to remove noise thru whatever means possible?
- ✓ Are data being edited to produce best result?
- ✓ Are data of satisfactory nature – will they be interpretable?
- ✓ In general, is contractor abiding by the terms of the contract?

Some Field QC, such as reporting on day activities and reviewing data, can now be done conveniently by email. Field reports or daily logs, plus data files, are small (Kbytes) and can be emailed to the client. Even if this necessitates a Sat phone, the cost is far cheaper than having a client rep in the field.

#### 4.8. MT Deliverables

Data – printed for each station

Main parameters including:

Apparent resistivity amplitude and phase

Strike and rotation (Impedance, Tipper information)

Dimensionality parameters (skew, ellipticity, tipper magnitude)

Polar Diagrams

Digital data – SEG/EDI format

Station locations

Map and/or digital UTM's (lat/longs)

Description of survey

Gear, personnel, dates, procedures

Problems, processing, noise, etc.

#### 4.9. Other systems or arrays for MT/AMT recording

##### 4.9.1. Stratagem –

A hybrid AMT/CSAMT system developed by EMI and Geometrics.

##### 4.9.2. EMAP- ElectroMagnetic Array Profiling –

Developed at UT-Austin in the 1980's. EMAP employs a continuous line of dipoles to record the E-field, normally laid out perpendicular to strike. H-field data are recorded at two locations near the profile and allow each dipole to be processed as with full MT parameters. Because of trademark issues, other companies have used an EMAP-type array but called it by a different name.

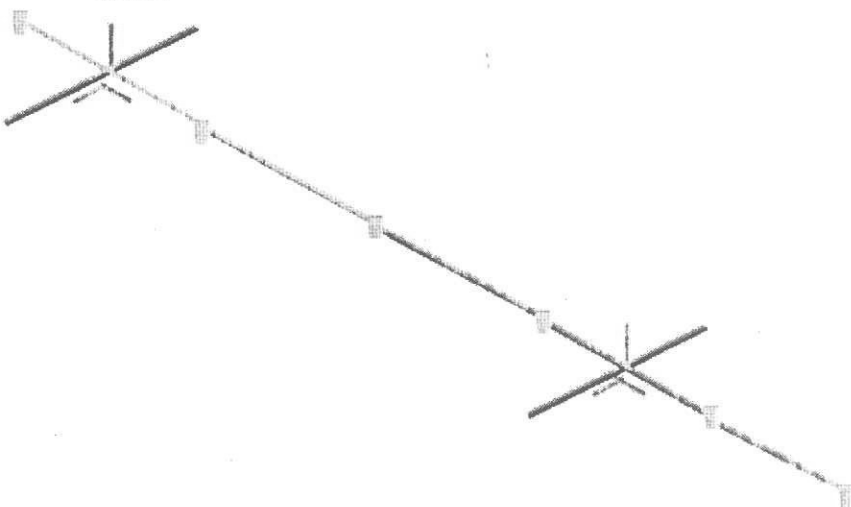


Figure 9: Example of EMAP layout

##### 4.9.3. TMT/MT-

Recording of at least two 5-component MT stations and numerous E-field only MT stations simultaneously. The two H-field stations are used to process the data from the E-field only stations.

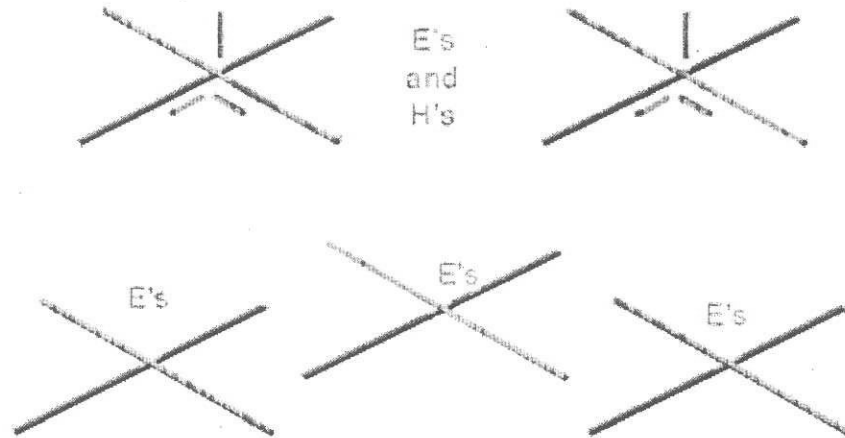


Figure 10: Example of MT/TMT layout

#### 4.9.4. MIMDAS- MIM Distributed Acquisition System

A proprietary system developed by MIM to record MT/AMT and other geophysical data

#### 4.10. MT Equipment Manufacturers (currently):

There are only three commercial MT equipment manufacturers in the world. Many other systems have been designed and built by private companies or universities.

Phoenix Geophysics – Toronto

EMI Instruments – California

Metronix - Germany

#### 4.11. MT Contractors (currently):

There are only a few MT contractors in the world. These listed are companies that specialize in MT acquisition. Other companies may perform MT acquisition, or claim to. A client should always check with other clients or colleagues before hiring a contractor whose capabilities are not known.

Geosystem – Milan, Toronto, San Francisco

Phoenix Geophysics – Toronto

Quantec – Reno NV

AOA Geophysics (Marine MT) – Austin TX

Geodatos – Chile

CNPC – China

NMC – Japan

IGNS – New Zealand

## 5. MT Interpretation

Everybody does it differently.....

Divided into

- Qualitative
- Quantitative

Luckily, there are WORKSTATIONS!

And also other programs. But, Workstations allow data viewing, editing, processing and modeling

What is the goal of the interpretation? Keep this in mind during the process!

Interpretation requires an estimate ahead of time for the resistivities of the expected targetshosts/background. Figures 1 and 2 show some average values for different rock types.

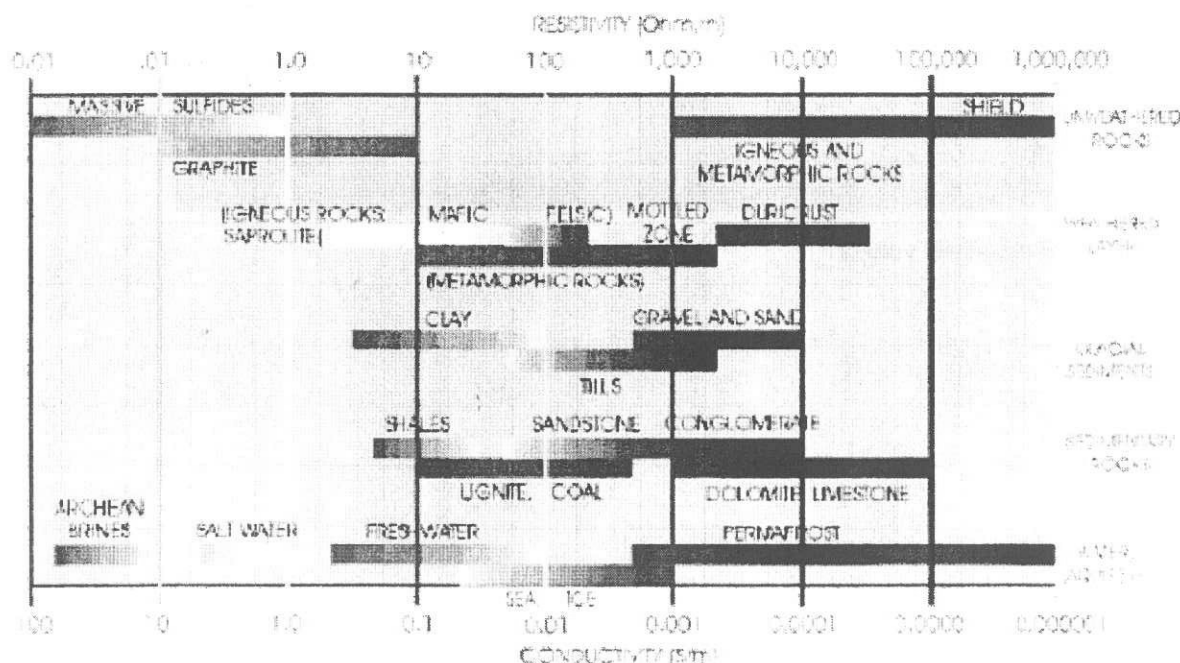


Figure 5-1: Typical resistivity values (Alan Jones)

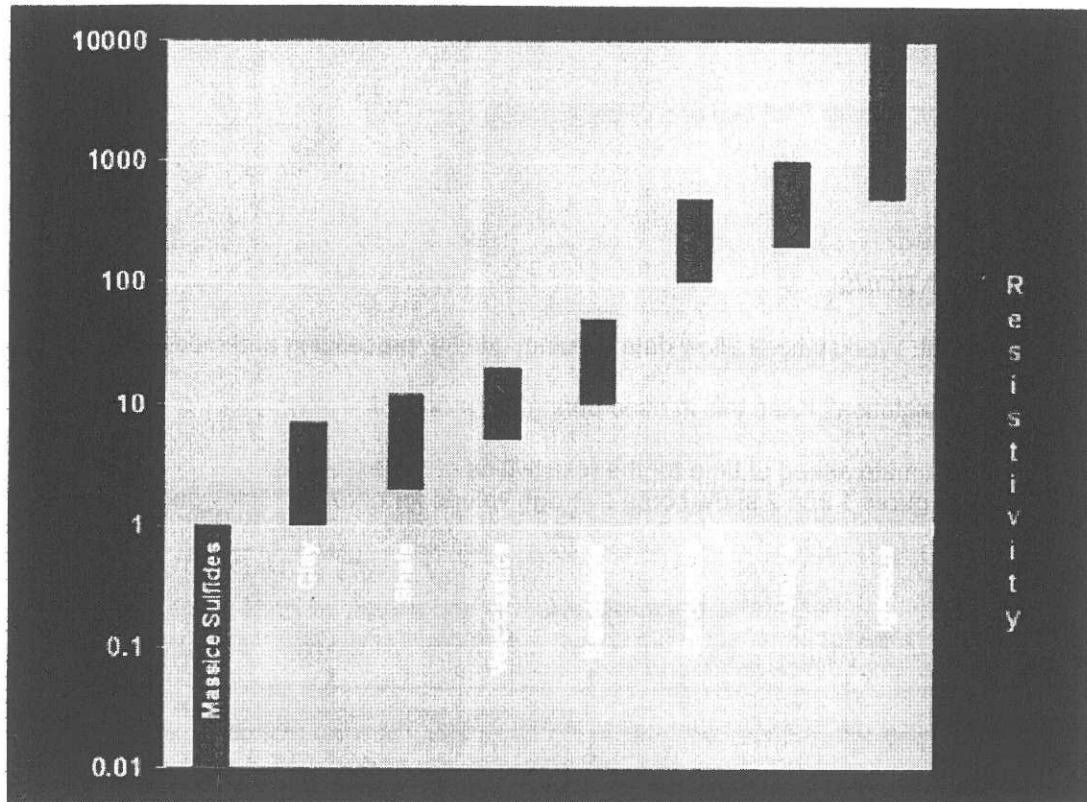


Figure 5-2: Typical resistivity values

## 5.1. MT Computed Parameters

Generally calculated parameters fall into one of three categories:

Interpreted Parameters.

Dimensionality Parameters.

Data Quality Parameters.

However, some fall into more than one category.

### 5.1.1. Interpreted Parameters

The interpreted parameters include the rotated apparent resistivity and phase, impedance polar diagrams, and tipper. The subsurface resistivity structures are determined directly from these parameters.

Figure 5-3 shows a typical plot of rotated apparent resistivity and phase, which is simply a way of expressing the surface impedance tensor. Also shown are plotted skew, ellipticity, tipper magnitude, tipper strike, impedance strike and impedance rotation.

Figure 5-4 shows the polar diagrams for the station in Figure 5-3. They are plotted for various frequencies.

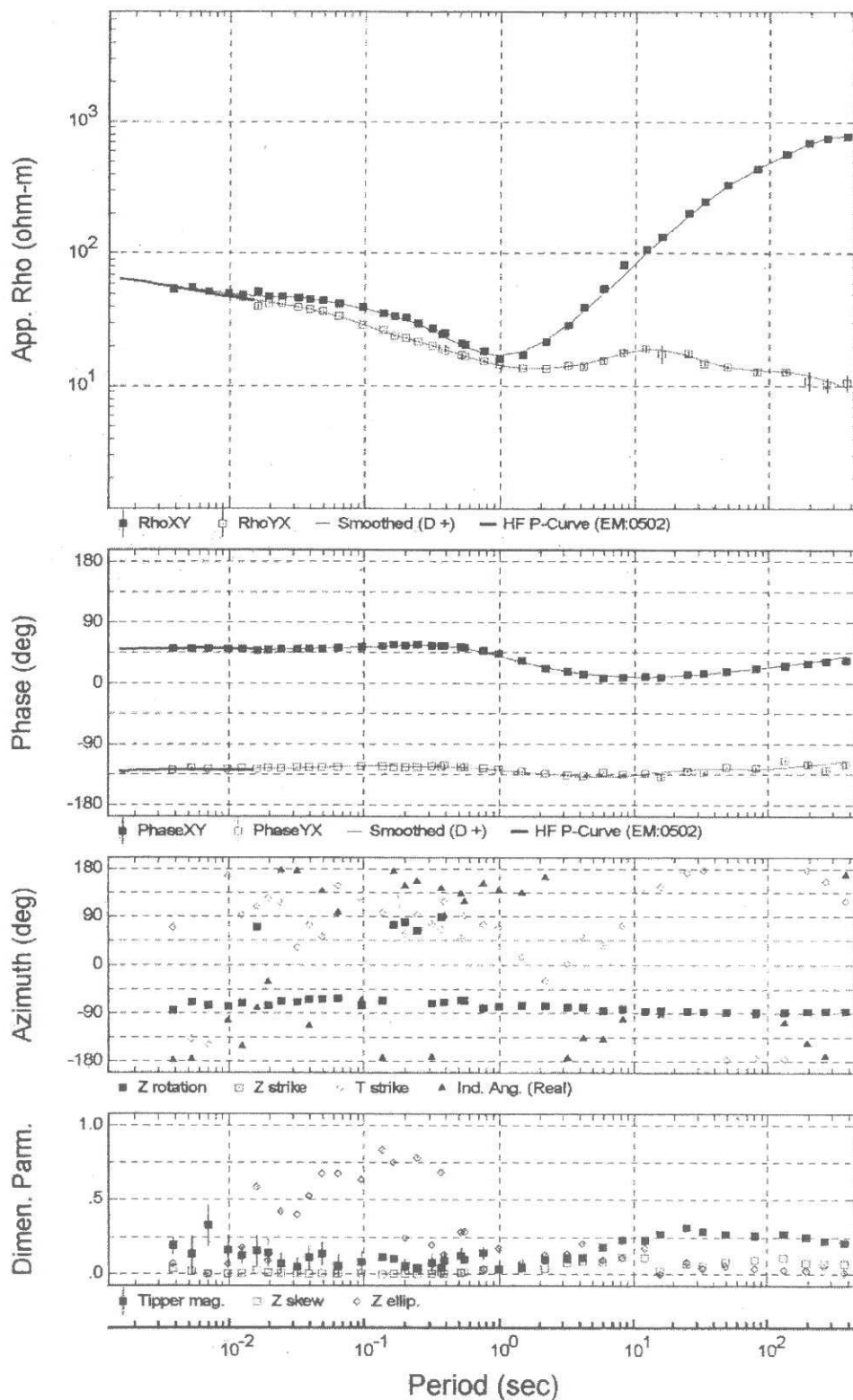


Figure 5-3: Example of Apparent Resistivity Amplitude and Phase plots (top) with rotation and dimensionality plots below

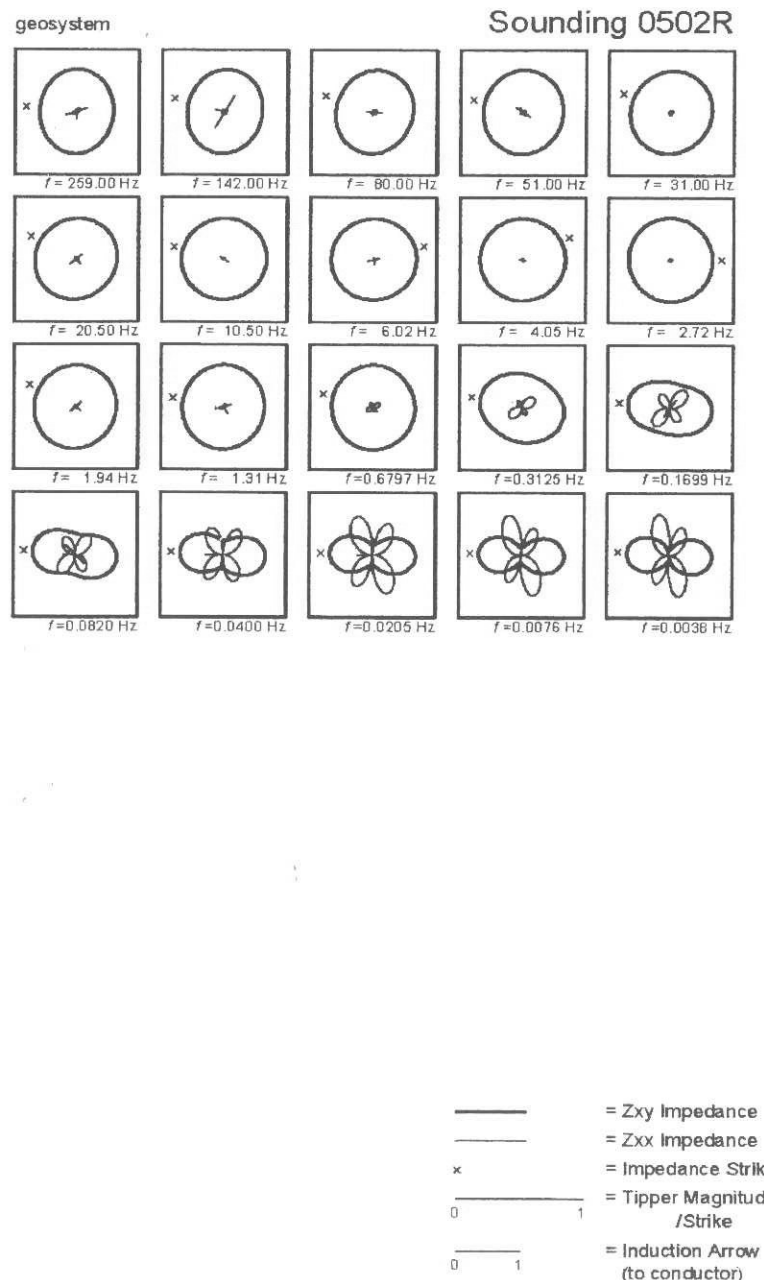


Figure 5-4: Example of Polar Diagrams plotted by frequency

## 5.2. MT Interpretation Steps

5. Data Quality
6. Data Dimensionality
7. Rotation
8. Assign TE and TM
9. Edit Data
10. Smooth Data
11. Correct for Static Shift
12. Perform 1-D inversions
13. Perform 2-D modeling; 3-D if needed or possible
14. Integrate other info
15. Repeat 9 and 10
16. Prepare report, maps, x-sections, etc.

### 5.2.1. Good Quality Data

Good quality data should have small error bars and show little to no distortion from noise or structure. The data should obey the 45° rule – an amplitude curve should not rise or fall on a log-log plot by more than 45°; phase should be within quadrant, i.e. not going beyond their plot bounds of 90°.

The data should look "good" – this comes with practice after reviewing MT data for awhile.

5.2.1.1. Sounding Curve Smoothness: Well behaved MT curves will show smooth variations between estimated E/H elements. Sudden offsets, rapid changes in curvature such as slope reversals across less than 0.5 log cycle of frequency, and curve slopes greater than 45-degrees on log- frequency versus log-apparent resistivity are physically implausible. It is desirable to have low scatter, moderate curvature, and well-joined frequency-band curve segments.

5.2.1.2. Other data quality parameters include coherencies and statistical errors. Generally, coherencies are a measure of agreement between a given observed field component and the corresponding component predicted from other measurements as calculated by Maxwell's equations. Coherencies of greater than 0.9 are generally acceptable. One type of coherency, called the predictability, is an indication of both data quality and dimensionality. Statistical errors, usually expressed as fractions or percent of a standard deviation, are the other principal data quality indicators.

### 5.2.1.3. Poor Quality Data

Poor quality data will show a low S/N ratio and usually will display large error bars. Distortion from noise (power, electric fences/pumps) may also be evident in curves that are not behaving normally.

The telling point in poor quality data are those that cannot be interpreted with confidence.

### 5.2.1.4. Distortion in Data

Some data can be distorted by structure proximity, i.e. faults, major vertical contacts. These data should be interpreted with 2-D codes; 1-D codes are very mis-leading and can over or under-estimate contacts giving a poor interpretation.

### 5.2.2. Data Dimensionality

The understanding of MT data dimensionality is critical to MT interpretation. Dimensionality parameters indicate the presence of three-dimensional closures in the subsurface resistivity structure. These calculated parameters provide information about the dimensionality in data, i.e. is it 1-D, 2-D, or 3-D?

Dimensionality parameters are provided for each frequency of data and at most stations dimensionality will change with frequency (depth) usually becoming more complex with depth.

There are several parameters to analyze data dimensionality: Skew, Ellipticity, Tipper Magnitude and Polar Diagrams. Examples of plots are shown in Figures 5-3 and 5-4.

#### 5.2.2.1. Skew

This is a measure of the ratio of the amplitudes of the diagonal impedance elements to the off-diagonal impedance elements. Lower values, less than about 0.3, are desirable. However, skew may be largely a function of earth resistivity inhomogeneities that can be accounted for by appropriate modeling. Other causes of high skew are local noise sources, local cultural features, and inhomogeneous or polarized source fields.

Ratio of impedance tensor, invariant with rotation

$$|Z_{xx}+Z_{yy}|/|Z_{xy}-Z_{yx}|$$

#### 5.2.2.2. Ellipticity

Ratio of impedance tensor, variant with rotation

$$|Z_{xx}(\theta)+Z_{yy}(\theta)| / |Z_{xy}(\theta)-Z_{yx}(\theta)|$$

#### 5.2.2.3. Tipper magnitude (more on Tipper later in Chapter)

Magnitude of Hz with respect to Hx and Hy

$$\text{Tipper} = \text{SQRT}(|T_x|^2 + |T_y|^2)$$

Tipper magnitude increases as structure becomes more 3-D

#### 5.2.2.4. Polar Diagrams

Plot Zxy and Zxx for each frequency, as in an aerial view of the XY plane.

1-D: Zxy should be circle; invariant with direction; Zxx should be minimal

2-D: Zxy is polarized (peanut shape); Zxx is small

3-D: Zxy, Zxx can be similar & strange

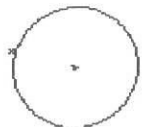


Figure 5-5: Polar Diagram indicating 1-D



Figure 5-6: Polar Diagram indicating 2-D



Figure 5-7: Polar Diagram indicating 3-D

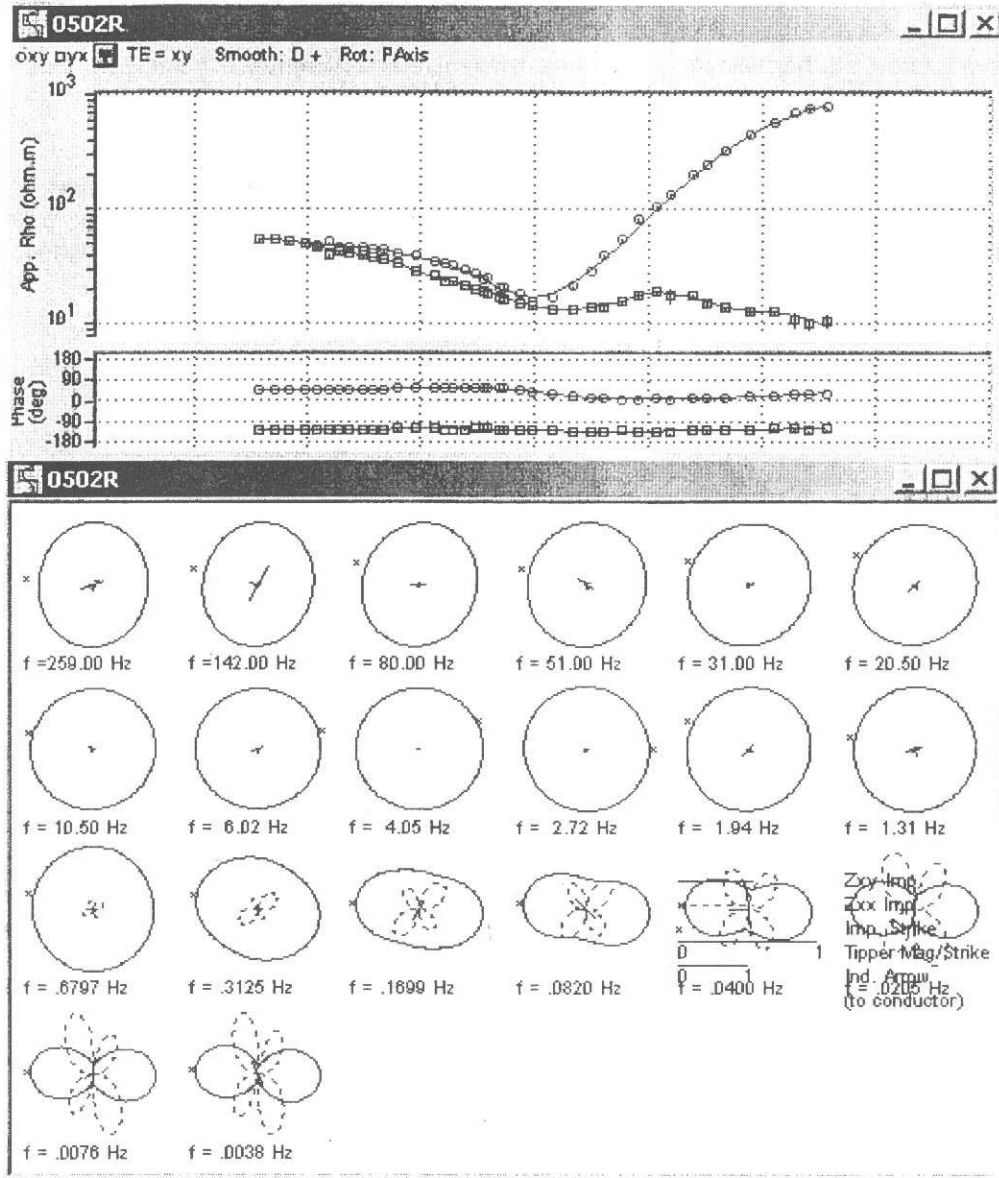


Figure 5-8: Polar diagrams for the above MT curves. Note that the section is 1-Dimensional until those frequencies below 0.7 Hz. The section becomes 3-D at about .04 Hz.

### 5.2.3. Rotation

Field data are rotated, mathematically, normally to maximize and minimize  $Z_{xy}$  and  $Z_{yx}$ . This aligns the data with the maximum and minimum (polarized) E-fields in subsurface. Rotation, like other parameters, is done for each frequency.

The result is two curves which are oriented parallel and perpendicular to Impedance strike. The rotation of the data should be close to geologic strike and dip. There is ambiguity in rotation – it alone does not provide the information as to which direction is strike and which is dip.

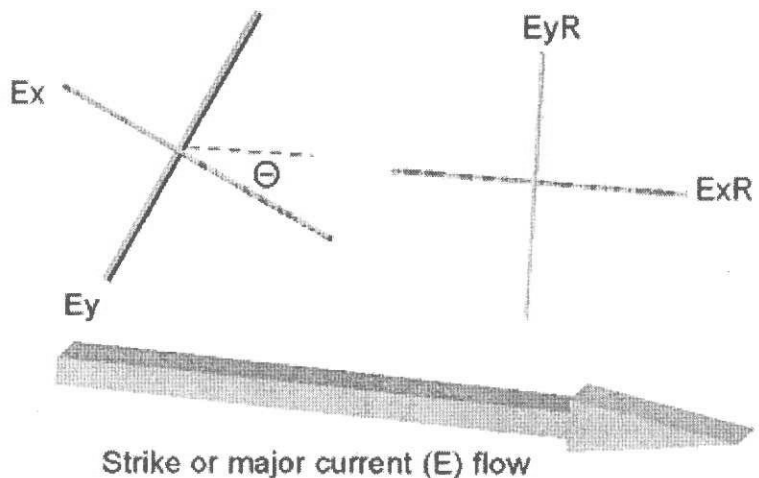


Figure 5-9: The data are rotated to be aligned with the maximum and minimum impedance values

#### 5.2.4. TE and TM

Assigning TE and TM – TE will be parallel to geologic strike.

Per a convention started in MT at its infancy, the polarized maximum and minimum E-field directions are designated as **TE** (transverse electric) and **TM** (transverse magnetic). TE is parallel to the predominant, or maximum, current flow. TM is perpendicular to it. The assignment of the names may seem ‘backwards’, but it was made by EE’s years ago and the names stuck.

##### 5.2.4.1. The ‘Tipper’ – this is info we get from Hz

The tipper is a measure of the ratio of the vertical (Hz) to the horizontal ( $H_x$ ,  $H_y$ ) magnetic fields. The tipper is a complex quantity with a magnitude and phase. Its coherency is a measure of the agreement between the observed vertical component (Hz) and that predicted from the behavior of the horizontal component ( $H_x$  and  $H_y$ ). The tipper is a measure of the degree of lateral inhomogeneity in the subsurface resistivity.

It can be thought of as the effect of ‘tipping’ part of the horizontal H field onto the vertical H field.

Tipper strike should indicate ‘geologic’ strike or which direction TE should be.  
If the Tipper data are ‘good’, they will give an indication of geologic strike. NOTE: If the data are 1-D, the Tipper will not be as meaningful since there is, in theory, no strike.

Use the Tipper or other knowledge (such as geology) to determine primary ‘strike’

Select xy or yx curve as parallel to strike and assign as ‘TE’

Done by comparing Zrotation (Impedance rotation) with Tipper strike – they should be close.

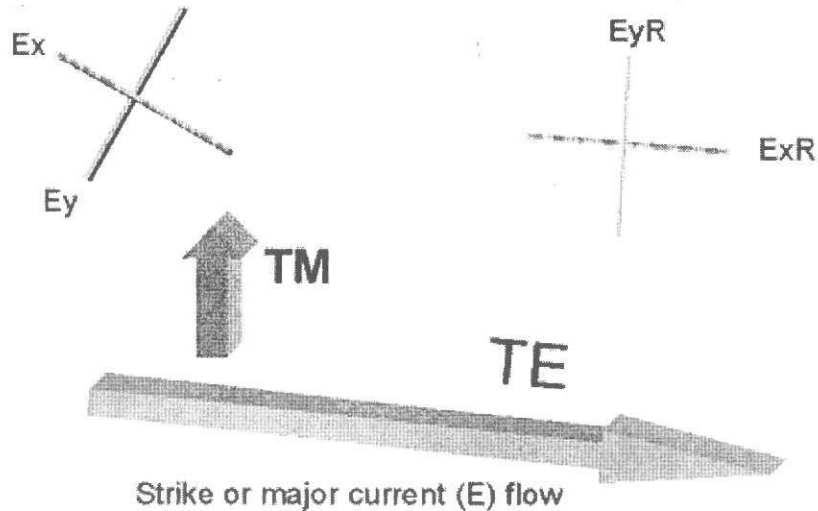


Figure 5-10: The data curves are assigned names of TE and TM, where TE is parallel to geologic strike or the predominant electric field

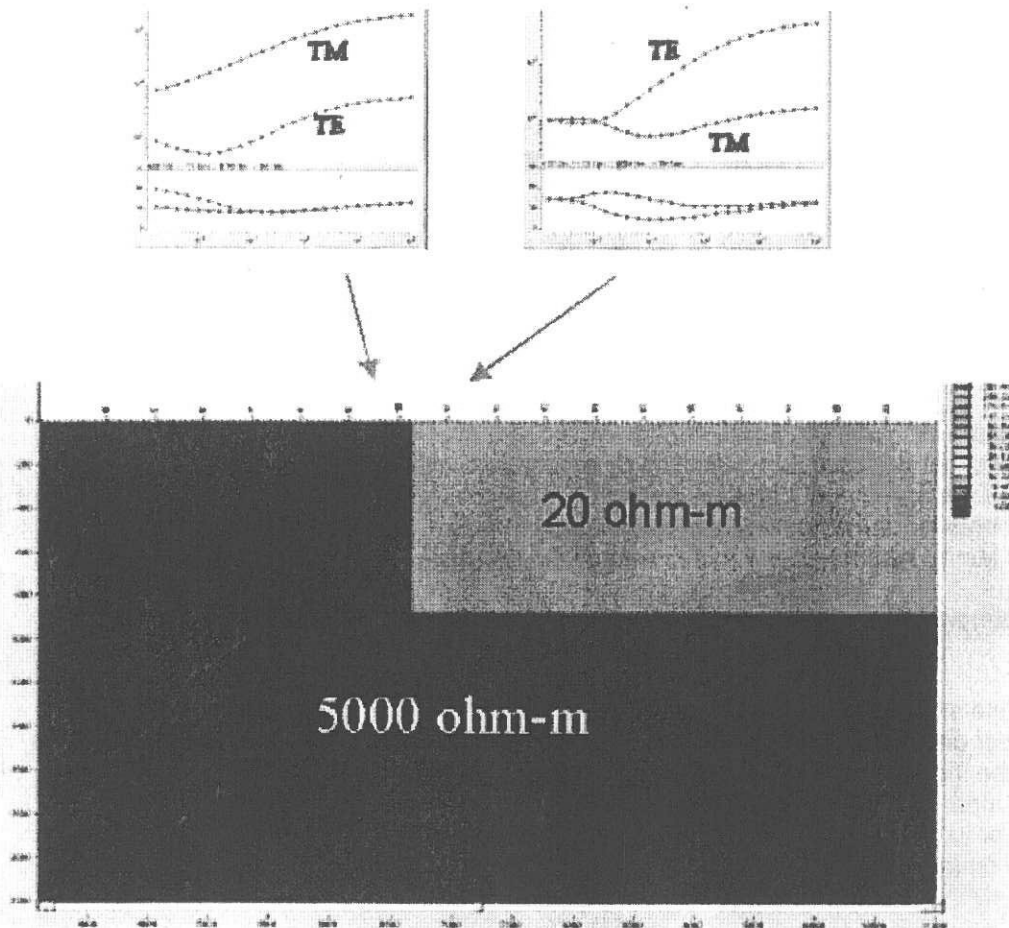


Figure 5-11: TE and TM will behave differently on either side of a major resistivity contact

#### 5.2.5. Edit Data

Data can be edited to 'throw out' poor data points. Normally, data can be 'marked' so that they are not deleted, just not used for interpretation.

There are various reasons to delete data:

- Suspicious behaviour (not obeying MT 'laws')
- Large error bars
- Known problems in frequencies from noise

#### 5.2.6. Smooth the Data

Smoothed curves are placed through the data for several reasons:

- Better behaviour during inversion
- Way to recover thru noisy portion of spectrum
- Method to interpolate thru missing data

-Several types of smoothing algorithms are available to the interpreter.

### 5.2.7. Correct for Static Shift

#### Static Shifts

Static shift corrections are necessary when there are systematic mode shifts in the data, due to the presence of nearby three-dimensional structures. In this case a "DC" shift in the magnitudes of the apparent resistivity curves is performed on one or both modes, depending on what is necessary to best approximate a one or two-dimensional response.

CAUSE: Near-surface inhomogeneities in resistivity - Variations in geology, lithology, weathering, fluid content, etc.

Occur when electrodes on or near anomalous body

Affects E-fields only

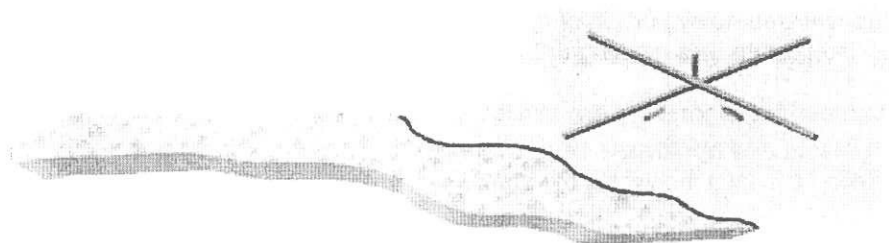
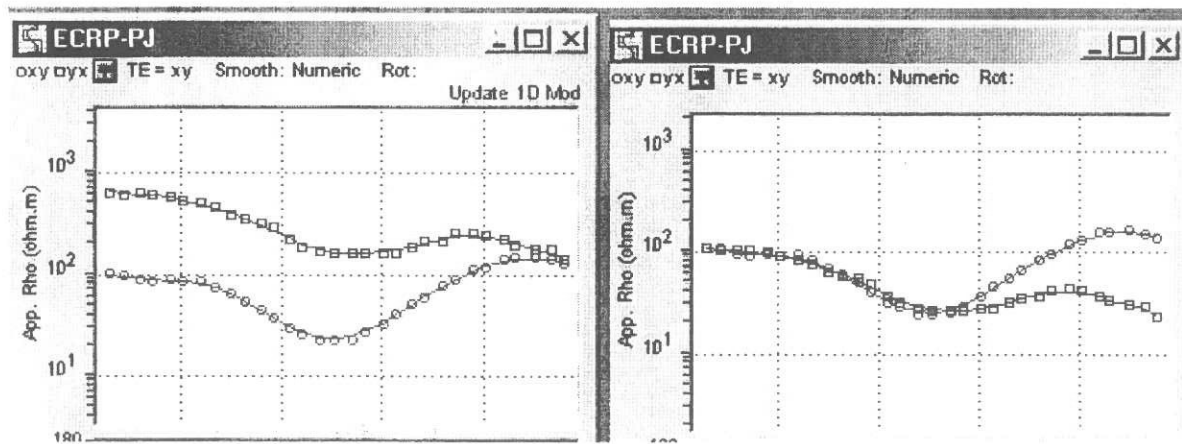


Figure 5-12: Static shifts are caused by near-surface changes in resistivity close to the E-field dipoles

Static Shifts: The effect in the data is a DC Offset between the two MT amplitude curves. The phase is not affected. Statics can greatly influence interpreted depths.



Resistivity curves before (left) and after (right) statics corrections have been applied.

#### Static Shift – Corrections

The Objective: To determine the true near-surface resistivity. The highest MT frequencies should approximate the near-surface resistivity. In order to accomplish the correction, there are a few approaches. Some approaches are:

AMT

TDEM (Time-Domain Electromagnetics)

Estimate or guess

TDEM (Time Domain Electromagnetics) is the most accurate, but requires additional separate acquisition and additional cost. A separate EM sounding is recorded at the MT station location, either before or after MT acquisition. TDEM uses a controlled-source (transmitter) and measures the shallow resistivity structure at the station without much distortion.

Many programs allow a direct comparison of the TDEM and MT data, in the frequency domain on the MT plots. This allows the interpreter to 'shift' the MT amplitude curves to match TDEM data.

Other solutions:

Compare the MT data to data from nearby MT stations. This will give a sense of near-surface resistivity for the area

Use general knowledge of surface geology to estimate what the near-surface resistivity should be

Use AMT (but AMT can show static effects also)

Static shifts are not always present and not always severe. Hence, corrections may not be necessary. Also, some modeling routines 'solve' for the statics problem.

A good reference is Sternberg et al (1998).

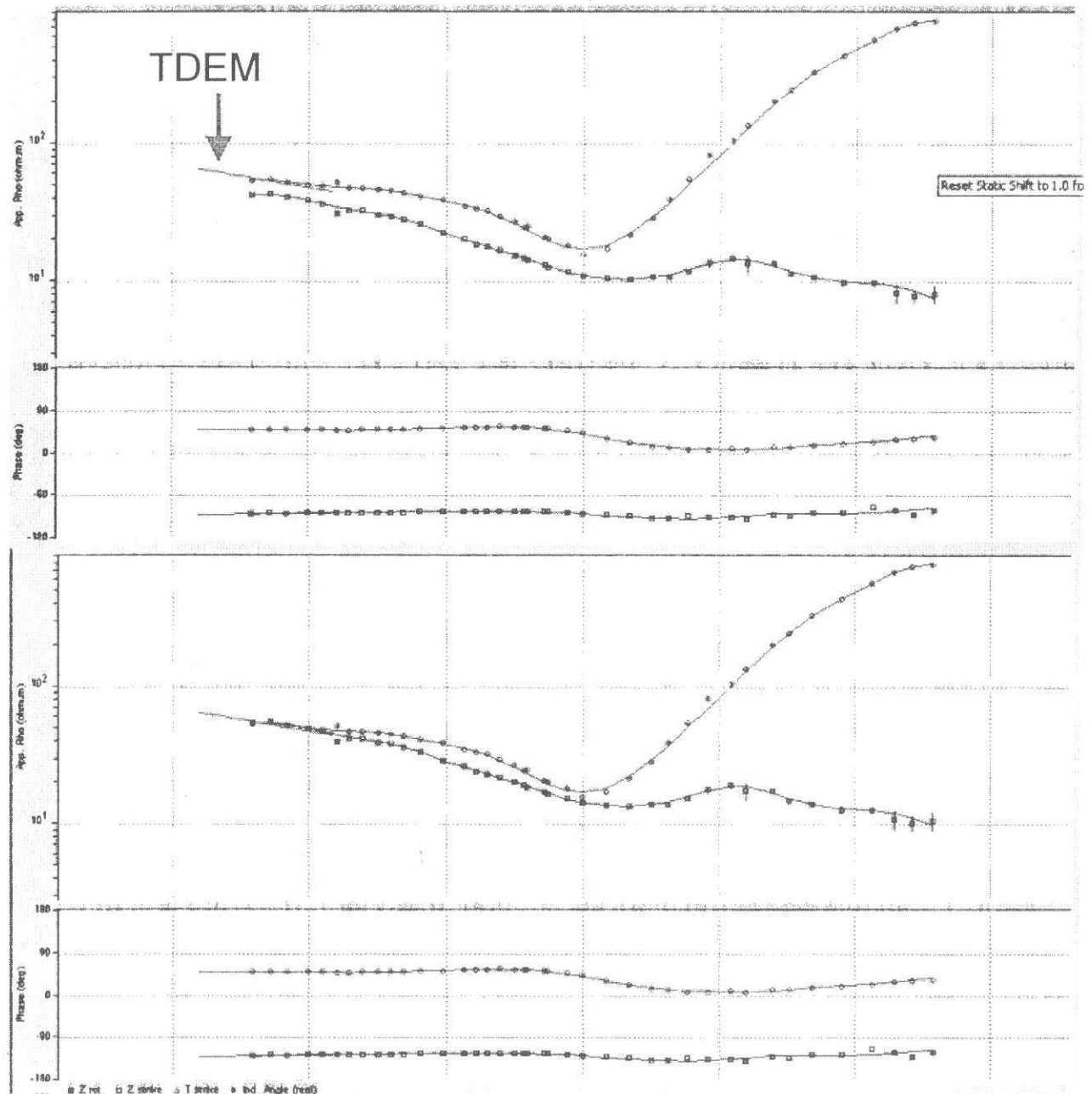


Figure 5-13: MT Curves before (top) and after (bottom) statics correction using TDEM data. The EM data have been 'placed' on the MT curves and are shown by the narrow line at high frequencies.

### 5.2.8. Numerical Modeling

In the present state of the art of numerical modeling technology, the following algorithms exist and are practical to use:

One-dimensional (1-D) forward solutions and inversion algorithms.

Two-dimensional (2-D) forward solutions and inversion algorithms.

Three-dimensional (3-D) forward solutions and inversion algorithms.

#### Modeling – In General

Use amplitude and phase and both modes (TE and TM)

Look at data – where is your ‘target’

Sometimes may be evident in only phase or only amplitude data

Be aware – don’t let computer do all the work!

#### 1-D Modeling

Many 1-D algorithms

Both forward and inverse

Useful for rough idea of subsurface

Useful for resolution studies (pre-survey)

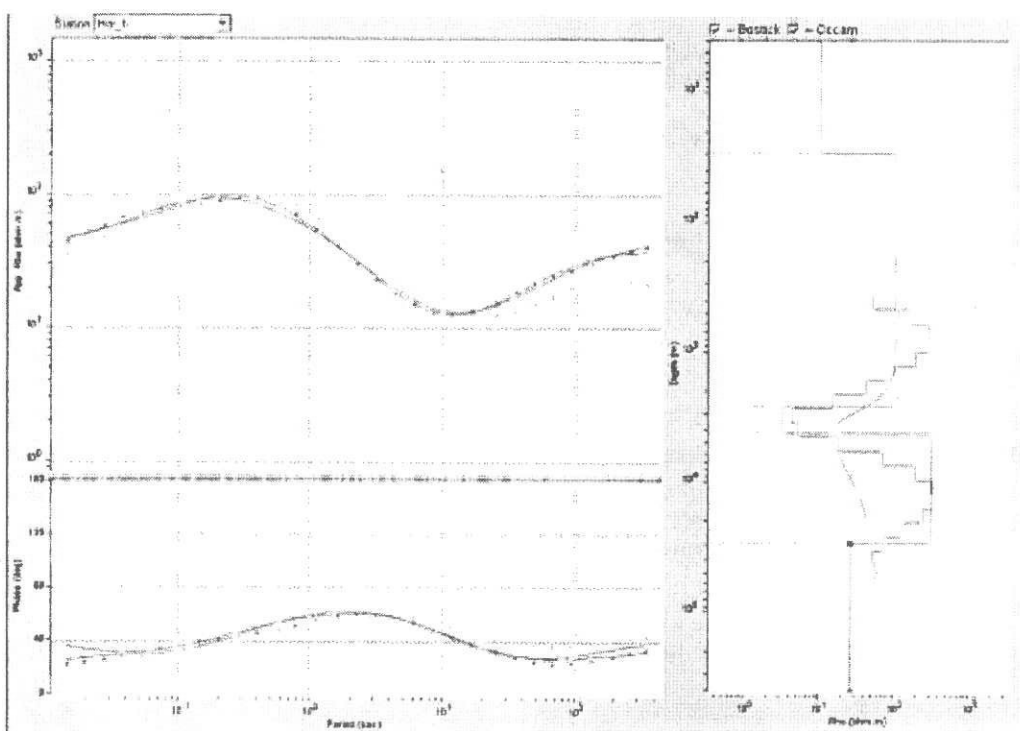


Figure 5-14: MT amplitude and phase curves (left) and three types of 1-D models. The smoothed curve is a Bostick inverse. The stepped curve is an Occam inverse. The 5-layer model is a layered forward/inverse.

1-D modeling can produce mis-leading results when applied to 2-D data. Distortion in the MT curves will cause the model to over or under estimate the true thicknesses, depending on which curve (TE or TM) is modeled and where the station is located with respect to major structural changes. The following figures help to demonstrate the problem.

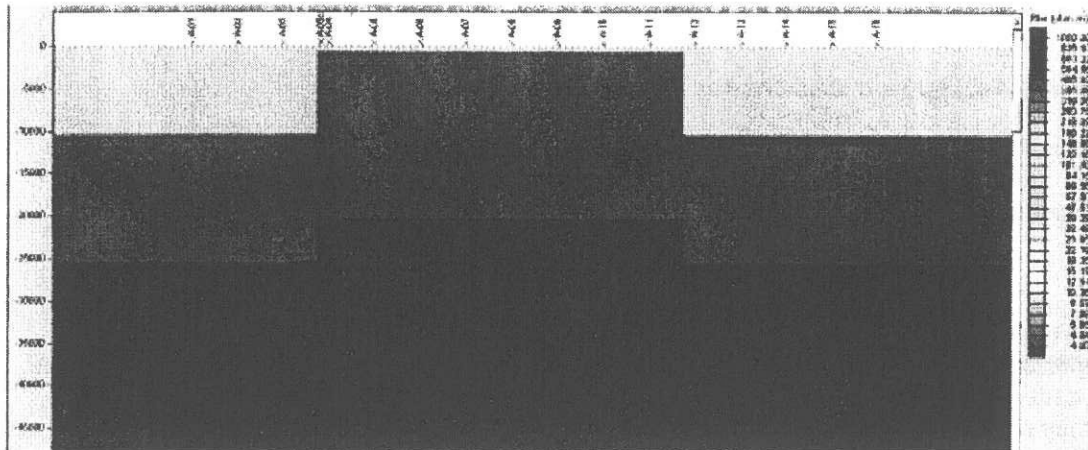


Figure 5-15: A 2-D structure. The top layer is 150 ohm-m, middle layer is 4 ohm-m and basement is 800 ohm-m. The station A-04 is located just to the right of fault.

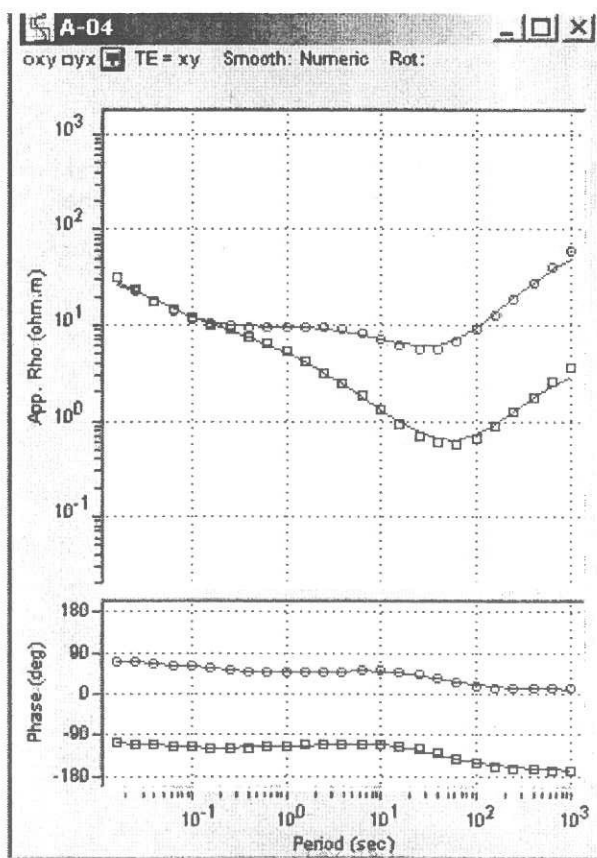


Figure 5-16: The amplitude and phase curves for station A-04. TE is the upper curve and TM is lower.

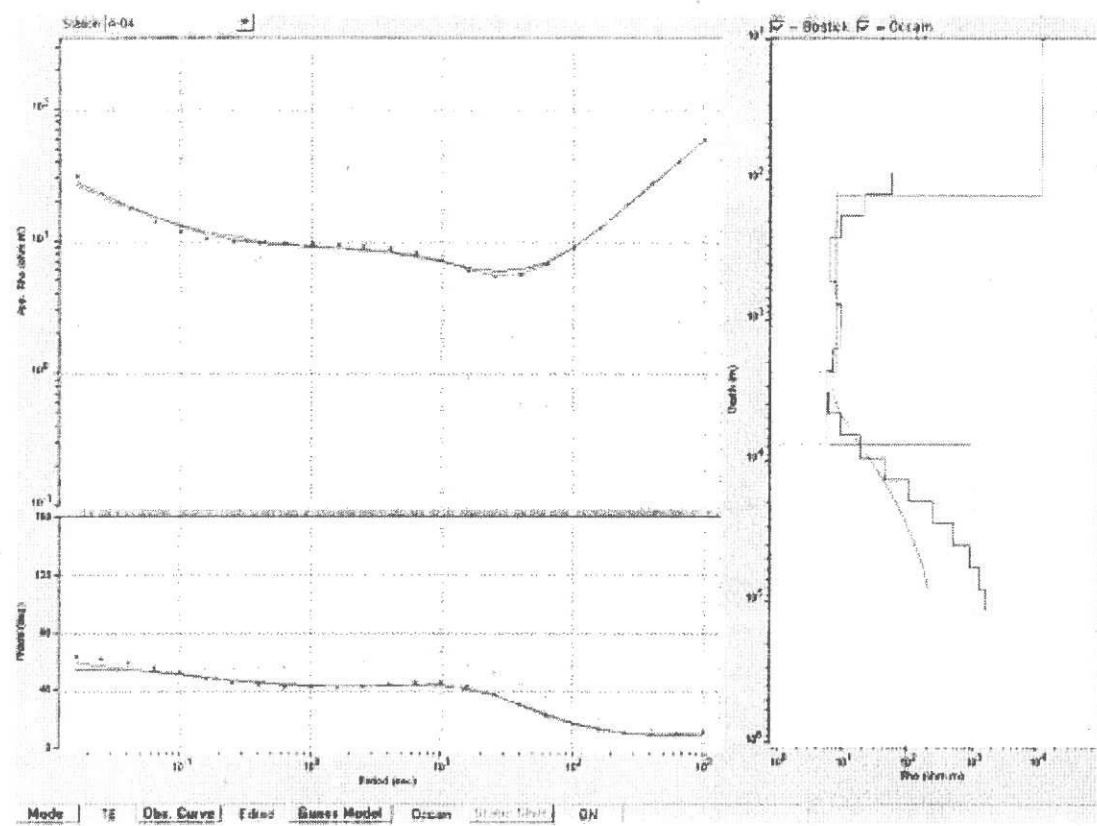


Figure 5-17: 1-D models for the TE mode, station A-04. The layered model gives thicknesses for the first two layers of 128m and 7359m, respectively. True thicknesses are 175m and 6000m. A 1-D model of the TE curve overestimates the true thicknesses.

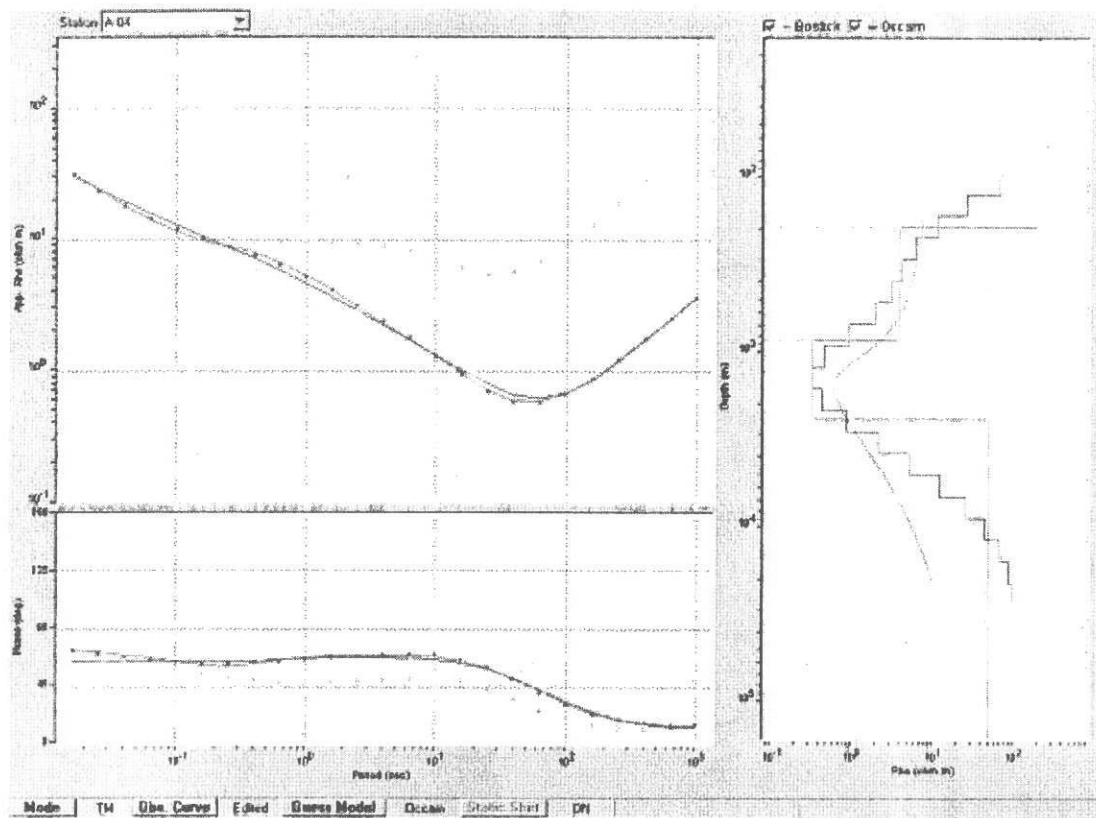


Figure 5-18 : 1-D models for the TM mode, station A-04. The layered model gives thicknesses for the first two layers of 192m and 2198m, respectively (combining layer 2 and 3 to make layer 2). True thicknesses are 175m and 6000m. A 1-D model of the TM curve underestimates the true thicknesses.

- 3-D Data – What to do?**
- Use 3-D modeling
  - Use various decomposition tools
  - Use 2-D with caution
  - Don't interpret 3-D portion of data

## **2-D and 3-D Modeling (see Mackie, included following chapter)**

### **Well Logs**

Well logs (electric logs) are extremely useful  
 Can tell roughly what resistivity of horizon is  
 Digital logs are best

### **Well logs – Resistivity indicator**

Digital Logs

- Can open in Excel or use other program
- Some workstations allow for MT modeling of e-logs
- Can run forward model off e-log data
- Determine MT response for E-log data

### **Interpretation: Good Results**

DO NOT rely just on inversions  
 CHECK your inversions with some forward models  
 CHECK for problems in models (boundary conditions, structures added out of 'area')  
 INTEGRATE your modeling with any other info you can get  
 Well logs, geology, other geophysics

### **Interpretation: Presentation**

MAKE sections look 'geologic'  
 DON'T overwhelm audience with MT details

### **Interpretation: Pre-Survey**

It is always good practice to run models prior to contracting for a survey.  
 This will ensure that efforts and money are worthwhile  
 Keeps clients and managers happy!

### **Interpretation: Summary of steps**

There is a fairly standard rational succession of interpretation procedures that are followed whenever a magnetotelluric data set is interpreted. These are summarized, in the order they are usually performed, as follows.

1. Qualitative analyses - followed by an immediate notification to the client if there are any significant preliminary conclusions.
2. Reformatting, Reprocessing, and Data Correction - if necessary.
3. One-dimensional inversions or forward models - if appropriate.

4. Unconstrained 2-D and/or 3-D inversions or fitted sections - as a first interpretative step in a profile analysis.
5. Constrained two-dimensional inversion - if sufficient geometric constraints (such as an interpreted seismic model or drilling data) exist to justify it.
6. Final trial-and-error refinement of 2-D resistivity models - incorporates available isolated constraints (well logs, surface geology) and most probable geologic hypotheses.
7. Construction of final interpreted geologic model - from refined resistivity section.



# Multi-dimensional Magnetotelluric Modeling and Inversion

Randall Mackie

*GSY-USA, Inc.  
2261 Market St., PMB 643  
San Francisco, California 94114*

*randy@gsy-usa.com*

October 2, 2002

# 1 Introduction

Early work in magnetotellurics (MT) always dealt with one-dimensional (1D) interpretations because they were simple and analytic solutions existed for the 1D problem. A 1D model is made up of a stack of horizontal layers and each layer is assumed to have a uniform electrical resistivity. We have come to learn, however, that 1D interpretations are rarely accurate and are often completely wrong or misleading, and consequently, MT has suffered from the poor results obtained by such interpretations. It is true that MT is a wave phenomenon and thus has analogies to seismic methods, but they must be used with care. MT is actually very closely related to the seismic phenomenon of surface waves. In both cases, information about the variation of the physical properties with depth is contained in the frequency response. It is often said that the damped nature of such waves reduces the depth resolution to some large fraction of the depth. When data are crude, this is correct, but the better the data, the more one can refine the interpretation and increase the resolution. Instrumentation and robust processing methods have improved considerably in recent years while interpretation technology has lagged behind. While this is due to the fact that smaller efforts have been put into MT than seismic, for example, it is also due to the fact that the MT interpretation problem is intrinsically more difficult. This is because MT is a very three-dimensional (3D) phenomena and because the electrical contrasts in nature can vary by orders of magnitude, making simplifications like perturbation methods inapplicable to MT. Compare this to seismic where velocity variations are typically very small, on the order of a few percent.

The 3D nature of MT shows up in two very different but very common situations. In the first, because of the continuity of current flow, small near surface regions with anomalous conductivity cause large changes in the electric field amplitudes over these areas. This effect is called a static shift since it occurs for all frequencies whose fields penetrate deeper than the anomalous region. (This term is borrowed from the seismic case where an anomalous near surface velocity change will cause a time shift of all reflections coming from below that anomalous zone.) The phase of the electric field does not change, however, and if one has data from neighboring regions, the static shift is easy to spot.

The second example, which is the regional problem, is not as well recognized as the static shift problem. The continuity of current, which caused the static shift, was also responsible for the lack of phase changes. The continuity of current implies that every current filament has its own phase which is invariant along its entire path. Thus, some current mixing is required to produce phase changes as a function of position. When different regions have different conductivity depth structures, they should have different magnetotelluric phases. However, if the conductivity structures discourage current mixing, these differences are reduced. Perhaps one of the most severe examples of this is the ocean-continent boundary. Because the ocean is such a good conductor, most of the current remains in the ocean even at periods as long as 12 hours. On the continents at these same long periods, most of the current is in the mantle. If there is a resistive crust that prevents the ocean currents from mixing easily with the mantle currents, then the result is that the telluric currents in the crust near the ocean will have phases associated with the ocean electric currents. These phase anomalies can persist inland for hundreds of kilometers. Consequently, any interpretation that does not include the ocean, even though it may be a great distance away from the survey area, will likely be incorrect or biased.

In resource exploration, we are not usually concerned with the mantle, but we can see similar

effects due to conductive basins in more resistive backgrounds. In this case, the current system in the conductive basin can be considerably affected by the more resistive background. To properly deal with this, one needs regional data, and multi-dimensional interpretation.

## 2 The Forward Problem

Interpreting MT data requires modeling to know if the interpretation is compatible with the data. In a 3D situation, the number of models that one could generate is so great that some sort of automated way is needed to find a model. The problem of finding a model that fits the observed data is called the inverse problem. Other terms one might hear are inverse boundary value problem, synthesis, or parameter estimation. The term inverse boundary value problem comes from its relationship to the boundary value problem, which is predicting the data given a model. This is also called the forward problem. The inverse boundary value problem is predicting the model given the data, a much more difficult problem than the forward problem. Inverse problems will be detailed in a later section.

There are five common approaches to solving the forward problem: analytic methods, boundary or volume integral methods, Fourier methods, finite difference, and finite element methods. There are also hybrid methods involving various combinations of these basic methods. In this course we will not make a complete study of the differences between the methods, but we can make a few general comments. First, analytical methods are usually restricted to very simple situations, such as the 1D problem [Kaufman and Keller, 1981] and the 2D problem consisting of a horizontal slab divided into three regions, which includes as special cases the vertical fault, the dike, and the quarter-space model [d'Erceville and Kunetz, 1962; Rankin, 1962, and Weaver, 1963]. Integral equation methods are probably the next best efficient method when the anomalous regions defines only a few boundaries and consequently they have seen a tremendous amount of work in 3D MT modeling efforts [e.g., Hohmann, 1975; Weidelt, 1975; Wannamaker et al., 1984; San Filipo and Hohmann, 1985; Wannamaker, 1991]. However, as the number of boundaries increases, the efficiency of the method decreases dramatically. In our inverse problem formulation that we will study later, we really want to be able to model a fully inhomogeneous media, and such problems are best suited to finite difference or finite element methods [e.g., Jones and Pascoe, 1972; Reddy et al., 1977; Mackie et al., 1993; Smith, 1996a; Smith, 1996b]. Finite element methods can more accurately model irregular boundaries, but finite difference equations are the simplest to implement. Finite difference equations are not very different from finite element methods, but we prefer the simplicity of finite difference schemes.

### 2.1 Finite Difference Equations In 3D

Our finite difference algorithm is based on the integral forms of Maxwell's equations rather than the differential forms, and although this leads to the same difference equations, it also has several important conceptual advantages. First, finite differences based on differential equations are approximations to the pointwise derivatives using numerical differences. However, starting from the integral forms of Maxwell's equations gives one a simple geometrical understanding of the coupling between the electric and magnetic fields. Furthermore, the resulting difference equations

result naturally from the application of contour integrals to flat surfaces defined by a regular discretization of space. And finally, the integral equations are involved with averages rather than approximations to derivatives, which seems to be a more natural approach to a discretized approximation than trying to define finite difference approximations to derivatives.

At the frequencies involved in MT exploration, conduction currents dominate over displacement currents. Therefore the integral forms of Maxwell's equations, assuming an  $e^{-i\omega t}$  time dependence, are given by

$$\oint \mathbf{H} \cdot d\mathbf{l} = \iint \mathbf{J} \cdot d\mathbf{S} = \iint \sigma \mathbf{E} \cdot d\mathbf{S} \quad (1)$$

$$\oint \mathbf{E} \cdot d\mathbf{l} = \iint i\mu\omega \mathbf{H} \cdot d\mathbf{S} \quad (2)$$

where in general  $\mu$  and  $\sigma$  are tensor quantities [Stratton, 1941]. We can define a difference scheme such that either (1) or (2) is exactly satisfied but not such that both are exactly satisfied. For example, if we divide Earth up into rectangular blocks with  $\mathbf{H}$  defined as the average along the block edges and  $\sigma\mathbf{E}$  defined as the average across the block faces, then the resulting difference equations would be exact for (1). However, this would be inconsistent with (2) since in that equation  $\mathbf{E}$  is defined as the average along a contour and  $\mathbf{H}$  is defined as the average across the surface enclosed by the contours. It is this inconsistency that makes these difference equations an approximation, but it should be remembered that all difference equations are approximations.

For our modeling algorithm we have chosen to divide Earth up into rectangular blocks with the  $\mathbf{H}$  fields defined along the block edges and the  $\mathbf{J}$  and  $\mathbf{E}$  fields defined along the normals to the block faces, as shown in Figure 1. This is equivalent to the staggered grid formulation of Yee [1966] and more recently of J. T. Smith [1993a]. With this formulation the contours for (1) are simply taken around the faces of the blocks, and the contours for (2) are taken around flat surfaces centered on the block edges and outlined by the normals to the block faces, as shown in Figure 1.

With the geometry shown in Figure 1, the  $x$  component of (1) is

$$\begin{aligned} & [H_z(i, j+1, k) - H_z(i, j, k)] \Delta z_k - [H_y(i, j, k+1) - H_y(i, j, k)] \Delta y_j \\ & = J_x(i, j, k) \Delta z_k \Delta y_j \end{aligned} \quad (3)$$

where  $\Delta z_k$  and  $\Delta y_j$  are the block spacings. The  $y$  and  $z$  components for this and the following equations can be derived in a similar fashion and therefore will not be written out for the sake of brevity.

Likewise, the  $x$  component of (2) can be written as

$$\begin{aligned} & [E_z(i, j, k) - E_z(i, j-1, k)] \Delta z_{k-1/2} - [E_y(i, j, k) - E_y(i, j, k-1)] \Delta y_{j-1/2} \\ & = i\omega\mu H_x(i, j, k) \Delta z_{k-1/2} \Delta y_{j-1/2}, \end{aligned} \quad (4)$$

where  $\Delta z_{k-1/2}$  and  $\Delta y_{j-1/2}$  are the distances between midpoints of the blocks defined by the normals to block faces.

Since the  $\mathbf{E}$  fields are specified as averages across block faces, they will suffer discontinuities if adjoining blocks have different conductivities. Thus we define the  $\mathbf{E}$  fields as the average of the  $\mathbf{E}$  fields on either side of the block face. Since  $\mathbf{J}$  is continuous, this can be written for the  $x$  component as

$$E_x(i, j, k) = \frac{\rho(i, j, k)\Delta x_i + \rho(i-1, j, k)\Delta x_{i-1}}{\Delta x_i + \Delta x_{i-1}} J_x(i, j, k) = \rho_x(i, j, k) J_x(i, j, k) \quad (5)$$

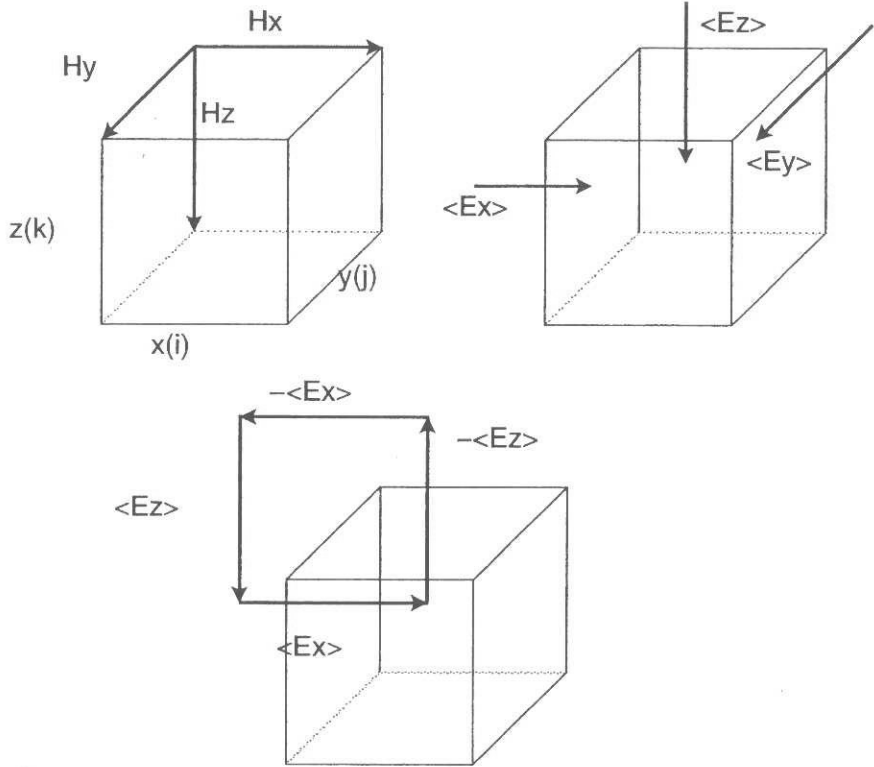


Figure 1: The difference equation geometry based on the integral forms of Maxwell's Equations.

where  $\rho_x(i, j, k)$  refers to the average resistivity in the  $x$  direction defined as in (5).

We can use (3) and its  $y$  and  $z$  components, along with (5), to eliminate the  $\mathbf{E}$  fields from (4). This results in a second-order equation in  $\mathbf{H}$ . The  $x$  component is given as

$$\begin{aligned}
 i\omega\mu H_x(i, j, k) \Delta x_i \Delta y_{j-1/2} \Delta z_{k-1/2} = & \\
 \rho_z(i, j, k) \left[ \frac{H_y(i+1, j, k) - H_y(i, j, k)}{\Delta x_i} + \frac{H_x(i, j, k) - H_x(i, j+1, k)}{\Delta y_j} \right] \Delta x_i \Delta z_{k-1/2} & \\
 - \rho_z(i, j-1, k) \left[ \frac{H_y(i+1, j-1, k) - H_y(i, j-1, k)}{\Delta x_i} + \frac{H_x(i, j-1, k) - H_x(i, j, k)}{\Delta y_{j-1}} \right] \Delta x_i \Delta z_{k-1/2} & \\
 - \rho_y(i, j, k) \left[ \frac{H_x(i, j, k+1) - H_x(i, j, k)}{\Delta z_k} + \frac{H_z(i, j, k) - H_z(i+1, j, k)}{\Delta x_i} \right] \Delta x_i \Delta y_{j-1/2} & \\
 + \rho_y(i, j, k-1) \left[ \frac{H_x(i, j, k) - H_x(i, j, k-1)}{\Delta z_{k-1}} + \frac{H_z(i, j, k-1) + H_z(i+1, j, k-1)}{\Delta x_i} \right] \Delta x_i \Delta y_{j-1/2} &
 \end{aligned} \tag{6}$$

Similar equations can be defined for the  $y$  and  $z$  components of the magnetic field. We group these second-order equations together in the form

$$\mathbf{A}\mathbf{x} = \begin{bmatrix} M_{xx} N_{xy} N_{xz} \\ N_{yx} M_{yy} N_{yz} \\ N_{zx} N_{zy} M_{zz} \end{bmatrix} \begin{bmatrix} H_x \\ H_y \\ H_z \end{bmatrix} = \mathbf{b}, \tag{7}$$

where  $\mathbf{b}$  contains the terms associated with the known boundary values and source field. This system of equations is sparse, symmetric, and complex (all elements are real except for the diagonal elements). Once this system has been solved for the  $\mathbf{H}$  fields, the  $\mathbf{E}$  fields can be determined by application of the curl of  $\mathbf{H}$  and Ohm's Law, equations (3) and (5). The  $\mathbf{H}$  fields can be directly interpolated to wherever they are required. Since the normal components of the  $\mathbf{E}$  field are discontinuous across conductivity contrasts, the currents  $\mathbf{J}$  are interpolated first and then converted to an electric field by use of Ohm's Law.

## 2.2 Boundary Conditions

In our modeling algorithm we assign the tangential  $\mathbf{H}$  fields on the boundaries of the model for the appropriate source polarization. These boundary values come from a two-dimensional (2-D) TM mode or TE mode calculation depending on whether or not a regional strike is detected. If a regional strike is detected, then the appropriate mode is used, depending on the strike and the polarization being solved, otherwise, a TE mode calculation for the appropriate edges of the model is done, and the values are interpolated to the interior of the model and used as starting values for a conjugate gradient solution.

We add several air layers on top of the Earth model with an approximately logarithmically increasing thickness for each air layer. The layers should be extended far enough above Earth to allow the longest wavelength perturbations to be damped out (we typically use a distance that is about three times the largest wavelength of the horizontal conductivity variations in the Earth model). These air layers are given a finite, but high, resistivity value of  $10^{10} \Omega m$  since the difference equations require a resistivity value for each model block, and this value provides a large contrast to Earth but is not too large to cause numerical instabilities. The air layers are necessary to allow the geometric perturbations in the  $\mathbf{H}$  field to damp out above Earth. The source field for the MT problem is a uniform current sheet that we put at Earth's surface. This current sheet can be put anywhere above Earth's surface as long as we allow for secondary outgoing fields above it. At the top of the air layers, a one-dimensional (1-D) plane wave impedance for outgoing fields is used. Likewise, a 1-D plane wave impedance for a layered media is used at the bottom of the Earth model.

## 2.3 Conjugate Gradient Relaxation

Conjugate gradient relaxation [Hestenes and Stiefel, 1952] is an iterative method for finding the solution to real, symmetric, and positive-definite systems of equations  $\mathbf{Ax} = \mathbf{b}$ , such as would arise in numerically solving partial differential equations. In theory, conjugate gradients will exactly solve a system of equations in a finite number of steps. In practice, this is not possible because of roundoff errors, but very accurate results are often obtained after a modest number of iterations for a wide range of problems.

The solution of the electromagnetic equations, however, is more complicated because it involves complex systems of equations, which though not hermitian (complex conjugate symmetric), are symmetric. The only complex elements in the second-order system of equations for the MT problem (see (6)) are on the diagonal of the matrix, and these are equal to  $i\mu\omega + \sum \rho$ . All other elements are real, related to the resistivities of the model blocks, and at the low frequencies

involved in MT exploration will almost always be larger in magnitude than the imaginary part of the diagonal terms. There are several possible ways to deal with complex symmetric systems, and such methods are explored in great detail by Sarkar et al. [1988] and Sarkar [1991].

One commonly-used approach is a recently developed algorithm called the quasi minimum residual (QMR) algorithm [Freund, 1992] that is related to the nonsymmetric Lanczos algorithm for complex matrices. In this algorithm a measure of the error closely related to the norm of the residual is minimized at each relaxation step. The resulting algorithm has a smoothly, but not monotonically, decreasing residual norm at each relaxation iteration.

However, the algorithm that we have come to prefer for the MT problem is the complex bi-conjugate gradient algorithm for general complex matrices [Jacobs, 1986]. While this algorithm in theory will exactly solve a complex system in a finite number of steps, it does not minimize any meaningful measure of the error. Consequently, the norm of the residual, which is often the only measure of the error that we have, may exhibit erratic fluctuations during the relaxation. (The norm of the residual at the *i*th iteration is given by  $\| \mathbf{r}_i \| = \| \mathbf{b} - \mathbf{Ax}_i \|$ .) Nonetheless, when used in conjunction with a good preconditioner and a scheme for eliminating any divergence of the magnetic field every few iterations [Mackie et al, 1994], we have found that it works extremely well with fairly smooth reduction of the norm of the residual. The preconditioner that we currently use is an incomplete LU decomposition of the diagonal sub-blocks of (7) with fill-in.

## 2.4 Meshing a 3D model

It is critical when building a 3D model that the mesh is designed to be as accurate as possible, which requires small block sizes. On the other hand, we want the total number of blocks to be as small as possible so that we can obtain a solution in a reasonable amount of time and without requiring the resources of a supercomputer. This is made worse by the fact in MT that we are typically dealing with frequencies from approximately 500 Hz - 0.001 Hz. Because of skin depth arguments, lower frequency data sample great depths and greater distances in the model. However, because of the damped nature of electromagnetic fields, we can accommodate all these requirements by models that have block sizes increasing with depth and out to the sides in an approximately logarithmic fashion. These types of meshes have been shown to be quite accurate over the frequency ranges of interest in MT. Some rules of thumb that can be used when building models for MT modeling and inversion follow.

### 2.4.1 VERTICAL DISCRETIZATION

- Surface layer thickness: 1/10 skin depth at shortest period in most conductive surface block
- increase the thickness of each layer by factor of 1.2 to 1.5 until the block thickness is  $\geq 1/3$  skin depth in the deep model at longest period.

### 2.4.2 HORIZONTAL DISCRETIZATION

- Columns widths can increase away from the stations by a factor of 1.5 until the block width is about the same width as the thickness of the deepest layer in the model. Ideally, one would want the model to be about twice as wide as it is deep.

- For typical MT surveys, column widths should be on the order of a few hundred meters. You may need to make them bigger for regional surveys, or when stations are widely spaced. If you have enough sites so as not to alias the lateral response variation, then one block/site should be fine.
- Block widths can increase by a factor of 1.2 to 1.5 in between stations depending on the spacing.
- You should try to make the block widths as uniform as possible within the area bounded by the stations.

## 2.5 Finite Difference Equations In 2D

We started out with the finite difference equations for 3D geometries because in a sense, they are easier to deal with because you have one set of equations to deal with the electromagnetic fields. In a 2D geometry, where the resistivity varies in only two dimensions, Maxwell's equations decouple into two different modes. One mode is called the transverse magnetic (TM) mode, in which the magnetic field is parallel to the strike direction. The second mode is called the transverse electric (TE) mode, in which the electric field is parallel to the strike direction. Everything we said about solving the 3D case is also applicable to the 2D case. Like the 3D case, we solve the 2D set of equations using difference equations.

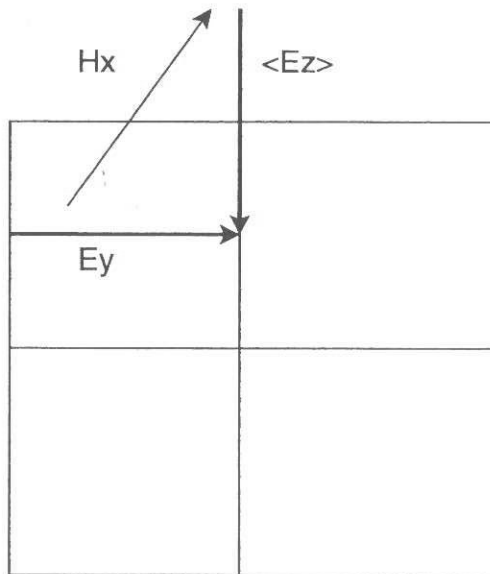


Figure 2: The difference equation geometry for the TM mode.

Assume the x-axis is along the strike direction, the y-axis is to the right, and the z-axis down. For the TM mode, we have the fields  $E_y$ ,  $E_z$ , and  $H_x$ . The resistivity is a function of  $y$  and  $z$  only, and is invariant in the  $x$  direction. With the geometry shown in Figure 2, we can write (1) for the

TM mode as

$$[H_x(j-1, k) - H_x(j, k)] \Delta x = J_z(j, k) \Delta x \Delta y_{j-1/2} \quad (8)$$

$$[H_x(j, k+1) - H_x(j, k)] \Delta x = J_y(j, k) \Delta x \Delta z_k \quad (9)$$

$H_x$  is invariant along the x-axis, and one can see that the  $\Delta x$  cancels out of both sides of the equations. We can also write down the x component of equation (2):

$$\begin{aligned} &[-E_y(j, k) + E_y(j, k-1)] \Delta y_j + [-E_z(j, k) + E_z(j+1, k)] \Delta z_{k-1/2} \\ &\quad = i\mu\omega H_x(j, k) \Delta y_j \Delta z_{k-1/2} \end{aligned} \quad (10)$$

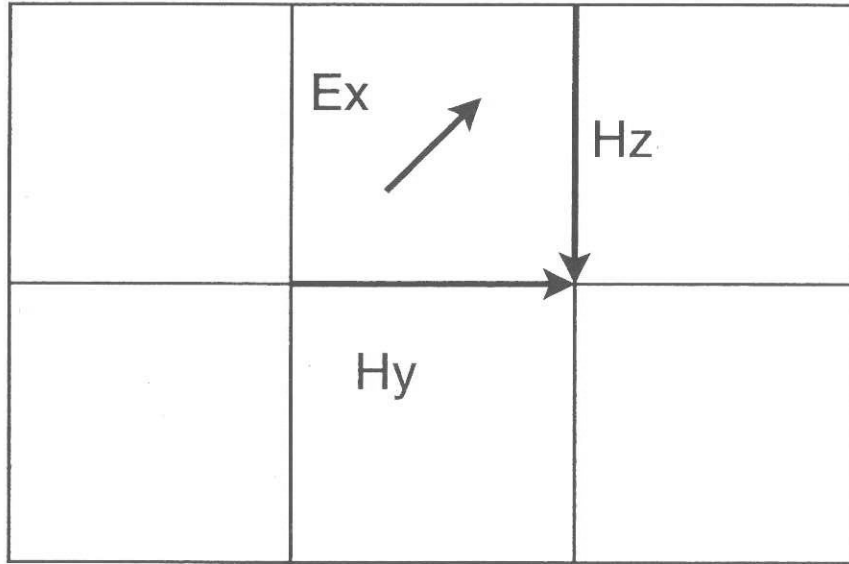


Figure 3: The difference equation geometry for the TE mode.

For the TE mode, we have the fields  $E_x$ ,  $H_y$ , and  $H_z$ . Using the difference equation geometry shown in Figure 3, we can then write down the equations for the TE mode as follows.

$$\begin{aligned} &[H_y(j, k) - H_y(j, k+1)] \Delta y_j + [H_z(j+1, k) - H_z(j, k)] \Delta z_k \\ &\quad = \sigma E_x(j, k) \Delta y_j \Delta z_k \end{aligned} \quad (11)$$

$$[E_x(j-1, k) - E_x(j, k)] \Delta x = i\mu\omega H_z(j, k) \Delta y_{j-1/2} \Delta x \quad (12)$$

$$[E_x(j, k) - E_x(j, k-1)] \Delta x = i\mu\omega H_y(j, k) \Delta z_{k-1/2} \Delta x \quad (13)$$

As in the 3D case, we can group these equations together into linear systems that are sparse, complex, and symmetric, and can be solved very quickly and efficiently with conjugate gradient algorithms. For more details on 2D finite difference solutions, see Swift [1967], Brewitt-Taylor and Weaver [1976], and Weaver [1994].

### 3 Inversion

Much of what is written below is taken verbatim from an article I co-authored with William Rodi at MIT [Rodi and Mackie, 2001], and is used here with his permission. Details on 2D MT inversion can be found in that article.

#### 3.1 Background

The standard approach to solving nonlinear inverse problems in geophysics has been iterated, linearized inversion. That is, the forward function (for predicting error-free data) is approximated with its first-order Taylor expansion about some reference model; a solution of the resulting linear inverse problem is computed; the solution is then taken as a new reference model and the process is repeated. Such schemes are generally some form of Newton's method (typically Gauss-Newton or Levenberg-Marquardt). When run to convergence they minimize an objective function over the space of models and, in this sense, produce an optimal solution of the nonlinear inverse problem. Most inversion algorithms for magnetotelluric (MT) data have been iterated, linearized methods. For 1-D earth models these include the algorithms of Wu [1968] and Jupp and Vozoff [1975], which obtain nonlinear least-squares solutions, and those of Smith and Booker [1988] and Constable, Parker and Constable [1987], which find nonlinear least-squares solutions subject to a smoothness constraint ('regularized' solutions). Jupp and Vozoff extended their algorithm to the case of 2-D models [Jupp and Vozoff, 1977] while algorithms for finding regularized solutions of the 2-D MT problem have been presented by Jiracek, Rodi and Vanyan [1987], Madden and Mackie [1989], Rodi [1989], deGroot-Hedlin and Constable [1990], and Smith and Booker [1991]. Mackie and Madden [1993] implemented an iterated, linearized inversion algorithm for 3-D MT data, as did Newman [1995] and Newman and Alumbaugh [1997] for the related problem of crosswell electromagnetic data. However, the usefulness of such algorithms in 3-D electromagnetic inverse problems has been hampered by severe computational difficulties, which we now discuss.

Compared to global optimization methods like grid search, Monte-Carlo search and genetic algorithms, inversion methods that make use of the Jacobian (first-order derivative) of the forward function, like those cited in the previous paragraph, generally require the testing of many fewer models to obtain an optimal solution of an inverse problem. This fact is of critical importance in 2-D and 3-D electromagnetic inverse problems where the forward function entails the numerical solution of Maxwell's equations, and is the reason that iterated, linearized methods have occupied center stage in electromagnetic inversion despite their greater susceptibility to finding locally rather than globally optimal solutions. On the other hand, generation of the Jacobian in these same problems multiplies the computational burden many times over that of evaluating the forward function alone, even when efficient reciprocity techniques [Madden, 1972; Rodi, 1976; McGillivray and Oldenburg, 1990] are exploited. Moreover, iterated, linearized inversion methods, done to prescription, have the additional computational chore of solving a linear system on the model space at each iteration step. These two tasks—generating the Jacobian and linear inversion—dominate the computations in 2-D and 3-D MT inversion, where the number of data and model parameters are typically in the hundreds or thousands. The computation of optimal solutions to the 2-D MT inverse problem can require several hours of CPU time on a modern workstation, while computing optimal solutions of the 3-D problem is impractical on the computers widely available today.

This computational challenge has motivated various algorithmic shortcuts in 2-D and 3-D MT inversion. One approach has been to approximate the Jacobian based on electromagnetic fields computed for homogeneous or 1-D earth models, which has been used in 2-D MT inversion by Smith and Booker [1991] in their ‘rapid relaxation inverse’ (RRI) and by Farquharson and Oldenburg [1996] for more general 2-D and 3-D electromagnetic problems. Other workers have sought approximate solutions of the linearized inverse problem. In this category is the method of Mackie and Madden [1993], which solves each step of a Gauss-Newton iteration incompletely using a truncated conjugate gradients technique. In addition to bypassing the complete solution of a large linear system, the algorithm avoids computation of the full Jacobian matrix in favor of computing only its action on specific vectors. Although not as fast as RRI, the Mackie-Madden algorithm does not employ approximations to the Jacobian and requires much less computer time *and* memory than the traditional iterated, linearized inversion methods (as we will demonstrate in this paper). Also in this category is the ‘subspace method’, applied by Oldenburg, McGillivray and Ellis [1993] to d.c. resistivity inversion and by others to various other geophysical inverse problems. This method reduces the computational burden by solving each linearized inverse problem on a small set of judiciously calculated ‘search directions’ in the model space.

In their use of incomplete solutions of the linearized inverse problem, the subspace and Mackie-Madden inversion methods depart from the strict schema of iterated, linearized inversion, with an accompanying reduction in the computer resources needed to solve large, nonlinear inverse problems. Our 2D and 3D MT inversion algorithms are based on an approach to electromagnetic inversion that is a further departure from the geophysical tradition: *nonlinear* conjugate gradients (NLCG), or conjugate gradients applied directly to the minimization of the objective function prescribed for the nonlinear inverse problem. The use of conjugate gradients for function minimization is a well-established optimization technique [Fletcher and Reeves, 1959; Polak, 1971] and was suggested for nonlinear geophysical inverse problems by Tarantola [1987]. It has been applied to varied geophysical problems, including crosswell traveltime tomography [Matarese and Rodi, 1991; Matarese, 1993], crosswell waveform tomography [Thompson, 1993; Reiter and Rodi, 1996], and d.c. resistivity [Ellis and Oldenburg, 1994; Shi, Rodi, Mackie and Zhang, 1996].

### 3.2 The Inverse Problem

We can write the inverse problem as

$$d = F(m) + e$$

where  $d$  is a data vector,  $m$  is a model vector,  $e$  is an error vector, and  $F$  is a forward modeling function, which could be, for example, our 3D finite difference modeling program described previously. In 2D MT inversion, we take  $d = [d^1 \ d^2 \ \dots \ d^N]^T$  with each  $d^i$  being any combination of the magnetic transfer function or the log amplitude or phase of  $\rho_{app}$  for a particular polarization (TE or TM), observation site, and frequency ( $\omega$ ). In our 3D MT inversion, the data are the real and imaginary parts of each element of the impedance tensor. We take  $m = [m^1 \ m^2 \ \dots \ m^M]^T$  to be a vector of parameters that define the resistivity function. Being consistent with the numerical forward modeling scheme, we let  $M$  be the number of model blocks and each  $m^j$  be the logarithm of resistivity ( $\log \rho$ ) for a unique block.

We solve the inverse problem in the sense of Tikhonov and Arsenin [1977], taking a ‘regularized solution’ to be a model minimizing an objective function,  $\Psi$ , defined by

$$\Psi(m) = (d - F(m))^T V^{-1} (d - F(m)) + \lambda m^T L^T L m \quad (14)$$

for given  $\lambda$ ,  $V$  and  $L$ . The ‘regularization parameter’,  $\lambda$ , is a positive number. The positive-definite matrix  $V$  plays the role of the variance of the error vector  $e$ . The second term of  $\Psi$  defines a ‘stabilizing functional’ on the model space. Typically the matrix  $L$  is chosen to be a simple, second-difference operator such that, when the grid of model blocks is uniform,  $Lm$  approximates the Laplacian of  $\log \rho$ .

### 3.3 Gauss-Newton Method

The **Gauss-Newton** algorithm is a common geophysical inversion method to minimize (14). This algorithm generates a model sequence  $m_0, m_1, \dots$ , by solving

$$(A_j^T R_{dd}^{-1} A_j + \tau L^T L)(m_{j+1} - m_j) = -\frac{1}{2} g_j \quad (15)$$

where

$$\begin{aligned} A_j &= \text{Frechet derivative of } F \text{ evaluated at } m_j \\ g_j &= \text{gradient of } S \text{ evaluated at } m_j \\ &= 2A_j^T R_{dd}^{-1} (F(m_j) - d) + 2\tau L^T L(m_j - m_o). \end{aligned}$$

- The model  $m_{j+1}$  solves a linearized version of the inverse problem, with  $F$  approximated by its linearization about  $m_j$ .
- The Gauss-Newton algorithm solves the linear system in (15) by inverting the matrix  $A_j^T R_{dd}^{-1} A_j + \tau L^T L$ . The elements of  $A_j$  are computed using reciprocity. This involves computing an extra MT forward problem for each frequency *and* each station.
- For numerical stability, a Marquardt-Levenberg modification of Gauss-Newton can be used, i.e.

$$m_{j+1} = m_j - \frac{1}{2} (A_j^T R_{dd}^{-1} A_j + \tau L^T L + \epsilon I)^{-1} g_j$$

where  $\epsilon$  is a small number.

- This algorithm is the conventional approach used in geophysical inverse problems, but for large models and large datasets, the computation time and memory requirements may become prohibitive. Consequently, this led us to develop a faster algorithm based on the method of conjugate gradients, described next.

### 3.4 Non-Linear Conjugate Gradients

**Non-linear conjugate gradients** applies directly to the minimization of (14). The model sequence is given by

$$m_{j+1} = m_j + \alpha_{j+1} h_{j+1}$$

where  $h_{j+1}$  is a given search direction.

- Like linear conjugate gradients, NLCG computes the search directions as

$$h_{j+1} = C_j g_j + \beta_j h_j,$$

where the operator  $C_j$  is known as the pre-conditioner.

- Unlike linear conjugate gradients,  $\alpha_{j+1}$  is computed to minimize the exact  $S$ . This involves an iterative line minimization procedure.

— In our NLCG algorithm, the line minimization automatically defaults to a one-step computation of  $\alpha_{k+1}$  when  $F$  can be well-approximated by its linear expansion about the previous model.

- Operations with  $A_j$  and  $A_j^T$  are computed efficiently using reciprocity of the forward problem. They require solving only two extra forward problems per frequency.

### 3.5 Efficiency Of Methods

— CPU and memory requirements for the NLCG method increase much less rapidly with problem size, allowing the use of larger model grids and data sets (more frequencies and stations) compared to the GN methods.

## References

- Brewitt-Taylor, C.R., and Weaver, J.T., 1976, On the finite difference solution of two-dimensional induction problems, *Geophys. J. R. Astron. Soc.*, **47**, 375–396.
- Constable, S.C., Parker, R.L., and Constable, C.G., 1987, Occam's inversion: A practical algorithm for generating smooth models from electromagnetic sounding data *Geophysics*, **52**, 289–300.
- deGroot-Hedlin, C., and Constable, S., 1990, Occam's inversion to generate smooth, two-dimensional models from magnetotelluric data, *Geophysics*, **55**, 1613–1624.
- Ellis, R.G., and Oldenburg, D.W., 1994, The pole-pole 3-D DC-resistivity inverse problem: A conjugate gradient approach, *Geophys. J. Int.*, **119**, 187–194.
- d'Erceville, I., and Kunetz, G., 1962, Some observations regarding naturally occurring electromagnetic fields in applied geophysics, *Geophysics*, **47**, 651–665.
- Farquharson, C.G., and Oldenburg, D.W., 1996, Approximate sensitivities for the electromagnetic inverse problem, *Geophys. J. Int.*, **126**, 235–252.
- Fletcher, R., and Reeves, C.M., 1959, Function minimization by conjugate gradients, *Computer Journal*, **7**, 149–154.
- Freund, R.W., 1992, Conjugate gradient-type methods for linear systems with complex symmetric coefficient matrices, *SIAM J. Sci. Stat. Comput.*, **13**, 425–448.
- Hestenes, M.R., and Stiefel, E., 1952, Methods of conjugate gradients for linear systems, *J. Res. Natl. Bur. Stand.*, **49**, 409–436.
- Hohmann, G.W., 1975, Three-dimensional induced polarization and electromagnetic modeling, *Geophysics*, **40**, 309–324.
- Jacobs, D.A.H., 1986, A generalization of the conjugate-gradient method to solve complex systems, *IMA J. Numer. Anal.*, **6**, 447–452.

- Jiracek, G.R., Rodi, W.L., and Vanyan, L.L., 1987, Implications of magnetotelluric modeling for the deep crustal environment in the Rio Grande rift Phys. Earth Planet. Interiors, **45**, 179–192.
- Jones, F.W., and Pascoe, L.J., 1972, The perturbation of alternating geomagnetic fields by three-dimensional conductivity inhomogeneities, Pure Appl. Geophys., **112**, 793–800.
- Jupp, D.L.B., and Vozoff, K., 1975, Stable iterative methods for the inversion of geophysical data Geophys. J. R. Astron. Soc., **42**, 957–976.
- Jupp, D.L.B., and Vozoff, K., 1977, Two-dimensional magnetotelluric inversion Geophys. J. R. Astron. Soc., **50**, 333–352.
- Kaufman, A.A., and Keller, G.V., 1981, *The Magnetotelluric Sounding Method*, Elsevier Scientific Publishing Company, New York.
- Levenberg, K., 1944, A method for the solution of certain non-linear problems in least squares, Quart. Appl. Math., **2**, 164–168.
- Mackie, R.L., Madden, T.R., and Wannamaker, P.E., 1993, Three-dimensional magnetotelluric modeling using difference equations—Theory and comparisons to integral equation solutions, Geophysics, **58**, 215–226.
- Mackie, R.L., Smith, J.T., and Madden, T.R., 1994, Three-dimensional electromagnetic modeling using finite difference equations: The magnetotelluric example, Radio Science, **29**, 923–935.
- Madden, T.R., 1972, Transmission systems and network analogies to geophysical forward and inverse problems, ONR Technical Report, **72-3**.
- Madden, T.R., and Mackie, R.L., 1989, Three-dimensional magnetotelluric modeling and inversion, Proc. IEEE, **77**, 318–333.
- Marquardt, D.W., 1963, An algorithm for least-squares estimation of nonlinear parameters, J. Soc. Indust. Appl. Math., **11**, 431–441.
- Matarese, J.R., 1993, *Nonlinear traveltome tomography*, Ph.D. Thesis, Massachusetts Institute of Technology, Cambridge, Massachusetts.
- Matarese, J.R., and Rodi, W.L., 1991, Nonlinear traveltome inversion of cross-well seismics: a minimum structure approach, 61st Annual International Meeting of the Society of Exploration Geophysicists, Expanded Abstracts, 917–921.
- McGillivray, P.R., and Oldenburg, D.W., 1990, Methods for calculating Frechet derivatives and sensitivities for the non-linear inverse problem: a comparative study, Geophysical Prospecting, **38**, 499–524.
- Newman, G., 1995, Crosswell electromagnetic inversion using integral and differential equations, Geophysics, **60**, 899–911.
- Newman, G.A., and Alumbaugh, D.L., 1997, Three-dimensional massively parallel electromagnetic inversion—I. Theory, Geophys. J. Int., **128**, 345–354.
- Oldenburg, D.W., McGillivray, P.R., and Ellis, R.G., 1993, Generalized subspace methods for large scale inverse problems, Geophys. J. Int., **114**, 12–20.
- Polak, E., 1971, *Computational methods in optimization: A unified approach*, Academic Press, New York.
- Rankin, D., 1962, The magnetotelluric effect on a dike, Geophysics, **27**, 666–676.
- Reddy, I.K., Rankin, D., and Phillips, R.J., 1977, Three-dimensional modeling in magnetotelluric and magnetic variational soundings, Geophys. J. Royal Astr. Soc., **51**, 313–325.
- Reiter, D.T., and Rodi, W., 1996, Nonlinear waveform tomography applied to crosshole seismic data, Geophysics, **61**, 902–913.

- Rodi, W.L., 1976, A technique for improving the accuracy of finite element solutions for magnetotelluric data, *Geophys. J. R. Astron. Soc.*, **44**, 483–506.
- Rodi, W.L., 1989, *Regularization and Backus-Gilbert estimation in nonlinear inverse problems: Application to magnetotellurics and surface waves*, Ph.D. Thesis, Pennsylvania State University, University Park.
- San Filipo, W.A., and Hohmann, G.W., 1985, Integral equation solution for the transient electromagnetic response of a three-dimensional body in a conductive halfspace, *Geophysics*, **50**, 798–809.
- Sarkar, T.K. (Ed.), 1991, *Application of Conjugate Gradient Method to Electromagnetics and Signal Analysis*, Elsevier Science, New York.
- Sarkar, T.K., Yang, X., and Arvas, E., 1988, A limited survey of various conjugate gradient methods for solving complex matrix equations arising in electromagnetic wave interactions, *Wave Motion*, **10**, 527–546.
- Shi, W., Rodi, W., Mackie, R.L., and Zhang, J., 1996, 3-D d.c. electrical resistivity inversion with application to a contamination site in the Aberjona Watershed, Proceedings from Symposium on the Application of Geophysics to Environmental and Engineering Problems (SAGEEP), Keystone, Colorado, Environmental and Engineering Geophysical Society, 1257–1267.
- Smith, J.T., 1996a, Conservative modeling of 3-D electromagnetic fields, Part I: Properties and error analysis, *Geophysics*, **61**, 1308–1318.
- Smith, J.T., 1996b, Conservative modeling of 3-D electromagnetic fields, Part II: Biconjugate gradient solution and an accelerator, *Geophysics*, **61**, 1319–1324.
- Smith, J.T., and Booker, J.R., 1988, Magnetotelluric inversion for minimum structure *Geophysics*, **53**, 1565–1576.
- Smith, J.T., and Booker, J.R., 1991, Rapid inversion of two- and three-dimensional magnetotelluric data *J. Geophys. Res.*, **96**, 3905–3922.
- Stratton, J.A., *Electromagnetic Theory*, McGraw-Hill, New York, 1941.
- Swift, C.M., 1967, Theoretical magnetotelluric and turam response from two-dimensional inhomogeneities, *Geophysics*, **36**, 38–52.
- Tarantola, A., 1987, *Inverse problem theory*, Elsevier.
- Thompson, D.R., 1993, *Nonlinear waveform tomography: theory and application to crosshole seismic data*, Ph.D. Thesis, Massachusetts Institute of Technology.
- Tikhonov, A.N., and Arsenin, V.Y., 1977, *Solutions of ill-posed problems*, V.H. Winston and Sons: Washington, D.C.
- Wannamaker, P.E., 1991, Advances in three-dimensional magnetotelluric modeling using integral equations, *Geophysics*, **56**, 1716–1728.
- Wannamaker, P.E., Hohmann, G.W., and San Filipo, W.A., 1984, Electromagnetic modeling of three-dimensional bodies in layered earths using integral equations, *Geophysics*, **49**, 60–74.
- Weaver, J.T., 1963, The electromagnetic field within a discontinuous conductor with reference to geomagnetic pulsations near a coastline, *Can. J. Phys.*, **41**, 484–495.
- Weaver, J.T., 1994, *Mathematical Methods for Geo-Electromagnetic Induction*, Research Studies Press Ltd., Taunton, Somerset, England.
- Weidelt, P., 1975, Electromagnetic induction in three-dimensional structures, *J. Geophys.*, **41**, 85–109.
- Wu, F.T., 1968, The inverse problem of magnetotelluric sounding, *Geophysics*, **33**, 972–979.

Yee, K.S., 1966, Numerical solution of initial boundary value problems involving Maxwell's equations in isotropic media, IEEE Trans. Antennas Propag., **AP-14**, 302–307.

## **References for MT Short Course**

### **History**

Vozoff, K., 1972, The magnetotelluric method in the exploration of sedimentary basins : Geophysics, Soc. of Expl. Geophys., **37**, 98-141. (\* Errata in GEO-38-4-0781; Discussion in GEO-41-02-0325-0328; Discussion and reply in GEO-62-2-691)

Cagniard, L., 1953, Basic theory of the magneto-telluric method of geophysical prospecting: Geophysics, Soc. of Expl. Geophys., **18**, 605-635.

Tikhonov, A. N., 1986, On determining electrical characteristics of the deep layers of the Earth's crust, in Vozoff, K., Ed., Magnetotelluric methods: Soc. of Expl. Geophys., 2-3. (\* Reprinted from Doklady, 73, 2, 295-297)

Cantwell, T. and Madden, T.R., 1960, Preliminary Report on Crustal Magneto-telluric Measurements: J. Geophys. Research, **65**, no. 12, 4202-4205.

### **Applications**

\*Zhang, P., King, A. and Watts, D., 1998, Using Magnetotellurics for Mineral Exploration: SEG 1998 Expanded Abstracts

\*Stevens, K.M., 1998, On the Detection of Ni-Cu Ore Hosting Structures in the Sudbury Igneous Complex Using the Magnetotelluric Method: SEG 1998 Expanded Abstracts

Balch, S.J., Crebs, T.J., King, A., and Verbiski, M., 1998, Geophysics of the Voisey's Bay Ni-Cu-Co Deposits: SEG 1998 Expanded Abstracts

\* Livelybrooks, D., Mareschal, M., Blais, E. and Smith, J. T., 1996, Magnetotelluric delineation of the Trillabelle massive sulfide body in Sudbury, Ontario : Geophysics, Soc. of Expl. Geophys., **61**, 971-986. (\* Discussion in GEO-62-5-1672)

Watts, M.D. and Balch, S.J., 2000, HEM-Constrained 2D inversion of AMT data over the Voisey's Bay nickel sulfide body, Labrador:SEG 2000 Expanded Abstracts

### **Processing:**

Gamble, T.D., Goubau, W.M., and Clarke, J., 1979, Magnetotellurics with a remote magnetic reference: Geophysics, **44**, 53-68.

Zerilli, A., 1998, Advances in Magnetotellurics applied to extreme noise environments: SEG Mining Workshop at the 68<sup>th</sup> Annual Meeting

Larsen , J.C., Mackie, R.L., Manzella, A., Fiordelisi, A., Rieven, S., 1996. Robust smooth magnetotelluric transfer functions. Geophys. J. Int. 124, pp. 801-819.

Oettinger, G., V. Haak, and J.C. Larsen (2001): Noise reduction in magnetotelluric time-series with a new signal-noise separation method and its application to a field in the Saxonian Granulite Massif. Geophys. J. Int., **146**(3), 659–669.

### **Interpretation Problems**

\*Chouteau, M. and Tournerie, B., 1999?, Analysis of Magentotelluric Data Showing Phase Rolling Out of Quadrant (PROQ): SEG 1999? Expanded Abstracts

**General:**

Vozoff, K., ed., 1986. Magnetotelluric Methods. Soc. Expl. Geophys. Reprint Ser. No. 5: Tulsa, OK, ISBN 0-931830-36-2.

Ward, S.,H., 1967, Electromagnetic Theory for Geophysical Applications: in Mining Geophysics, Vol. II: SEG, pp. 13-372.

Zhdanov, M.S, and Keller, G.V.,1994, The Geoelectrical Methods in Geophysical Exploration, Elsevier.

**Static Shifts**

Sternberg, B.K., Washburne, J.C., and Pellerin, L., 1988, Correction for the static shift in magnetotellurics using transient electromagnetic soundings: Geophysics, vol. 53, p. 1459-1468

## **Resources – MT contractors, manufacturers and software (workstations)**

### Manufacturers:

Phoenix Geophysics, Toronto [www.phoenix-geophysics.com](http://www.phoenix-geophysics.com)

EMI Instruments, Berkeley [www.emiinc.com](http://www.emiinc.com)

Metronix, Germany [www.metronix.de](http://www.metronix.de)

Zonge Engineering, Tucson [www.zonge.com](http://www.zonge.com)

### Contractors:

Geosystem, Milan, SFrancisco and Toronto [www.geosystem.net](http://www.geosystem.net)

Phoenix Geophysics, Toronto [www.phoenix-geophysics.com](http://www.phoenix-geophysics.com)

Quantec , Reno

Geodatos, Chile [www.geodatos.cl](http://www.geodatos.cl)

AOA Geophysics, Austin [www.aoageophysics.com](http://www.aoageophysics.com)

### Software:

Geosystem, Milan, SFrancisco and Toronto [www.geosystem.net](http://www.geosystem.net)

Geotools (owned by AOA), Austin [www.aoageophysics.com](http://www.aoageophysics.com)

Interpex, Golden CO [www.interpex.com](http://www.interpex.com)

### Other info:

MTNet <http://www.cg.nrcan.gc.ca/mtnet/>

Lightning storms; Solar data - tracking for activity

<http://sec.noaa.gov>

Canada-  
<http://www.spaceweather.gc.ca/>



# Continuing Education



Karen - Interpretation

If we add H-field components to our array  
Can we calculate a true strike/directionality

Increased sample frequency will increase resolution  
up to what point.

TE is aligned with strike & TM is perpendicular

H<sub>a</sub> component is very important for TE determination  
Airloop for Amr - How big? Ask big guy!

TM will be upper curve on resistive side

TE " " " " " conductive side

Workstation Programs &- data editing, etc,

WingLink - (good system!) Geotools - AOA (out of support?)  
Basic C \$4000

Gravity/Magnetics module

One of these will be necessary!

Can we use H<sub>a</sub> airloop as sensor loop for  
EM static shift correction or RIP Array!!

Phase data maybe most important parameter but  
under utilized and/or exploited - what exactly  
is it showing us?

Map displays "look" geologic!

MT short course @ NWMA in Spokane??

# Continuing Education



10/6 - Alan Jones - data/PPT's on website - MTNET

Complex Analytic Signal - check on this!

Jackknife estimator superior to parametric estimates

Jones Robust Processing - available - Phoenix system

Static shift doesn't affect phase!

Amr Remote cannot be too far away - high freqs,  
can be incoherent - probably less than 5Kms  
multiple remotes - Low freq remotes & high freq. remotes

Stratagem Geometrics

# Continuing Education



Randy Macie - MT Modeling 20/30

Likes Finite Differences rather than Finite Elements

Mesh

Surface layer  $\approx 1/10^{\text{th}}$  skin depth at highest frequency.

Watch curve fitting in a separate window ??

Starts w/ TM mode as it is less complicated & doesn't require air component

